Impacts of future climate on Tasmanian rivers

by

James C. Bennett, B.A./B.Sc., B.Ant.Stud.(hons), Grad.Dip.Ed.

Submitted in fulfilment of the requirements

for the degree of Master of Science

Institute for Marine and Antarctic Studies

University of Tasmania

November 2013

I declare that this thesis contains no material which has been accepted for a degree or diploma by the University or any other institution, except by way of background information and duly acknowledged in the thesis, and that, to the best of my knowledge and belief, this thesis contains no material previously published or written by another person, except where due acknowledgement is made in the text of the thesis, nor does the thesis contain any material that infringes copyright.

Signed: _____

James Bennett

Date: _____

Signed: _____

James Bennett

Date: _____

Abstract

Changes to streamflows caused by climate change may have major impacts on the management of water for hydro-electricity generation and agriculture in Tasmania, Australia. This thesis describes changes to surface water availability in Tasmania for the 21st century assessed from a series of high-resolution regional climate and hydrological models. Surface water projections are generated by bias-correcting regional climate model (RCM) simulations, passing the bias-corrected RCM simulations through rainfall-runoff models, and then passing runoff through river models that simulate water diversions and consumption.

The bias-correction applied to daily RCM simulations is a quantile mapping technique that aligns empirical frequency distributions of RCM variables to observations. We show that quantile mapping of empirical distributions can be highly effective in correcting biases in RCM outputs. Cross-validation shows biases are effectively reduced across the range of cumulative frequency distributions, with few exceptions. The bias-correction is not as effective at correcting biases for values at or near zero (e.g. in rainfall simulations), although even here the bias-correction improves biases in the uncorrected simulations. In addition, the bias-correction improves frequency characteristics of variables such as the number of rain days.

The bias-correction effectively preserves long-term changes (e.g. to the mean and variance) to variables projected by the uncorrected RCM simulations. Correlations between key variables are also largely preserved, thus the bias-corrected outputs largely reflect the dynamics of the underlying RCM. However, the bias-corrected simulations still exhibit some of the deficiencies of the RCM simulations, for example the tendency to underestimate both the magnitude and duration of large, multi-day rain events.

Bias-corrected outputs from six fine-scale (10 km^2) simulations of daily rainfall and potential evapotranspiration generated with the CSIRO Conformal Cubic Atmospheric Model (CCAM), a variable-resolution RCM, are used as direct inputs to the hydrological models AWBM, IHACRES, Sacramento, SIMHYD and SMAR-G to project Tasmanian runoff. The performance of the hydrological models is assessed against 86 streamflow gauges across Tasmania. The SIMHYD model is the least biased (median bias =−3%) while IHACRES has the largest bias (median bias =−22%). We find the hydrological models that best simulate observed streamflows produce similar streamflow projections.

There is much greater variation in projections between RCM simulations than between hydrological models. Marked decreases of up to 30% are projected for annual runoff in central Tasmania, while runoff is generally projected to increase in the east. Daily streamflow variability is projected to increase for most

of Tasmania, consistent with increases in rainfall intensity. Inter-annual variability of streamflows is projected to increase across most of Tasmania.

Changes to rivers are assessed by passing runoff projections through models that account for water diversions and water use, including hydro-electric power generation. Of the 78 rivers modelled, on average 32 are projected to have changes to mean annual flows of more than ±10% by 2100. On average, 28 of the 78 rivers modelled are projected to have decreased flows by 2100. The likely reduction in runoff to the central highlands will mean reduced inflows to irrigation storages. For example, the mean inflows to Lake Crescent/Sorell and Meander Dam are likely to fall by 20% and 13% respectively. Conversely, large irrigation storages supplying the Macquarie and Coal river catchments are projected to experience increased inflows by 2100. Hydropower generation is projected to decrease by 6%, mainly caused by decreased runoff from the central highlands.

This is the first major Australian study to use high-resolution bias-corrected rainfall and potential evapotranspiration projections as direct inputs to hydrological models. Our study shows that these simulations are capable of producing realistic streamflows. The fine spatial resolution of the runoff projections allows us to generate plausible scenarios of river flows at the catchment scale, which is most relevant to water managers. The surface-water projections generated in this study are being used to inform water planning and policy by the Tasmanian government.

Acknowledgements

For me, writing a thesis while working full-time and parenting two young children would have been impossible without the heroic efforts of my wife, Nina. Nina took on a huge proportion of our child-rearing and domestic tasks when I wrote this thesis, and the accompanying exhaustion and offense to her feminist ideals, for months on end and without complaint. Her efforts are as much responsible for this thesis as mine, and I am terrifically grateful.

Frieda (5) and Sam (2) did everything they could to distract me from writing this thesis, and I couldn't be more thankful for it.

Thanks to my supervisory team of Nathan Bindoff (IMAS), Fiona Ling (Entura) and David Post (CSIRO). This thesis came out of my secondment to the Climate Futures for Tasmania project at the ACE CRC (www.acecrc.org.au/Research/Climate_Futures) when I was employed as a consultant at Entura. Fiona arranged the secondment, encouraged me to pursue post-graduate study, envisaged the water and catchments modelling component of the Climate Futures for Tasmania project, stepped in when I needed help and left me the freedom to find my own way when I did not. If that were not enough, I owe Fiona my career in hydrology, a career I enjoy far too much to admit in polite company. David ran the Tasmania Sustainable Yields project, and then magnanimously threw his support behind what could have been seen as competing research carried out by Climate Futures for Tasmania. This thesis owes a great debt to the Tasmania Sustainable Yields project, and to David. Climate Futures for Tasmania was borne largely out of Nathan's conviction that scientists should provide local information on climate change to empower people to act in their own interests. Nathan took the risk of employing me as an underqualified and overenthusiastic analyst, for which I am very grateful. Aside from being excellent supervisors, Fiona, David and Nathan have shown by example how to pursue highly successful careers and scientific excellence through modesty and good humour, and by treating all of their colleagues with empathy and honour. It is an example I try to emulate.

Heartfelt thanks to the Climate Futures for Tasmania team of Stuart Corney, Suzie Gaynor, Greg Holz and Chris White (all ACE CRC) for a whirlwind 20 months of enjoyable productivity. Special thanks to Michael Grose (ACE CRC and CSIRO), for the extra help, code, and discussions both serious and light. Thanks to my then manager, Crispin Smythe (then of Entura), for supporting my secondment and my career.

Bryce Graham (DPIPWE) ensured the Climate Futures for Tasmania water and catchments model outputs would be usable by the Tasmanian government to inform policy, and selflessly took the time to impart to me the real and (more often) imagined inadequacies of the Carlton football club.

Roger Parkyn (Hydro Tasmania) configured the Temsim hydro-electricity generation model and Katherine Brown (Entura) ran runoff scenarios through Temsim. Stuart Allie (Hydro Tasmania) prepared

and supplied Fig 5.5. Jin Teng (CSIRO) provided evapotranspiration algorithms. Bill Budd (ACE CRC) kept the Climate Futures analysts from repeating the mistakes of analysts past. Simon Wotherspoon gave advice on the bias-correction, and generously taught me time series analysis. Francis Chiew, Marie Ekström, Jin Teng, Neil Viney (all CSIRO), Fiona Dyer (University of Canberra), Kelvin Michael (IMAS) and Danielle Verdon-Kidd (University of Newcastle) gave comments that improved papers and reports that contributed to this thesis. Ashish Sharma (University of New South Wales) and an anonymous assessor gave thorough and expeditious assessments of this thesis and valuable suggestions for improvement. Thanks all.

Thanks to the hydrologists whose work developing models for the Tasmania Sustainable Yields project made the Climate Futures for Tasmania water and catchments component possible: Kim Robinson, Mark Willis, Jayson Peterson, Vila Gupta (then all Entura), Neil Viney and Ang Yang (CSIRO).

I am grateful to John Morrongiello (CSIRO) and David Ikedife (Entura) for inviting me to contribute to a review article on climate change impacts on Australian native fish.

QJ Wang (CSIRO) and the CSIRO streamflow forecasting team allowed me some (work) time and computing resources to complete this thesis – thanks.

Thanks to my parents, Ernest and Josephine Bennett, for child minding, temporary accommodation and countless small, helpful things. Extra thanks to Jo and Ernest for enabling me to spend four glamorous weeks as a full time post-graduate student.

Climate Futures for Tasmania was supported by the Australian government's Cooperative Research Centres Program through the ACE CRC. Thanks to Tony Press and Kate Maloney (ACE CRC) for administrative support. Climate Futures for Tasmania received financial and in-kind support from the federal Department of Sustainability, Environment, Water, Populations and Communities, the Tasmanian Department of Primary Industries, Parks Water and Environment, the federal Attorney General's Department, the Tasmanian State Emergency Service, the Bureau of Meteorology, Hydro Tasmania, Geoscience Australia, CSIRO, the Tasmanian Institute for Agricultural Research and the Tasmanian Partnership for Advanced Computing.

I acknowledge the modelling groups, the Program for Climate Model Diagnosis and Intercomparison (PCMDI) and the WCRP's Working Group on Coupled Modelling (WGCM) for their roles in making available the WCRP CMIP3 multi-model dataset. Support of this dataset is provided by the Office of Science, U.S. Department of Energy.

Publications arising from research completed during candidature

Refereed journal papers

1. **Bennett JC**, Grose MR, Corney SP, White CJ, Holz GK, Katzfey JJ, Post DA, Bindoff NL. 2013. Performance of an empirical bias-correction of a high-resolution climate dataset. *International Journal of Climatology*, published online. DOI: 10.1002/joc.3830.
2. **Bennett JC**, Ling FLN, Post DA, Grose MR, Corney SP, Graham B, Holz GK, Katzfey JJ, Bindoff NL. 2012. High-resolution projections of surface water availability for Tasmania, Australia. *Hydrology and Earth System Sciences* 16: 1287-1303. DOI: 10.5194/hess-16-1287-2012.
3. Corney S, Grose M, **Bennett JC**, White C, Katzfey J, McGregor J, Holz G, Bindoff NL. 2013. Performance of downscaled regional climate simulations using a variable-resolution regional climate model: Tasmania as a test case. *Journal of Geophysical Research: Atmospheres***:** 2013JD020087. DOI: 10.1002/2013jd020087.
4. Grose MR, Corney SP, Katzfey JJ, **Bennett JC**, Holz GK, White CJ, Bindoff NL. 2013. A regional response in mean circulation and rainfall to projected climate warming. *Climate Dynamics* **40:** 2035-2048. DOI: 10.1007/s00382-012-1405-1.
5. Morrongiello JR, Beatty SJ, **Bennett JC**, Crook DA, Ikedife DNEN, Kennard MJ, Kerezsy A, Lintermans M, McNeil DG, Pusey BJ, Rayner T. 2011. Climate change and its implications for Australia's freshwater fish. *Marine and Freshwater Research* **62:** 1082-1098. DOI: 10.1071/MF10308.

Refereed conference paper

1. **Bennett JC**, Grose MR, Post DA, Ling FLN, Corney SP, Bindoff NL. 2011. Performance of quantile-quantile bias-correction for use in hydroclimatological projections. *MODSIM2011, 19th International Congress on Modelling and Simulation*. Modelling and Simulation Society of Australia and New Zealand: Perth. Available online at http://www.mssanz.org.au/modsim2011/F5/bennett.pdf.

Referred technical report

1. **Bennett JC**, Ling FLN, Graham B, Corney SP, Holz GK, Grose MR, White CJ, Post DA, Gaynor SM, Bindoff NL. 2010. Climate Futures for Tasmania: water and catchments. Cooperative Research Centre: Hobart. Available online at http://www.climatechange.tas.gov.au/government_action/climate_futures/

Statement of co-authorship

The following people contributed to the publication of the work included in this thesis:

Paper 1/Chapter 3 (Performance of an empirical bias-correction of a high-resolution climate dataset):

- **James Bennett** (70%) – Conceived and implemented cross-validation and all other verification analyses; generated cross-validated bias-corrected RCM outputs; assisted in testing and implementing bias-correction method, jointly conceived all validation methods, carried out all analyses, wrote paper.
- Michael Grose (10%) – Developed and coded bias-correction method; contributed analyses.
- Stuart Corney (10%) – Developed and coded bias-correction method; contributed analyses.
- Christopher White (2%) – Contributed verification analyses.
- Greg Holz (2%) - Suggested bias-correction and assisted in bias-correction method development.
- Jack Katzfey (2%) – Configured CCAM and assisted with running CCAM.
- David Post (2%) – Assisted in development of cross-validation method.
- Nathaniel Bindoff (2%) – Conceived wider project, edited and augmented paper, supervised research.

Paper 2/Chapter 4 (High-resolution projections of surface water availability for Tasmania):

- **James Bennett** (80%) – Conceived hydro-climatological modelling method, generated bias-corrected RCM outputs, carried out all runoff and river system modelling, jointly conceived all validation methods, carried out all analyses, wrote paper.
- Fiona Ling (6%) – Conceived modelling method, supervised modelling and research.
- David Post (3%) – Conceived cross-validation and validation methods, edited paper, supervised research.
- Michael Grose (2%) – Developed bias-correction method, assisted with analyses.
- Stuart Corney (2%) – Ran CCAM, developed bias-correction method
- Bryce Graham (1%) - Supervised hydrological modelling.
- Greg Holz (1%) – Assisted in method development.
- Jack Katzfey (1%) – Configured CCAM and assisted with running CCAM, edited and augmented paper.
- Nathaniel Bindoff (4%) – Conceived wider project, edited and augmented paper, supervised research.

Conference Paper 1/Appendix A (Performance of quantile-quantile bias-correction for use in hydroclimatological projections):

- **James Bennett** (85%) - Conceived and implemented cross-validation and all other verification analyses; generated cross-validated bias-corrected RCM outputs; assisted in testing and implementing bias-correction method, jointly conceived all validation methods, carried out all analyses, wrote paper.
- Michael Grose (5%) – Developed and coded bias-correction method; contributed analyses.
- David Post (4%) – Conceived cross-validation and validation methods, edited paper, supervised research.
- Stuart Corney (2%) - Developed and coded bias-correction method.
- Fiona Ling (2%) - Edited paper, supervised research.
- Nathaniel Bindoff (2%) - Edited paper, supervised research.

We the undersigned agree with the above stated proportion of work undertaken for each of the above published (or accepted for publication) peer-reviewed manuscripts contributing to this thesis:

Signed: _____

Prof. Nathaniel L. Bindoff

Supervisor

Institute for Marine and Antarctic Studies

Date: _____

Signed: _____

Prof. Mike Coffin

Director

Institute for Marine and Antarctic Studies

Date: _____

Abbreviations used in this thesis

APET	Areal potential evapotranspiration
AR4	IPCC Fourth Assessment Report
AWAP	Australian Water Availability Project gridded climate data
BoM	Bureau of Meteorology
BoM-HQ	Bureau of Meteorology High Quality interpolated climate data
CCAM	Conformal Cubic Atmospheric Model
C-C	Clausius-Clapeyron relationship
DPIPWE	Department of Primary Industries, Parks, Water and Environment
GCM	coupled ocean-atmosphere Global Climate Model
IPCC	Intergovernmental Panel on Climate Change
NSE	Nash-Sutcliffe Efficiency
RCM	Regional Climate Model
SILO	Queensland Department of Natural Resources gridded climate data
SRES	Special Report on Emissions Scenarios
SST	Sea Surface Temperature
Temsim	Tasmanian Electricity Market Simulation Model

Contents

1 Introduction

Water in rivers and lakes ('surface-water') remains the most important source of fresh water to many of the world's communities and ecosystems. One troubling possibility of continued human greenhouse gas emissions is a change to the availability of surface water. No less troubling are the inexorably increasing rates of human water use caused both by population growth and increased per capita consumption (Oki and Kanae, 2006). Informed planning for future water use will help us maintain this fundamentally important resource. This thesis contributes to this effort by assessing future surface water availability for Tasmania, Australia, with particular focus on the potential effects of climate change.

1.1 Anthropogenic climate change and the hydrological cycle

Heat from the sun's radiation evaporates water from the oceans and land. Water vapour in the atmosphere is transported by winds, and coalesces into clouds. Moisture condenses out of supersaturated air and falls as rain, snow and ice on land and oceans. Water falling on land is absorbed into the surface or runs off into rivers and lakes; subsurface water percolates into rivers or aquifers. The rate of rainfall has a profound effect on how much water flows into rivers: high intensity rainfall results in proportionally more runoff than low intensity rainfall. Snow or ice may melt quickly, or they may fall in cold regions and be bound in glaciers. Glaciers, aquifers and rivers complete the hydrological cycle by returning water to the oceans and the atmosphere.

Earth's atmosphere and oceans have warmed since the mid-20th century. The evidence includes rises in surface temperature records (Thompson et al., 2008), rising ocean temperatures (Domingues et al., 2008), paleoclimate reconstructions (Mann et al., 2008), retreat of glaciers and ice caps (Hock et al., 2009), reduced polar ice-sheets (Allison et al., 2009) and rising sea levels (Rahmstorf et al., 2007). The Intergovernmental panel on climate change (IPCC) fourth assessment report (AR4) – possibly the largest review of scientific literature ever published – concluded that warming of the climate system in the second half of the 20th century was ''unequivocal'' (IPCC, 2007). During this period, human emissions of carbon dioxide (CO_2) raised atmospheric CO_2 concentration to the highest level in at least 800,000 years (Lüthi et al., 2008). The warming effect of CO_2 and other greenhouse gases is consistent with our understanding of atmospheric physics and observations (e.g. Arrhenius, 1896; Hansen et al., 2011; Hansen et al., 2005). IPCC (2007) AR4 concluded that "most of the observed increase in global average temperatures since the mid-20th century is *very likely* due to the observed increase in anthropogenic greenhouse gas concentrations" (their italics).

In theory, changes to the radiative heat balance of the earth caused by anthropogenic greenhouse gas emissions will have wide-reaching effects on the global hydrological cycle. Saturation vapour pressure

(analogous to the water-holding capacity of the atmosphere) is closely tied to temperature. Saturation vapour pressure is bound to temperature by the Clausius-Clapeyron (C-C) relationship, which holds that the saturation vapor pressure increases by about 7% for each 1 °K temperature increase for temperatures typical of the earth's surface. For theoretical calculations, relative humidity is often assumed to remain constant with changes in temperature (e.g. Allen and Ingram, 2002; Arrhenius, 1896). Precipitation is not expected to increase at the C-C rate, principally because the additional latent heat released from the added precipitation cannot be transported out of the troposphere quickly enough (Allen and Ingram, 2002). These ostensibly contradictory forces – i.e., increased moisture in the atmosphere without a compensating increase in precipitation – are reconciled by the slowing of tropospheric mass transport, resulting in longer atmospheric residence times of water vapour and a slowing of the hydrological cycle (Held and Soden, 2006). A slower hydrological cycle implies that rain will tend to fall in more intense bursts interspersed by longer dry periods (Stephens and Hu, 2010; Trenberth, 2011). In addition, if relative humidity in the lower troposphere remains unchanged, and if changes in winds are negligible, water available for runoff (precipitation (*P)* minus evaporation (*E*)) also scales with C-C, as described by Held and Soden (2006). From this thermodynamic argument it follows that current spatial patterns of $P - E$ will be amplified by increases in temperature so that dry regions become dryer and wet regions become wetter (Trenberth, 2011), or, to use Chou and Neelin's (2004) memorable phrase, 'the rich get richer and the poor get poorer'.

Observed changes in the global hydrological cycle often follow theoretical predictions, with several notable exceptions. We note that a number of hydro-climatic variables have patchy spatial coverage and short records (see, e.g., Sherwood et al., 2010a; Trenberth et al., 2007), and we confine our discussion to those studies that have strong grounding in quality controlled data. There appears to have been a net increase in global surface specific humidity since at least the mid-1970s, approximately in line with the Clausius-Clapeyron relationship (Sherwood et al., 2010a; Willett et al., 2008). This increase has been formally attributed to anthropogenic global warming (Willett et al., 2007). Over the same period global surface relative humidity has not changed significantly (Willett et al., 2008). These increases in specific humidity with no change in relative humidity are theoretically consistent with warming, as described above. The 'rich get richer' hypothesis appears to have some support in observed precipitation changes, although there is considerable regional variation in trends. Observed precipitation increases in the mid latitudes of the northern hemisphere, drying in the northern subtropics and tropics, and moistening of the southern tropics and tropics for 1925-1999 have all been at least partly attributed to anthropogenic global warming (Zhang et al., 2007). The 'rich-get-richer' mechanism has been indirectly (but clearly) observed over oceans through changes in sea surface salinity since 1950 (Durack et al., 2012). Globally, the incidence of drought appears to have increased in the 20th century (Dai, 2011; Dai et al., 2004). At the same time, extreme rainfall indices generally show increases when averaged globally for the second half of the 20th century (Alexander et al., 2006) and increases to precipitation extremes (Min et al., 2011) and regional flooding (Pall et al., 2011) have been ascribed to anthropogenic global warming. Increasing

trends in drought and rainfall intensity support the theoretical prediction of more intense rainfalls interspersed by longer dry periods. Indeed, an index that measures increases in both dry spell length and precipitation intensity (described as 'hydroclimatic intensity') has also shown global increases in the latter half of the 20th century (Giorgi et al., 2011).

The agreements between theoretical predictions and observations already described are somewhat undermined by Wentz et al. (2007), who found that global net precipitation increased at the same rate as total atmospheric water over the period 1986-2007. If the assumption that rainfall will increase at a rate slower than C-C with rising temperatures stands on less-than-solid ground, much else becomes shaky. For example, dry spells need not necessarily become longer as atmospheric residence times of water vapour need not increase, and while more rain will fall, it need not necessarily fall with increased intensities (but if it does not, then the frequency of rainfall must increase). Wentz et al. (2007) could not explain the findings of their study with respect to theoretical predictions (represented by global climate models), but rather offered that 20 years may not be a long enough period over which to measure such trends, or that there may be some measurement error in the satellite data that they used. However, Durack et al. (2012) have reported changes in rainfall over oceans since 1950 that correspond to C-C scaling, supporting Wentz et al. (2007). Taken at face value, Wentz et al.'s (2007) findings are unsettling for those of us investigating the impacts of climate change on hydrology, as they imply a fundamental misunderstanding of possible changes to the hydrological cycle under increased warming (and one that is carried into dynamical climate models, which enforce theoretical thermodynamic constraints on rainfall increases).

The thermodynamic hydrological responses to warming discussed thus far do not account for the marked regional variations in hydrological responses to warming driven by climate dynamics. For example, coupled ocean-atmosphere global climate models (GCMs) project a 'widening' of the tropics (a poleward expansion of the Hadley cell) and this is supported by observational studies (e.g. Lucas et al., 2012; Nguyen et al., 2013). The poleward expansion of the Hadley cell drives spatial and vertical changes in relative humidity (e.g., relative humidity may increase in the mid latitudes) (Sherwood et al., 2010b). While these changes in relative humidity are small compared to changes in specific humidity, their influence on cloud formation may be significant (Sherwood, 2010). At much smaller scales, topography and land/ocean boundaries can influence regional hydrological responses to warming (Hagemann et al., 2009). Dynamical climate models attempt to simulate both the dynamics and thermodynamics of the hydrological cycle, and are therefore designed to describe regional differences in climate change. For this reason dynamical climate models are commonly used to assess the impacts of a warming climate on regional hydrology, in particular changes to atmospheric variables such as rainfall and evaporation. The use of dynamical regional climate models (RCMs) to reprocess GCM simulations at higher resolution for a particular area offers the possibility of improved simulations of regionally important climate processes. The advantages of regional climate modelling, together with the dynamical climate modelling method we apply to this study, are discussed in Chapter 2.

1.2 Assessing climate change impacts on regional hydrology

Changes to regional runoff and river flows are most often assessed with a combination of climate models and hydrological models (see reviews by Fowler et al., 2007; Maraun et al., 2010). The hydrological models are usually forced by rainfall and a measure of evaporation, and then account for soil moisture fluxes and land surface processes to simulate river flows. Typically, hydrological models are simple conceptualisations of catchment processes, and usually do not conserve mass (i.e., incoming rainfall need not be balanced by outgoing streamflows and evaporation). These models are most often parameterised for each catchment (or subcatchment) by matching simulated river flows to observed hydrographs. Dynamical climate models conserve mass, so that water is never lost from the hydrological cycle. Combining hydrological models with climate models has the notable disadvantage of disrupting the water mass balance. Conserving the water balance may be particularly important if, for example, water fluxes from soil to atmosphere are not realistically constrained (Milly and Dunne, 2011). However, runoff or river flows simulated directly by dynamical climate models often do not agree well with observations. There are a number of causes for this, including: insufficiently detailed representation of important regional hydrological process (e.g. sea/land boundaries) (Hagemann et al., 2009), inaccurate representation of the size or function of surface moisture stores (van den Hurk et al., 2005), inadequate representation of catchment characteristics (e.g. topography, slope, channel networks, flow routing), biases in other hydrological variables that are then conveyed to surface water simulations when the water mass balance is closed, or some combination of these. Reasonably realistic simulations of river flows are particularly important if they are to be used in other impact models such as hydro-electricity generation models or irrigation models, as these may rely on empirically derived decision rules (as is the case in this study; see Chapter 5).

For climate change impact studies, hydrological models can be forced indirectly by adjusting historical observations to resemble the future climate projected by climate models (e.g. Chiew et al., 2009), or directly by using time series of hydrological variables generated by climate models to force hydrological models (e.g. Akhtar et al., 2009; Kilsby et al., 2007; Wood et al., 2004). Fowler and Kilsby (2007) point out that indirect forcing methods often do not explicitly account for changes to rainfall variability or to changes in the sequences of wet and dry days, even though these are likely to have significant impacts on streamflow.

Forcing hydrological models directly with climate model outputs has the advantage that the complex dynamical and thermodynamic changes to rainfall projected by climate models, including changes in regional rainfall distribution, changes to seasonal rainfall, changes to rainfall extremes, and changes to rainfall frequencies, will be reflected in projections of streamflow. This allows more meaningful assessment of climate change impacts on streamflow volumes and variability. Accordingly, we attempt this approach.

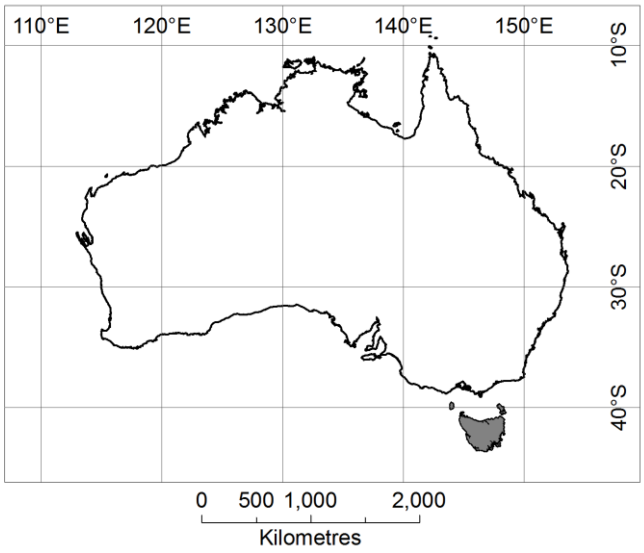

Fig 1.1 Tasmania's location (shaded) in relation to the Australian continent.

1.3 Study area: Tasmania

Tasmania is Australia's smallest (~70,000 km²) and most southerly state, in addition to being Australia's only island state. Tasmania is mountainous, with mountain ranges in the north-east (Ben Lomond Plateau), centre (central highlands), west and south all exceeding 1000 m in elevation. Tasmania lies in the path of the 'Roaring Forties' winds (Fig 1.1), and the prevailing westerly weather combines with the mountains to make western Tasmania one of the wettest places in Australia. Mean annual rainfalls exceed 2000 mm for much of the west and rise to more than 4000 mm on some mountain peaks (Fig 1.2a). Rainfall in the west is highest in the austral winter (June-July-August, JJA) and lowest in summer (December-January-February, DJF). Snowfalls are common on Tasmanian mountains, however snow typically melts within a few weeks and seasonal snowmelt is not an important component of Tasmanian streamflows. Mean annual rainfall follows a sharp gradient from west to east, with the central midlands and eastern lowlands averaging less than 600 mm (Fig 1.2a). In contrast to the winter-dominant rainfall in the west and north-west, rainfall in the east does not show a strong seasonal cycle. Low pressure systems off the east coast cause occasional high-intensity rain storms over eastern Tasmania. Despite the low and less reliable rainfall, agriculture is an important industry in the lowlands of the east. The central, western and south-western mountains are of high conservation value and much of this unpopulated region is listed as a UNESCO world heritage area.

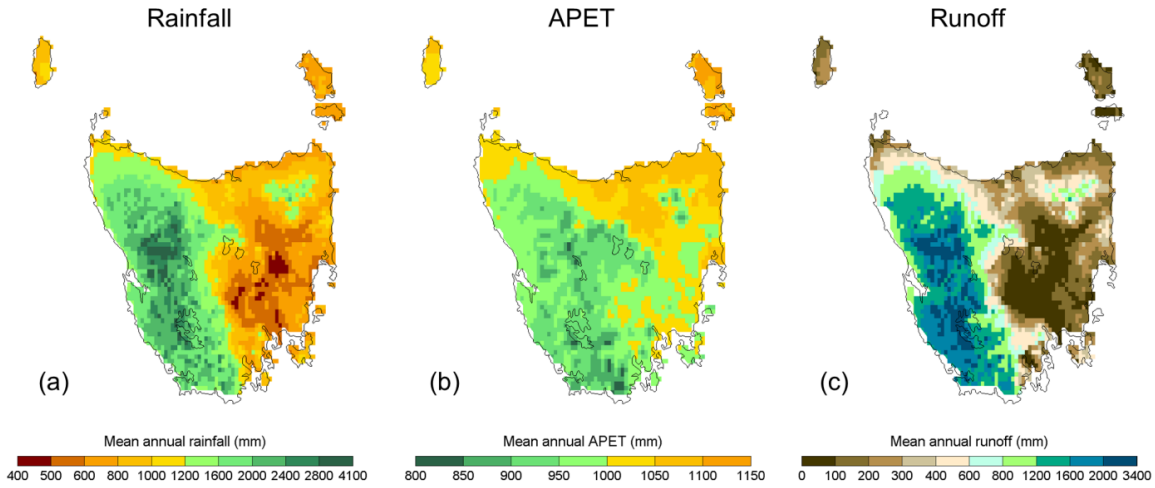

Fig 1.2 Tasmanian historical climate (1961-2007) derived from the SILO climate dataset (Jeffrey et al., 2001). (a) Mean annual rainfall. (b) Mean annual Morton's (1983) wet APET calculated from SILO temperature, solar radiation and vapour pressure. (c) Mean annual runoff generated with the SIMHYD model using SILO variables.

Mean annual areal potential evapotranspiration (APET) is highest (>1100 mm) in the central north of Tasmania and declines to <850 mm in the south and west (Fig 1.2b). These patterns of APET and rainfall combine to give Tasmania a very steep west-to-east gradient in mean annual runoff, from >3000 mm on the western mountains to <100 mm in some eastern areas (Fig 1.2c). An exception to this west-to-east gradient is the small, mountainous Ben Lomond plateau in the north-east of Tasmania, where high mean annual runoff (>1200 mm) occurs.

1.3.1 Recent trends in Tasmanian rainfall

Tasmanian mean annual rainfall for 1930-2009 from three different observational datasets is shown in Fig 1.3. Two of the datasets, the Bureau of Meteorology high- quality dataset (Lavery et al., 1997) (BoM-HQ) and the Australian water availability project (AWAP) gridded dataset (Jones et al., 2009) show decreasing rainfall since 1930. The SILO gridded dataset (Jeffrey et al., 2001) shows no clear trend in Tasmanian rainfall from during the 20th century. SILO and AWAP both interpolate observations to grids using various interpolation techniques. Discrepancies may arise between the two datasets because AWAP data are corrected to preserve trends in selected high-quality stations to reduce network-derived inhomogenities (i.e., artificially large changes in time series caused by the commissioning or decommissioning of observing stations) (Fawcett et al., 2010), whereas SILO data are not. Mean Tasmanian rainfall is dominated by the rainfall contribution of the wet western region, and this area has a

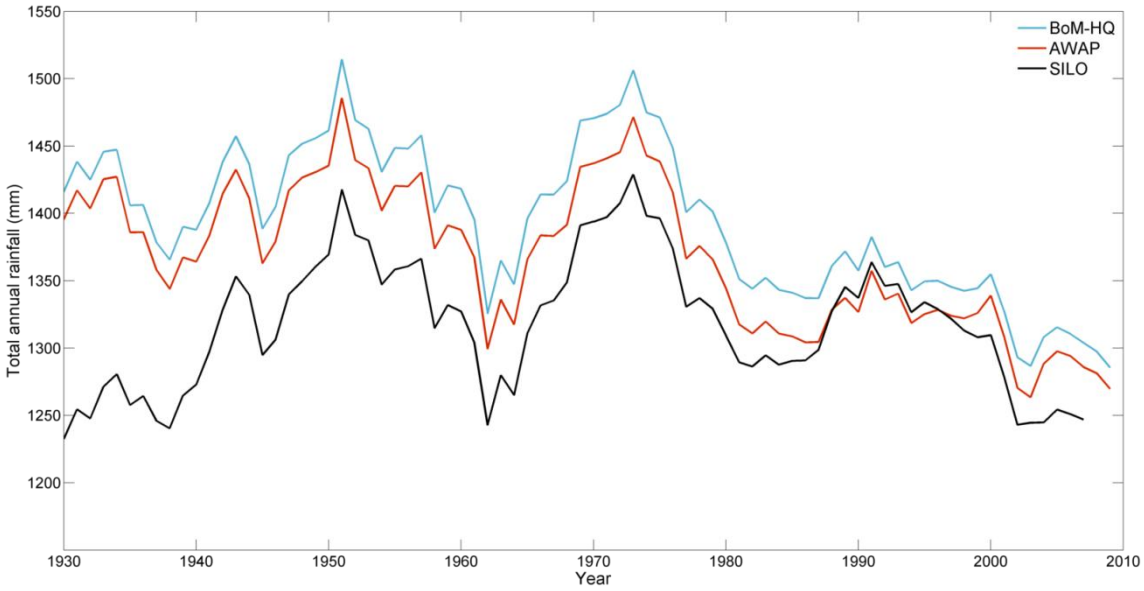

Fig 1.3 Tasmanian mean annual rainfall from the AWAP, SILO and BoM-HQ datasets from 1930-2008. The three curves are smoothed with an 11-year moving average. Datasets described in text.

sparse observing network, especially before 1950. Interpolation discrepancies over western Tasmania are the likely cause of the discrepancies in 20th century rainfall trends between the SILO and AWAP datasets. All three datasets indicate that Tasmanian rainfall has declined since about 1980. The decline is particularly marked from the late 1990s to 2008, a period described as the 'Millennium Drought' over south-east Australia. The severely low rainfalls of the Millennium Drought over south-east Australia are probably unprecedented in the historical record (van Dijk et al., 2013), and the drought has been linked to a more southerly position of the subtropical ridge of high pressure (Timbal and Drosdowsky, 2013), a well-known signal of global warming. However, the Millenium drought has not yet been formally attributed to anthropogenic global warming.

More detailed analyses of Tasmanian rainfall trends and how well these are replicated by the high resolution climate simulations used in this study are presented in Chapter 2.

1.3.2 Previous studies of climate change impacts on Tasmania

Tasmania's highly uneven rainfall distribution is not well represented by GCMs (Corney et al 2010). The most recent GCMs available for this study were generated for phase 3 of the climate model intercomparison project (CMIP3). Most CMIP3 GCMs have horizontal resolutions of 150 km or more, and as Tasmania is approximately 300 km wide these models cannot realistically simulate Tasmania's spatial variation in rainfall. This makes Tasmania an ideal candidate for fine-scale climate modelling. Tasmania has been the subject of a major hydroclimatological study by Post et al. (2012) that reviewed

future availability of surface water in Tasmania to 2030. Post et al. (2012) used pattern scaling (Mitchell, 2003) of global climate models (GCMs) and a series of hydrological models to better replicate spatial variation in Tasmanian runoff. Post et al.'s (2012) median future scenario projected decreased mean annual runoff in Tasmania's central highlands and north-eastern highlands of up to 30% by 2030, with little change elsewhere. No region was projected to experience increased runoff under the median scenario by 2030. The other notable study of climate change impacts on Tasmania's water resources was carried out by McIntosh et al (2005), who used an earlier version of CCAM to dynamically downscale the CSIRO-Mk3 GCM to 2040. McIntosh et al (2005) also projected a decrease in rainfall in eastern Tasmania.

1.4 Thesis aims and scope

The thesis had its genesis in the Climate Futures for Tasmania project (http://www.acecrc.org.au/Research/Climate%20Futures). There are plans to develop substantial new irrigation infrastructure in Tasmania (see http://www.tasmanianirrigation.com.au/) in light of declining agricultural yields in the Murray Darling Basin and south-west Western Australia. In addition, Tasmania relies heavily on hydro-electricity to meet its power needs. Both irrigation and hydro-electric infrastructure are operated on very long (40+-year) timescales. Climate Futures for Tasmania sought to produce longer-term high-resolution projections of surface water availability to inform water management planning in Tasmania for the 21st century.

This thesis draws on the multi-climate model and hydrological modelling approach of Post et al. (2012) and the fine resolution regional climate modelling of McIntosh et al (2005) to extend high-resolution projections of Tasmanian surface water to 2100.

The aims of this Masters project are to:

1) Devise a robust method to project surface water yields in Tasmania to 2100 with the most advanced climate projections and hydrological models available.
2) Generate projections of Tasmanian runoff and river flow to 2100.
3) Describe and analyse changes to surface water yields in Tasmania to 2100.

Only changes caused by anthropogenic climate change are considered. Possible future changes to land and water use could have substantial impacts on Tasmanian catchments, but these are not considered in this study.

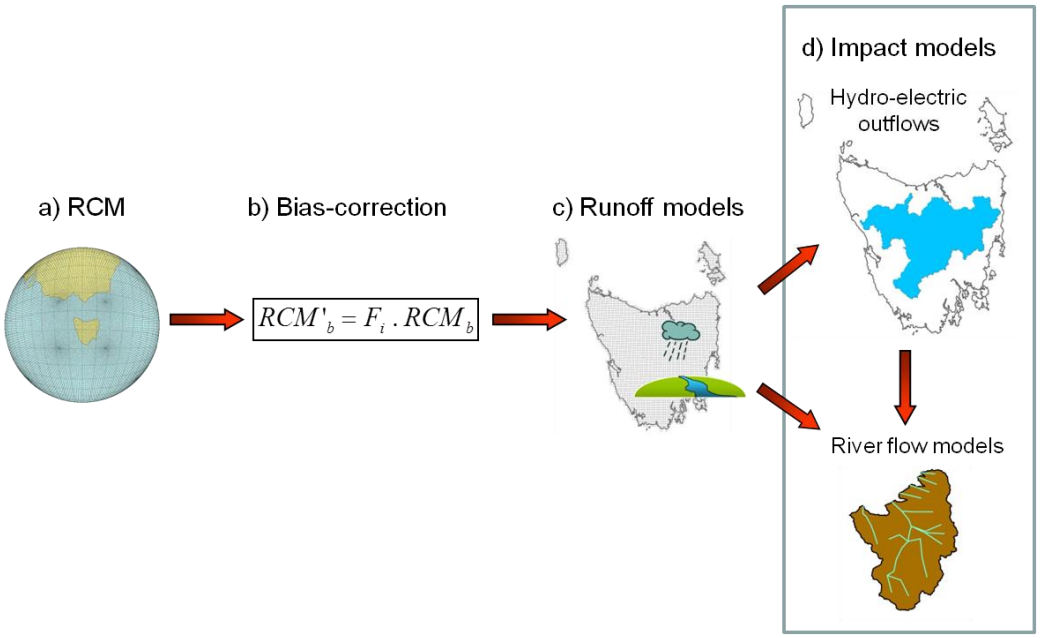

Fig 1.4 Schematic of hydro-climatological modelling used in this thesis. See text for description.

1.5 Thesis overview

This thesis describes the methods and results of an assessment of the availability of surface water in Tasmania, Australia, for the 21st century, performed using state-of-the-art climate and hydrological models. A schematic of the modelling method is given in Fig 1.4. RCM simulations of rainfall and potential evapotranspiration for 1961-2100 (Fig 1.4a) are bias-corrected (Fig 1.4b) and used to force rainfall-runoff models (Fig 1.4c) to quantify surface water availability. Impact models that simulate outflows from hydro-electric power stations, dam operations and water extractions (Fig 1.4d) are then used to simulate inflows to important water storages and flows in Tasmanian rivers.

Thesis chapters are ordered accordingly:

- Chapter 1 (present chapter) reviews the observed and potential effects of anthropogenic climate change on the hydrological cycle, and reviews methods used to assess possible future changes to surface water. The study area is introduced. The aims and scope of the thesis are described.
- Chapter 2 describes the regional climate simulations, (including edited excerpts from Corney et al., 2013), and discusses the extent to which the RCM simulations used in this study add value to GCM simulations.
- Chapter 3 describes the bias-correction and the performance of the bias-correction method (an edited reproduction of Bennett et al., 2013).

- Chapter 4 describes the runoff simulations (an edited reproduction of Bennett et al., 2012).
- Chapter 5 describes the effects of runoff changes on inflows to hydropower storages, irrigation storages and river flows in Tasmania (edited excerpts from Bennett et al., 2010).
- Chapter 6 summarises the thesis and suggests possible future work.

2 Regional climate model simulations from the Conformal Cubic Atmospheric Model

This chapter gives a description of the high-resolution climate simulations used in this study. The simulations were generated by Corney et al. (2010) – that is, with only minor contribution from the primary author of this thesis (though all analyses included in this chapter were conceived and carried out by the author of this thesis). However, the simulations underpin the hydrological projections described later, and are therefore described in some detail. Fig 2.1 and Fig 2.2 are included in a paper accepted for publication by the *Journal of Geophysical Research* as:

Corney SP, Grose MR, Bennett JC, Katzfey JJ, McGregor JL, Holz GK, White CJ, Bindoff NL. 2013. Performance of downscaled regional climate simulations using a variable-resolution climate model - Tasmania as a test case. *Journal of Geophysical Research (Atmospheres)***:** accepted for publication July 2013.

2.1 RCM simulations

We use regional climate simulations of 1961-2100 produced with the CSIRO Conformal Cubic Atmospheric Model (CCAM) (Corney et al., 2013; Corney et al., 2010). CCAM is a variable-resolution global atmospheric model (McGregor and Dix, 2008); that is, CCAM simulates global atmosphere and the horizontal resolution of this simulation varies by location. The highest resolution grid cells are positioned over the study area, as detailed below. Variable-resolution global atmospheric models have been shown to simulate rainfall and related processes realistically at a range of scales and locations (Berbery and Fox-Rabinovitz, 2003; Boé and Terray, 2007; Zou et al., 2010). Although a global model, CCAM is designed to increase resolution over small regions, and we refer to the CCAM simulations in this study as RCM simulations. CCAM has no lateral boundaries and accordingly does not suffer from the problems associated with lateral boundaries in limited area RCMs (Fox-Rabinovitz et al., 2008). CCAM has been used for regional climate studies in Australia (Charles et al., 2007; Chiew et al., 2010; Post et al., 2012) and internationally (Engelbrecht et al., 2009; Lal et al., 2008).

CCAM was forced with sea surface temperature (SST) and sea ice from six CMIP3 GCMs, the most recent GCM simulations available (Meehl et al., 2007) (Table 2.1). CCAM simulations were produced for the B1 and A2 emissions scenarios (Nakićenović and Swart, 2000), however we use only the A2 high emissions scenario to produce hydrological projections in this study. Radiative forcings for the CCAM simulations, including atmospheric concentrations of greenhouse gases, were taken from the future emissions scenarios to correspond to the GCM forcings. For convenience, each RCM simulation will be referred to by the GCM used to force it.

Each GCM was downscaled in two stages: stage two is nested inside stage one. The two stages were necessary to allow CCAM to resolve synoptic processes everywhere on earth for the 10 km² regional simulations (Thatcher and McGregor, 2011). Stage one uses only the bias-corrected SSTs and sea ice from GCMs, together with radiative forcings, to produce atmospheric simulations with a horizontal resolution of ~50 km² (0.5°) over Australia. Stage two used the same GCM SSTs and sea ice forcings (and radiative forcings) as stage one, and is also forced by spectral nudging (Thatcher and McGregor, 2009) of atmospheric variables from the stage one simulations. Stage two produces an approximate horizontal resolution of ~10 km² (0.1^o) over Tasmania. Because stage two is nested inside stage one, CCAM is forced only by SSTs and sea ice from GCMs to produce high resolution simulations over Tasmania.

2.1.1 SST bias-correction

Correcting GCM SST biases improved the simulation of seasonal precipitation patterns (Ashfaq et al., 2010) and precipitable water (Held and Soden, 2006) in GCM experiments, and improved rainfall simulations by CCAM in experiments over tropical regions (Nguyen et al., 2011). GCM SST biases exceed ±8°C in some regions for the GCMs used in our study (Fig 2.1a, and see Randall et al., 2007), with the largest biases occurring at high latitudes and near the west coasts of South America and Africa.

For the RCM simulations in this study, mean monthly biases in the GCM SSTs were corrected before downscaling. The correction was a simple mean bias-correction (Katzfey et al., 2009) to the Reynolds (1988) SST dataset. To correct mean monthly biases, we calculate SST biases for each GCM and for each calendar month by subtracting mean GCM SST from mean observed SST:

$$Bias_{SST} = \overline{SST}_{OBS} - \overline{SST}_{GCM} \tag{2.1}$$

We then add the bias to the GCM SST, and use bias-corrected SST fields to force CCAM.

The bias-correction removes SST biases very effectively under split-sample cross-validation tests applied to the GFDL-CM2.0 GCM (the remaining GCMs give very similar results). To carry out split-sample cross-validation we train the bias-correction using odd years from the period 1951-1999 and then evaluate the bias-corrected SSTs against even years from the same period. In almost all regions cross-validated biases are less than ±0.5°C (Fig 2.1). No cross-validated SST biases are greater than ±1°C for any of the six GCMs. While the bias-correction of SST is another potential source of uncertainty in the RCM simulations, the cross-validation results indicate that uncertainties introduced by SST bias-correction are likely to be small. We note, however, that cross-validation with historical data does not necessarily show stable performance for simulations of future climate, nor do small variations in RCM forcings necessarily lead to small variations in RCM outputs.

Table 2.1 List of global climate models downscaled in this study

Institute[a] (country)	GCM	Horizontal resolution (no. of land cells covering Tasmania)	Confidence in ENSO simulation (van Oldenborgh et al., 2005)	SST persistence skill rank (of 23 GCMs) (skill score) (Johnson et al., 2011)
CSIRO (Australia)	CSIRO-Mk3.5 (Run 1, Run 2, Run 3)	1.9° (3-cell peninsula)	Not Assessed	7 (0.33)
MPI (Germany)	ECHAM5/MPI-OM	1.9° (1-cell island)	High	4 (0.35)
GFDL/NOAA (USA)	GFDL-CM2.0	2.5° (5-cell peninsula)	High	6 (0.34)
GFDL/NOAA (USA)	GFDL-CM2.1	2.5° (5-cell peninsula)	High	2 (0.38)
CCSR/NIES/ FRCGC (Japan)	MIROC3.2(medres)	2.8° (0 land cells)	Medium	15 (0.24)
UKMO (UK)	UKMO-HadCM3	3.75° (0 land cells)	High	8 (0.32)

[a]Abbreviations are described at http://www-pcmdi.llnl.gov/ipcc/about_ipcc.php

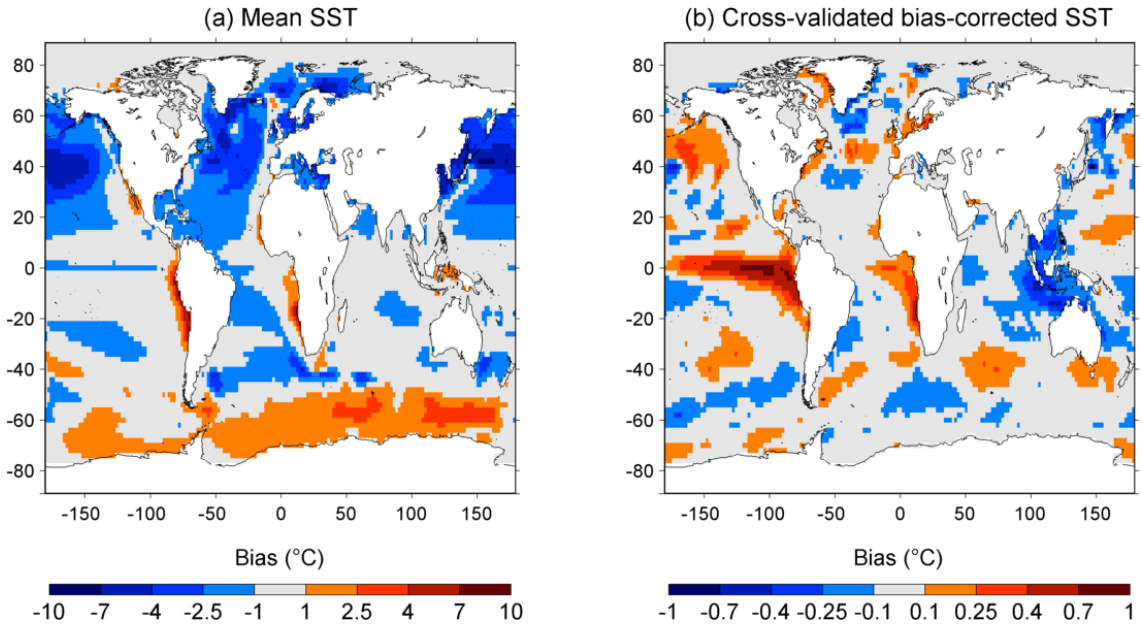

Fig 2.1 Uncorrected and bias-corrected SST biases for GFDL-CM2.0: (a) Mean annual bias in for the period 1961-1999 and (b) cross-validated mean annual SST biases calculated for the even years between 1950-1999 (1950,1952,...,1998) when trained using the odd years between 1950-1999 (1951, 1953, ..., 1999). Note the difference in colourscales between (a) and (b).

2.2 Adding value to GCM downscaling

Several recent studies have discussed the extent to which the computational (and often financial) expense of RCM experiments adds value to GCM projections (e.g. Di Luca et al., 2013; Feser et al., 2011) , including an excoriating critique of RCM downscaling by Pielke and Wilby (2012). RCMs have been shown to add value in coastal (Di Luca et al., 2013; Feser et al., 2011) and mountainous (or topographically varied) regions (Feser et al., 2011, and references therein). Our study addresses the Australian state of Tasmania, a mountainous island with a strong maritime influence on its temperate climate and high spatial variation in rainfall. Accordingly, an RCM is highly likely to add value to GCM projections over Tasmania. In addition, Tasmania lies on the boundary between a region where GCMs project precipitation will increase (to the south) and a region where GCMs project precipitation will decrease (to the north) (Christensen et al., 2007). An RCM allows us to refine the location of this boundary (Grose et al., 2013b).

Pielke and Wilby (2012) make five criticisms of RCM studies: 1) forcing GCMs do not include all first order climate forcings and feedbacks; 2) forcing GCMs do not simulate major climate features well, for example the El Niño southern oscillation (ENSO); 3) RCMs are heavily dependent on boundary conditions, and hence they inherit errors from GCMs; 4) small RCM domains mean RCMs do not

improve GCM predictions of the larger-scale atmospheric features; 5) The resolution of lateral boundary conditions between GCMs and RCMs is mismatched, so errors caused by coarse resolution are passed from the GCM to the RCM. We address these criticisms as follows:

1. The first criticism applies to GCMs and we do not discuss it here, except to say that while GCMs are imperfect, they remain the best attempt to describe future climate scenarios.
2. Some GCMs simulate major climate features better than others. van Oldenborgh et al. (2005) showed that five of the GCMs selected for our study - ECHAM5/MPI-OM, GFDL-CM2.0, GFDL-CM2.1, MIROC3.2(medres) and UKMO-HadCM3 - were the best-performed of all CMIP3 GCMs in simulating ENSO (the sixth GCM, CSIRO-Mk3.5, was not available at the time of the van Oldenborgh et al. (2005) study) (Table 2.1). In addition, several of the six GCMs have been shown to simulate SST persistence characteristics in comparison to other GCMs by a more recent study (Johnson et al., 2011; not available at the conception of our study): five of the six GCMs were ranked in the top eight GCMs for SST persistence (Table 2.1). We note, however, that MIROC3.2(medres) did not simulate SST persistence well in relation to other GCMs.
3. CCAM is configured to be forced at only one, horizontal, boundary (i.e., the ocean) (Corney et al., 2013). This allows biases in GCM sea surface temperatures (SST) to be corrected before downscaling (Corney et al., 2013; Nguyen et al., 2011). In short, coarse biases in GCMs SST are not inherited by CCAM in these simulations.
4. CCAM's domain is global, allowing more realistic simulation of larger-scale atmospheric features such as cut-off lows (Grose et al., 2013a) and mean circulation over Tasmania (Grose et al., 2013b) in comparison to GCMs.
5. CCAM has no lateral boundaries. The bias-corrected GCM SST used to force CCAM's lower horizontal boundary are regridded to match CCAM's conformal cubic grid. Because SST vary less in space and time than atmospheric variables, differences in the GCM and CCAM SST grids are unlikely to have deleterious effects of the kind described for lateral boundaries by Pielke and Wilby (2012). Indeed, Pielke and Wilby (2012) make no mention of horizontal boundaries in their critique.

Demonstrating added value is difficult, in part because global climate models are designed to simulate global- and continental-scale climates, and cannot hope to replicate sub-grid scale features, while it is not possible to assess regional models over the very large domains covered by GCMs. We have used Taylor (2001) diagrams to assess the capacity of the simulations to simulate the spatial distributions present in observations independent of spatial resolution. Simulated rainfall in the historical climate (1961-1990) has been compared to gridded AWAP observations (Jones et al., 2009) (Fig 2.2) for the host GCMs as well as the two downscaled resolutions (0.5° and 0.1°). We tested each set of simulations at its native resolution over a domain that suited its purpose. Using different domains to compare model performance has the obvious detraction that we are not comparing performance in similar climates. However this analysis shows how well models at each resolution perform the task for which they are designed, and

indicates the level of value the downscaling adds to GCM simulations. Only land cells are assessed. GCMs are regridded to match the highest-resolution GCM (CSIRO-Mk3.5, an approximate horizontal resolution of 2°). For GCMs, we have assessed only regions where all six GCMs have land cells (Fig 2.2, left hand column). We use a continent-scale domain to assess GCMs (Fig 2.2), following other studies (e.g. Smith and Chandler, 2010). The 0.5° simulations are assessed over southeast Australia, while the 0.1° simulations are assessed over Tasmania (Fig 2.2). AWAP rainfalls are regridded on to the 2° and 0.5° grids in order to match the resolution of the simulations.

Spatial correlations improve from 0.6-0.8 in the GCM simulations to ~0.9 in the 0.5° and 0.1° downscaled simulations, and spatial variance more closely matches AWAP observations in the downscaled simulations (Fig 2.2, right hand column). These represent marked increases in skill over raw GCM simulations, as observed mean annual rainfalls show considerably greater spatial variation and span markedly larger ranges of values in the 0.5° and 0.1° modeling output. The root mean square differences (RMSD) decrease from the GCM to 0.5° simulations, but then increase again in the 0.1° complexity of the spatial pattern of Tasmanian rainfall (and the higher overall rainfall) in relation to rainfall of south-eastern Australia. The spatial standard deviation in the 0.1° simulations is much closer to the variability of AWAP than is the case for the 0.5° or GCM simulations. Overall, the fact that the spatial biases are similar or even improved as we downscale from GCMs to finer resolution indicates that the CCAM simulations are performing with comparable, or improved, fidelity for their target resolution compared to the host GCM.

There is a notable reduction in model spread in both spatial correlation and standard deviation in CCAM compared to the GCM simulations. For example, considerable differences in spatial deviation exist between the GCMs, yet the 0.5° simulations forced by those GCMs are largely indistinguishable from each other (Fig 2.2). The reduction of spread in the ensemble is caused by a combination of the bias-correction of SSTs before downscaling and the use of a single downscaling model. CCAM generates its own atmosphere, and therefore applies a consistent set of parameters and physical equations to GCM SSTs, thereby reducing the variation between simulations. Other downscaling methods may show a different spread of RMSD and correlation coefficients given the same GCM inputs. This SST bias-correction is a likely cause for the clustering of simulations, especially in regard to RMSD, however the magnitude of this clustering cannot be quantified without more controlled tests.

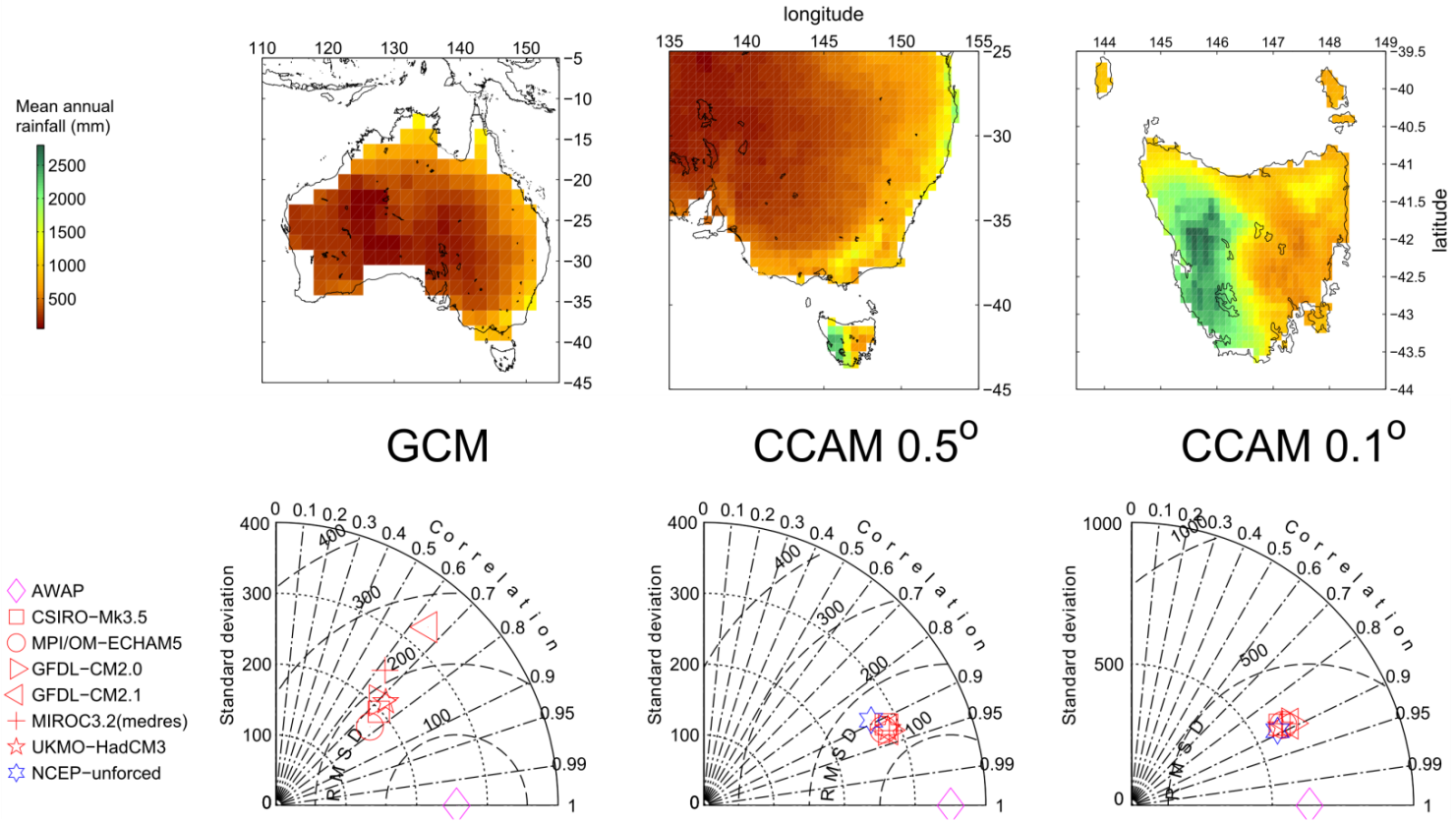

Fig 2.2 Performance of rainfall simulations at different resolutions and over different domains. Top row shows mean annual rainfall for 1961-1990 from the AWAP dataset for grid cells and domains used to assess the GCM simulations (~2.0°) (left), the 0.5° RCM simulations (centre) and the 0.1° RCM simulations (right). Bottom row shows Taylor (2001) diagrams comparing spatial characteristics of simulated rainfalls with corresponding AWAP rainfalls shown in top row. Magenta diamonds show AWAP rainfalls. Blue hexagrams show control RCM simulations forced by NCEP reanalysis.

3 Performance of an empirical bias-correction of a high-resolution climate dataset

This is an edited version of a paper that has been accepted for publication by the *International Journal of Climatology* as:

Bennett JC, Grose MR, Corney SP, White CJ, Holz GK, Katzfey JJ, Post DA, Bindoff NL. 2013. Performance of an empirical bias-correction of a high-resolution climate dataset. *International Journal of Climatology,* **published online**. DOI: 10.1002/joc.3830.

Some of the introductory material has been moved to Chapter 1, while description of the regional climate simulations (already detailed in Chapter 2) has been abridged.

3.1 Abstract

We describe the method and performance of a bias-correction applied to high-resolution (~10 km) simulations from a stretched-grid regional climate model (RCM) over Tasmania, Australia. The bias-correction is a quantile mapping of empirical cumulative frequency distributions. Corrections are applied at a daily time step to five variables: rainfall, potential evaporation, solar radiation, maximum temperature and minimum temperature. Corrections are calculated independently for each season.

We show that quantile mapping of empirical distributions can be highly effective in correcting biases in RCM outputs. Cross-validation shows biases are effectively reduced across the range of cumulative frequency distributions, with few exceptions. The bias-correction is not as effective at correcting biases for values at or near zero (e.g. in rainfall simulations), although even here the bias-correction improves biases evident in the uncorrected simulations. In addition, the bias-correction improves frequency characteristics of variables such as the number of rain days.

We use a detrending technique to apply the bias-correction to 140-year time series of RCM variables. We show that the bias-correction effectively preserves long-term changes (e.g. to the mean and variance) to variables projected by the uncorrected RCM simulations. Correlations between key variables are also largely preserved, thus the bias-corrected outputs reflect the dynamics of the underlying RCM. However, the bias-corrected simulations still exhibit some of the deficiencies of the RCM simulations, for example the tendency to underestimate the magnitude and duration of large, multi-day rain events, and the tendency to underestimate the duration of dry spells.

The bias-corrected simulations for six downscaled GCMs for the A2 and B1 emissions scenarios are available to researchers from http://www.tpac.org.au.

3.2 Introduction

Policymakers are increasingly expected to plan for future climate change caused by anthropogenic global warming, but are often missing vital detailed information about how climate could change in their local areas (Kerr, 2011). Global climate models (GCMs) are usually too coarsely resolved to provide more than generic projections for local catchments, bioregions or agricultural production areas. The problem is particularly acute when using impact models and indices, including hydrological, ecosystem and agricultural models, which require local, unbiased inputs that are on the same temporal and spatial scales as observations. In response, GCM projections may be downscaled with dynamical regional climate models (RCMs) to generate climate change scenarios at a resolution that better reflect intra-regional differences due to factors such as topography and therefore better suit end user requirements.

Despite the increase in resolution, RCM simulations often remain too biased to be used directly in impact models such as rainfall-runoff models. For example, uncorrected climate model outputs have been shown to cause very large biases in hydrological models (Wood et al., 2004) and biophysical crop models (Ines and Hansen, 2006). Biophysical or hydrological models are calibrated with observations, so if climate variables from RCM projections are to be used in these models, they must be on the same scale as observations. This challenge can be overcome by either perturbing historical datasets with projected anomalies (e.g. Post et al., 2012) or using some form of bias-correction (e.g. Dosio and Paruolo, 2011).

Our study presents a bias-correction approach that produces corrected RCM simulations that are suitable for direct use in impact models. We correct simulations from a variable-resolution (or stretched-grid) RCM, the Conformal Cubic Atmospheric Model (CCAM) over Tasmania, Australia. CCAM is configured to be forced at only one horizontal boundary (i.e., the ocean - see Corney et al., 2013). Forcing CCAM only with SST allows biases in GCM sea surface temperatures (SST) to be corrected before downscaling (Corney et al., 2013; Nguyen et al., 2011). In short, coarse biases in GCMs SST are not inherited by CCAM in these simulations. As a consequence of the SST bias-correction and the high resolution of the CCAM simulations, CCAM simulates historical Tasmanian climate with a high degree of realism, including seasonal and spatial distributions of rainfall (Corney et al., 2013). However, CCAM is still too coarsely resolved to accurately represent key climate variables in some Tasmanian regions, preventing direct application in impact models.

The bias-correction we present uses a quantile mapping (or histogram equalisation) method, which is applied to individual variables generated by CCAM. Quantile mapping has been shown to be effective at correcting climate model biases across a range of values and variables (e.g. Li et al., 2010). Quantile mapping corrections have been shown to be generally stationary when applied to RCMs (Lafon et al., 2013; Maraun, 2012), provided that biases do not change too greatly in future. This indicates that quantile mapping can be suitable for simulations of future climate. Further, Chen et al. (2011) have shown that

uncertainties generated by quantile mapping are small in relation to uncertainties from GCMs or emissions scenarios for the purpose of impact modelling.

Our quantile mapping bias-correction method is distinguished from previous methods by three elements: 1) we use empirical frequency distributions to calculate our quantiles; 2) we detrend RCM simulations (and some observed variables) before calculating corrections; 3) we calculate and apply our corrections independently for each season. Aligning empirical frequency distributions of observations and CCAM outputs avoids the need to parameterise idealised frequency distributions and the uncertainty associated with these parameters. Detrending variables before bias-correction conserves trends from the original RCM variables in the bias-corrected variables, and this allows us to apply our empirical bias-correction to long RCM time series. Applying the corrections seasonally rather than annually maintains distinct climate change responses for the four seasons. However, applying the correction seasonally and using empirical distributions fits the correction very closely to observations. This increases the likelihood that the correction will be over-fitted to the historical period, and therefore may not be as robust when applied to future periods. We demonstrate that our corrections are not overfitted by using robust cross-validation.

Most bias-correction approaches rely on two assumptions: 1) the statistical relationships used to generate the bias-correction will not change substantially in the future, and 2) corrections are unlikely to substantially disrupt the spatio-temporal relationships between and within climate variables that have been carefully circumscribed by the RCM (Ehret et al., 2012). If these assumptions cannot be validated, the bias-correction may obviate the major advantages of RCM downscaling for impact modelling. To address the first assumption, a major aim of this study is to assess how well the bias-correction performs under cross-validation. Cross-validation using different conditions for the training period gives some indication of how well the bias-correction method performs for simulations of future climate (Teutschbein and Seibert, 2012).

We present a technique we call *ensemble cross-validation* to verify the bias-corrected CCAM outputs against observations. This technique cross-validates the bias-correction using three different and independent realisations from one of the GCMs. Ensemble cross-validation enables us to make use of all available observations for training, rather than so called 'split-sample' cross-validation methods (as used, e.g., by Lafon et al., 2013), which require a portion of observations to be reserved for validation.

One of the major benefits of using RCM outputs in impact assessments is that variables are in dynamical balance (Fowler et al., 2007). Dynamical RCM outputs cohere temporally and spatially across multiple variables, and rely less on the assumption that historical relationships between large- and local-scale climate variables will remain fixed in a warmer future world (Fowler et al., 2007; Maraun et al., 2010). To address the assumption that dynamical relationships between variables are not disrupted, we describe the extent to which important correlations are retained between bias-corrected variables.

As with many previous studies, we train and apply our bias-correction to daily data. As a consequence, errors in measures that rely on autocorrelation – for example, the length of no-rain periods – are not explicitly corrected. There is some evidence that correcting daily data can improve errors in autocorrelated metrics such as drought indices (Piani et al., 2010a), however errors in autocorrelated metrics are not routinely reported. For this study, we investigate the effects of the bias-correction on both consecutive rain days and multi-day rainstorms to assess whether these can be improved by correcting daily data.

The paper is structured as follows: Section 3.3 describes CCAM, the observational data; Section 3.4 presents the bias-corrected method and the verification and results are discussed in sections 3.5 and 3.6. Finally, a summary of the results and concluding remarks are presented in section 3.7.

3.3 Methods

3.3.1 Model and observation data

Regional climate simulations used in this study are generated with CCAM, a variable-resolution global atmospheric model (McGregor and Dix, 2008). CCAM is forced by six GCMs (Chapter 2, Table 2.1) run under two emissions scenarios, A2 (high emissions) and B1 (low emissions) (Nakićenović and Swart, 2000). We focus on the A2 emissions scenario when analysing future changes. For the CSIRO-Mk3.5 GCM, the downscaled simulations of the three independent realisations are used. These realisations are the perturbed-initial-conditions ensemble from CMIP3. Each of the CSIRO-Mk3.5 runs are initialised with different initial conditions in 1871 and evolved for 90 years. We refer to the three CSIRO-Mk3.5 realisations as Run 1, Run 2 and Run 3, following CMIP3 nomenclature. For convenience, we refer to each downscaled simulation by its host GCM.

Five CCAM variables are selected for bias-correction: daily rainfall, daily potential evaporation (PE), daily surface short-wave downward radiation (henceforth *solar radiation*), daily minimum temperature (Tmin) and daily maximum temperature (Tmax). These are the key variables used in many hydrological and biophysical models.

3.3.2 Observation data

CCAM outputs are bias-corrected to observations from the Australian Water Availability Project (AWAP) (Jones et al., 2009). We regrid AWAP data from a ~5 km grid to a ~10 km grid to align with the CCAM outputs. Rainfall, Tmin and Tmax are corrected to AWAP data over the training period 1961-2007. AWAP uses satellite PE and solar radiation data to interpolate gridded observations from 1990 onward. Satellite measurements give a more realistic variance in AWAP PE and solar radiation than station data alone, and accordingly we correct PE and solar radiation to observations for the period 1990-2007.

3.4 Bias-correction

The variables that are bounded by zero values - rainfall, PE, solar radiation - are corrected by multiplying correction factors ('multiplicative quantile mapping'). The two temperature variables, Tmin and Tmax, are corrected by adding corrections ('additive quantile mapping').

3.4.1 Rainfall, evaporation and solar radiation: multiplicative quantile mapping

Corrections are calculated independently for the seasons December-January-February (DJF), March-April-May (MAM), June-July-August (JJA), and September-October-November (SON). We begin by concatenating all data points from one season, *S*, to form continuous seasonal time series for simulations and observations, $X_{RCM,S}$ and $X_{O,S}$, respectively, where *X* is one of rainfall, PE or solar radiation. We calculate correction factors at each grid cell by

$$F_i = \begin{cases} \dfrac{P_i(X_{O,S})}{P_i(X_{RCM,S})} : P_i(X_{RCM,S}) > 0 \\ 1 : P_i(X_{RCM,S}) = 0 \end{cases} \text{ and } i = \{0.5, 1.5, ..., 99.5\} \quad , \tag{2}$$

where F_i is the correction factor at the i^{th} percentile, and $P_i(X_{O,S})$ and $P_i(X_{RCM,S})$ are the i^{th} percentiles of observations and CCAM simulations, respectively, for each season *S*. Correction factors are calculated for each percentile from 0.5 to 99.5 (0.5^{th}, 1.5^{th}, ..., 99.5^{th}). Corrections were tested at larger intervals (e.g. 5th percentiles, deciles) however these resulted in unsmooth cumulative frequency distributions (not shown). Percentiles are calculated from all data, including zero values. When CCAM outputs are zero, the correction factor is set to 1 ($F_i = 1$). We also trialled corrections calculated weekly, monthly and annually (not shown), with seasonal corrections resulting in the smoothest cumulative frequency distributions.

When correcting rainfall, we force any rain day with rainfall of less than 0.2 mm to zero in both observed and modelled rainfall time series. The threshold of 0.2 mm is chosen because it is the lower resolution limit of the Bureau of Meteorology rain gauges that are the basis of the AWAP dataset.

Quantile mapping assumes that corrections can be conferred from ranked historical simulations to equivalent ranks in future simulations. Before we rank points in the RCM simulations (by consigning them to percentile 'bins'), we detrend each 140-year RCM time series. Detrending simulations ensures that trends are neither damped nor amplified by the bias-correction. We detrend each season by subtracting a 30-year moving average. To do this, we first concatenate all data points from one season to form a continuous simulated time series, $X_{RCM,S,t}$, for a given daily variable for season *S* and time *t=1, 2, ..., T*. We then calculate $Y_{RCM,S}$, the detrended seasonal time series, as

$$Y_{RCM,S,t} = X_{RCM,S,t} - \overline{X_{RCM,S,t}} \quad , \tag{3}$$

where $\overline{X_{RCM,S,t}}$ is the 30-year moving average of $X_{RCM,S}$ centred on time *t*. To calculate $\overline{X_{RCM,S,t}}$ at all values of *t* we pad the the begining of the time series $X_{RCM,S}$ with 15 years of repeated $X_{S,1}$ and we pad the end of *Xs* with 15 years of repeated $X_{RCM,S,T}$, and calculate $\overline{X_{RCM,S,t}}$ from the padded time series.

Each $Y_{RCM,S,t}$ is consigned to a percentile 'bin', *b*, of 0-1, 1-2, …, 99-100 percentiles, and assigned a rank that accords to the bin. For each time, *t*, The rank for $Y_{RCM,S,t}$ is transferred to each member of the original (undetrended) series, $X_{RCM,S,t}$. Bias-corrected outputs, $X'_{RCM,S,b}$, are then calculated by

$$X'_{RCM,S,b} = F_i \,.\, X_{RCM,S,b} : i = \{0.5,1.5,...,99.5\} \; and \begin{cases} \{i-0.5 \le b < i+0.5\} : b < 99.5 \\ \{i-0.5 \le b \le i+0.5\} : b = 99.5 \end{cases}, \quad (4)$$

where *b* is the percentile bin. Note that we do not correct detrended data (the detrended series is used only to calculate ranks), which means that we do not need to reapply a trend to the corrected RCM simulations. Eq. 4 applies the correction factor calculated for the 0.5th percentile to the 0-1 percentile bin, the factor for the 1.5th percentile to the 1-2 percentile bin, and so on up to the factor for the 99.5th percentile, which is applied to the 99-100 percentile bin. The correction is not tailored to extreme events, as it applies the same correction to all values that fall in the top percentile. Caution should be exercised if using these outputs for analyses of extremes.

Correction factors are generally close to 1 because of the realistic simulation of the Tasmanian climate by CCAM. The largest correction factors occur when correcting rainfall. Fig 3.1A shows an example of the rainfall correction factors for all grid cells for MAM (other seasons show very similar results). Corrections are less than 1.5 and greater than 0.5 in most grid cells for rainfalls larger than the 60th percentile. Corrections of lower rainfall values at or near zero (30th-60th percentile) are more marked, as rainfall in a number of grid cells is scaled to zero to match observations. Where both the simulated and observed rainfalls are zeros (rainfalls <30th percentile), correction factors are forced to 1.

3.4.2 Temperature: additive quantile mapping

Before Tmin and Tmax corrections are calculated, we detrend each season in the uncorrected simulation and AWAP data for the training period (1961-2007) by subtracting a 30-year moving average, as shown in Eq. 3. This is necessary for Tmin and Tmax to account for the marked trend of observed temperature increases across Tasmania during the training period. If we did not detrend these variables, higher values would be sampled mostly from the latter part of the period, and this could have the effect of correcting out (or exacerbating) trends in the simulations if the AWAP data and the simulations have different rates of temperature increases.

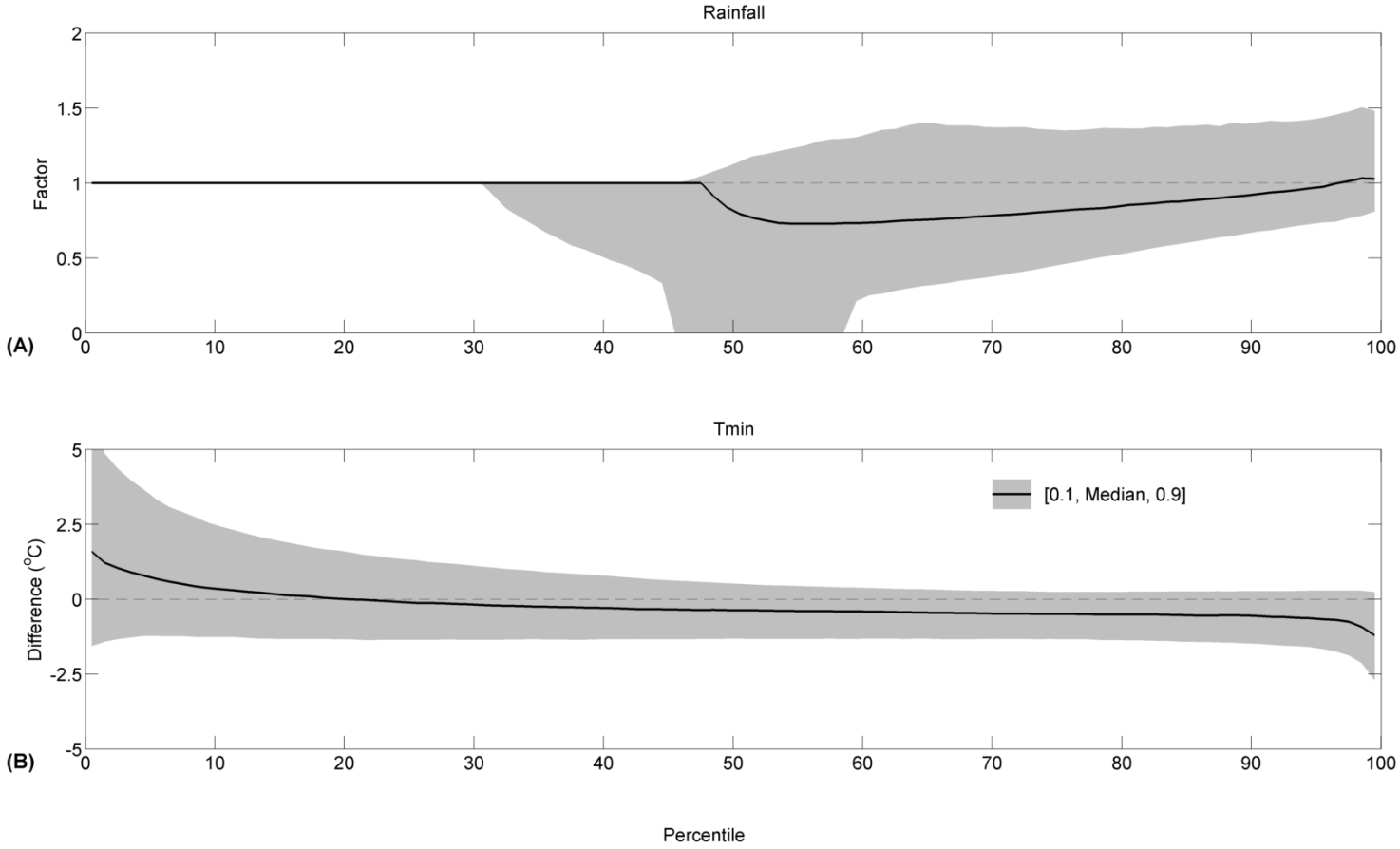

Fig 3.1 Distribution of bias-corrections applied across the cumulative frequency distribution for (A) rainfall and (B) Tmin for MAM. All grid cells from the CSIRO-Mk3.5 Run 1, Run 2 and Run 3 simulations are combined to calculate the median and range of corrections. Solid line shows corrections at the median grid cell. Confidence bounds show [0.1, 0.9] ranges of corrections across all grid cells. Results are similar for all seasons and models (not shown).

After detrending Tmin and Tmax, we calculate corrections at each grid cell,

$$D_i = P_i(X_{O,S}) - P_i(X_{RCM,S}) : i = \{0.5,1.5,...,99.5\}, \quad (5)$$

where X is Tmin or Tmax, D_i is the correction at the i^{th} percentile, and the other terms are as already described. Percentiles are calculated as described for the multiplicative quantile mapping, above.

CCAM outputs are detrended seasonally (Eq. 3) and ranked as for the multiplicative quantile mapping before corrections are applied. Bias-corrected Tmin and Tmax are calculated by

$$X'_{RCM,S,b} = D_i + X_{RCM,S,b} : i = \{0.5,1.5,...,99.5\} \; and \begin{cases} \{i - 0.5 \le b < i + 0.5\} : b < 99.5 \\ \{i - 0.5 \le b \le i + 0.5\} : b = 99.5 \end{cases}, \quad (6)$$

where terms are as described above.

As with the multiplicative corrections, corrections are generally small because CCAM simulates Tasmanian climate realistically. The largest additive corrections occur when correcting Tmin. Fig 3.1B shows Tmin corrections for all grid cells for MAM (other seasons show very similar results). Corrections are within ±2.5°C for most grid cells for all Tmin values larger than the 10th percentile.

3.5 Verification

3.5.1 Definition of bias and mean error

We use the definition of 'bias' suggested by Ehret et al. (2012); "the correspondence between a mean [simulation] and mean observation averaged over a certain domain and time". We use *bias* only to describe errors in average Tmax, Tmin, rainfall, PE and solar radiation. For a given measure of temperature, *T*,

$$B_T = \overline{T_{RCM}} - \overline{T_{Obs}}, \quad (7)$$

where B_T is the bias, $\overline{T_{RCM}}$ is the average of modelled T and $\overline{T_{Obs}}$ is the average of observed T.

For rainfall, solar radiation and PE, we define bias as the proportional differences in mean forecasts and mean observations, normalised by the mean observations. For rainfall, *R*, bias is defined as

$$B_R = \frac{\overline{R_{RCM}} - \overline{R_{Obs}}}{\overline{R_{Obs}}} \times 100\%, \quad (8)$$

where B_R is the bias, $\overline{R_{RCM}}$ is the average of modelled R and $\overline{R_{Obs}}$ is the average of observed R.

When reporting errors in other measures, for example errors in quantiles or errors in the number of rain days, we use the term *mean error*. Mean errors are calculated as for equations 7 and 8, but the term is applied to measures other than mean Tmax, Tmin, rainfall, PE and solar radiation.

3.5.2 Ensemble cross-validation

We verify the performance of the bias-correction with cross-validation. We use the ensemble of three CSIRO-Mk3.5 runs for this purpose, as each run represents a plausible and independent realisation of historical climate. For example, we calibrate the bias-correction for CSIRO-Mk3.5 Run 1 and then apply the correction to CSIRO-Mk3.5 Run 2 and CSIRO-Mk3.5 Run 3. We repeat this process for each combination of CSIRO-M3.5 runs, producing six cross-validated bias-corrected realisations for each variable. The performance of each of these realisations is then assessed against observations. We call this method *ensemble cross-validation.*

Ensemble cross-validation allows us to include all 47 years of observations to train and validate the bias-correction, allowing us to generate stable frequency distributions. We note that even though the ensemble cross-validation is based on runs from the same forcing GCM, the realisations of climate during the bias-correction training period are quite different. These differences are illustrated by the realisations of Tasmania-wide rainfall presented in Fig 3.2, which shows, for example, that CSIRO-Mk3.5 Run 1 is markedly drier than CSIRO-Mk3.5 Run 3 during the training period. The differences in the realisations ensure that the ensemble cross-validation is a rigorous test of the bias-correction, as well as allowing as much data as possible to be included. To further ensure that we do not overrate the performance of the bias-correction, we report the largest biases generated under ensemble cross-validation.

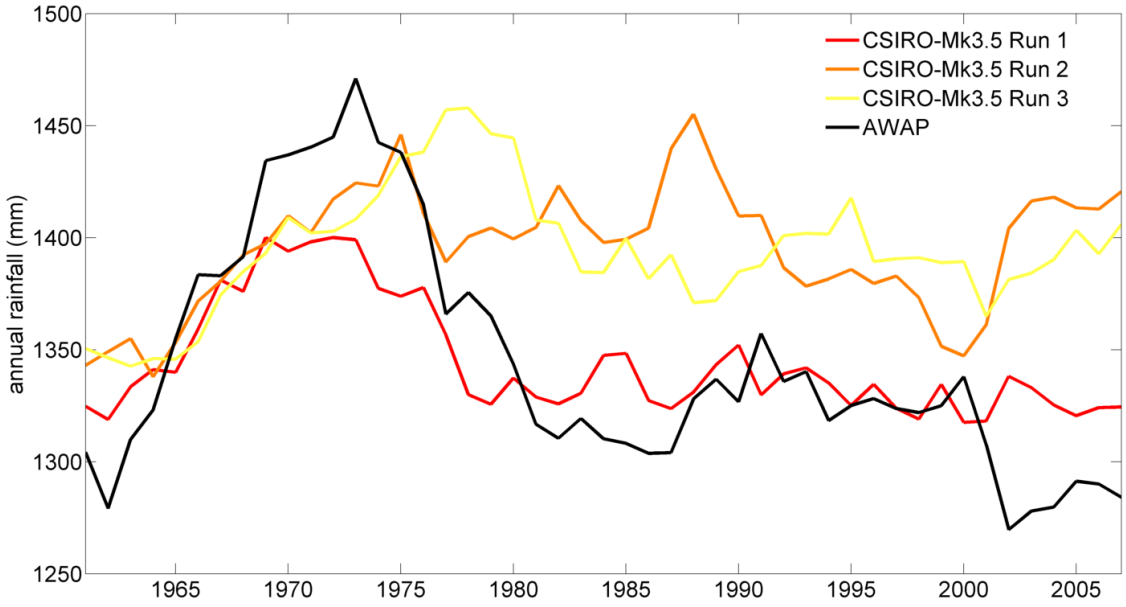

Fig 3.2 Different realisations of Tasmania-wide rainfall given by the downscaled CSIRO-Mk3.5 ensemble members during the bias-correction training/cross-validation period. Observations (AWAP) are given by the black line. Time series have been smoothed with an 11-year moving average.

3.6 Results

3.6.1 Performance in the historical period

The bias-correction successfully reduces biases during the historical period (1961-2007) under ensemble cross-validation.

Fig 3.3 shows minimum biases in the original RCM simulations (Fig 3.3A-E) and maximum cross-validation biases after bias-correction (Fig 3.3F-J). The original RCM simulations of PE and particularly solar radiation have modest biases (within ±5% in most areas – Fig 3.3B-C). The spatial patterns of Tmax and Tmin are also reasonably well represented by the original simulations, though there is a persistent tendency to underestimate Tmax for most of the state by 1°C or more (Fig 3.3D), and a tendency to overestimate Tmin in the warmer eastern parts of Tasmania by >1°C (Fig 3.3E). The most pronounced biases occur for simulations of rainfall, in particular in the central north, a region with steep topographic and rainfall gradients. CCAM tends to underestimate rain falling on the central and north-west mountains by 30% or more, while it tends to greatly overestimate rainfall (>100%) in the low-rainfall Tamar valley region in the central north of Tasmania. Rainfall biases in the uncorrected simulations are high in the north-east largely because the ~10 km grid size does not effectively resolve finer scale orographic rainfall effects (in this case, a rain shadow caused by a steep topographic gradient from the mountainous central plateau [>1000 m elevation] to the lowlands in the east, see Corney et al., 2013).

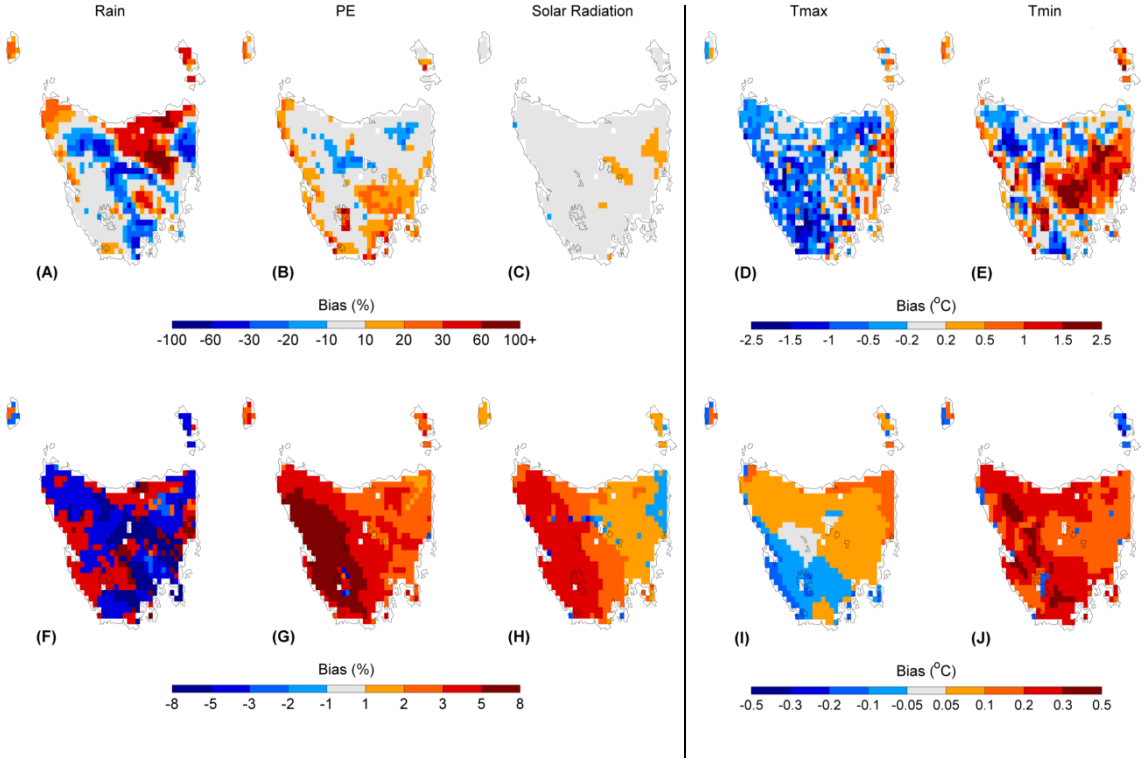

Fig 3.3 Biases in uncorrected and bias-corrected simulations. Top row shows minimum biases in uncorrected simulations from in the CSIRO-Mk3.5 ensemble: average annual (A) rainfall, (B) potential evaporation (PE), (C) solar radiation, (D) Tmax and (E) Tmin. Bottom row shows cross-validated biases after bias-correcting the CSIRO-Mk3.5 ensemble: average annual (F) rainfall, (G) potential evaporation (PE), (H) solar radiation, (I) Tmax and (J) Tmin. Biases in the bias-corrected simulations (F-H) correspond to the largest absolute biases from the six cross-validated bias-corrected CSIRO-Mk3.5 realisations at each grid cell. Where the largest absolute bias corresponds to a negative bias, this is plotted as a negative bias. Note the different colour scales for uncorrected and bias-corrected simulations.

The bias-correction reduces cross-validation biases for annual rainfall, PE and solar radiation to within ±5% in most areas (Fig 3.3F-H). The largest cross-validation Tmin and Tmax biases after bias-correction are within ±0.1°C for most of Tasmania (Fig 3.3I-J). We note that the rainfall biases under ensemble cross-validation (Fig 3.3F) are very similar to those reported by Bennett et al. (2012) for the same RCM simulations, whoused conventional split-sample cross-validation. The largest rainfall biases after bias-correction (up to 8%, Fig 3.3F) are similar to the cross-validated interpolation errors reported for AWAP rainfall data over Tasmania by Jones et al. (2009). Similarly, temperature biases are less than the Australia-wide RMSE for AWAP temperature data (Jones et al. 2009). Biases for PE are largest in western Tasmania (Fig 3.3G), an area of low annual PE (<850 mm.yr^{-1}) and high annual rainfall (>2000 mm.yr^{-1}). In a small number of grid cells with very low PE, the cross-validated bias-corrected PE simulations can be slightly more biased than the uncorrected simulations.

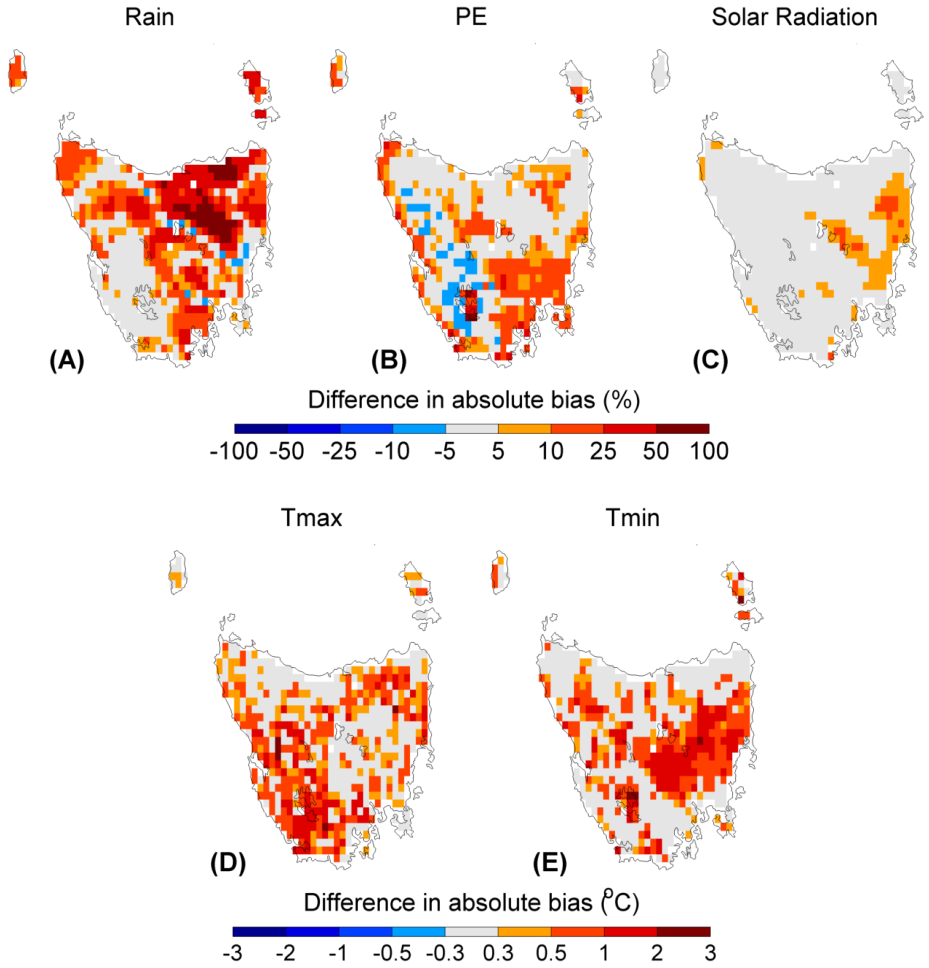

Fig 3.4 Improvement of absolute biases in average annual (A) rainfall, (B) potential evaporation (PE), (C) solar radiation, (D) Tmax and (E) Tmin in the CSIRO-Mk3.5 ensemble. Improvements are calculated by subtracting the largest absolute biases in the six cross-validated bias-corrected CSIRO-Mk3.5 simulations from the smallest absolute biases in the three uncorrected CSIRO-Mk3.5 simulations. Positive values indicate improvements caused by the bias-correction; negative values show reduced performance.

Fig 3.4 shows the improvement in annual biases by comparing the smallest biases in the uncorrected CSIRO-Mk3.5 simulations to the largest biases in the cross-validated bias-corrected CSIRO-Mk3.5 simulations. The bias-correction reduces biases in all grid cells for Tmin, Tmax and solar radiation. Rainfall biases are improved in all but 11 (of 720) grid cells and are corrected by up to 100% in lower rainfall areas in the east, and particularly the north-east (Fig 3.4A), where the underestimation of the steep rainfall gradient is effectively corrected. Solar radiation biases are not improved greatly (Fig 3.4C), as the biases in the uncorrected simulations are already small.

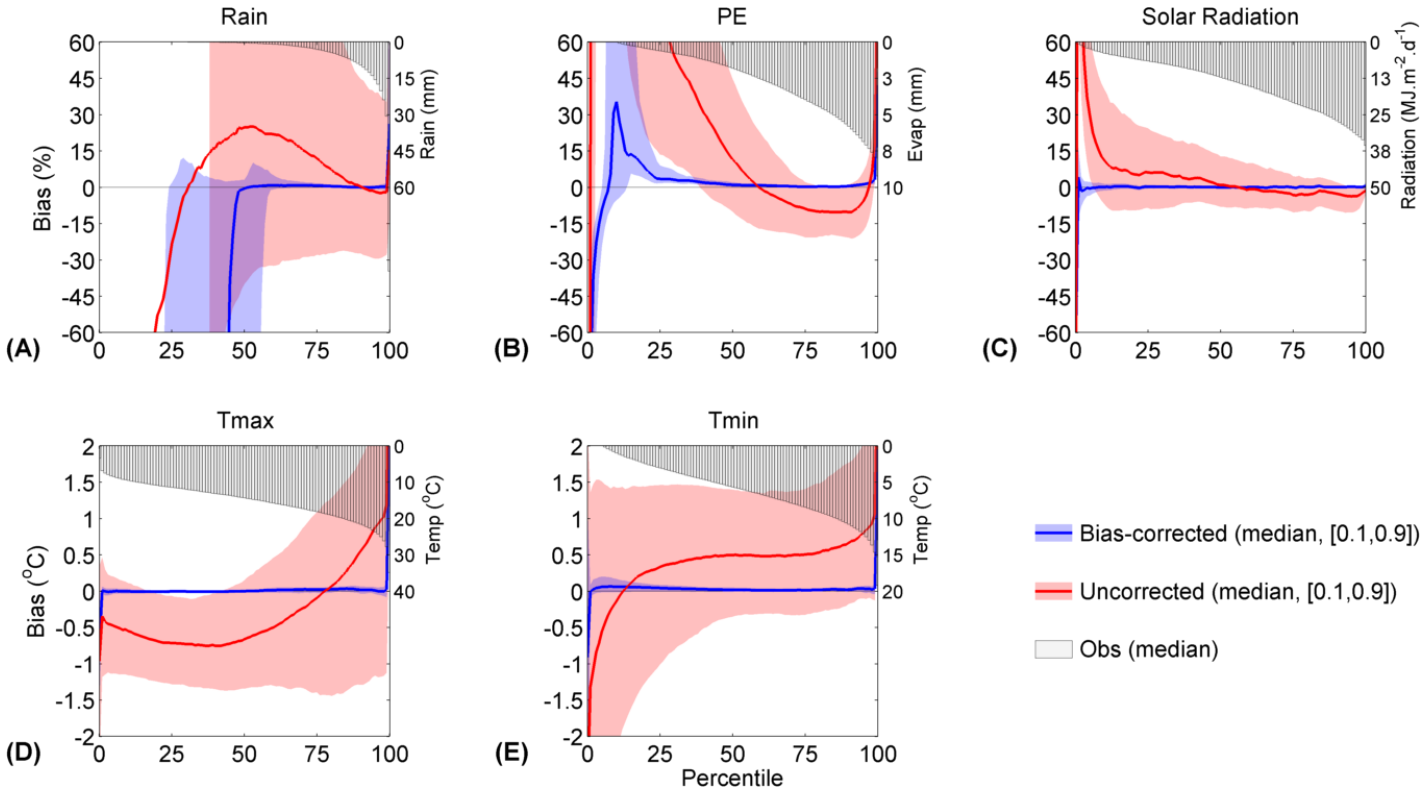

Fig 3.5 Distribution of mean errors of grid-cells across the cumulative frequency distributions of (A) daily rainfall, (B) potential evaporation (PE), (C) solar radiation, (D) Tmax and (E) Tmin in the CSIRO-Mk3.5 ensemble. Horizontal axis gives the cumulative frequency distribution (expressed as percentiles). All grid cells from all corrected and uncorrected CSIRO-Mk3.5 realisations are combined to calculate the median and range of mean errors. Transparent blue and red confidence bounds show [0.1, 0.9] ranges of biases across all grid cells for cross-validated bias-corrected outputs and uncorrected outputs. Solid blue and red lines show mean error for the median grid cell. Narrower bands indicate that grid cells are closer to the median grid cell. Grey bars show values of AWAP observations at the median grid cell for each percentile (right-hand vertical axis).

As expected with quantile mapping, mean errors are removed across the cumulative frequency distributions. Fig 3.5 shows mean errors in the cross-validated bias-corrected simulations for the full cumulative frequency distributions of each variable. Characteristics of mean errors in individual grid cells are summarised by showing the median bias from all grid cells, as well as the [0.1, 0.9] range of mean errors for all grid cells. In general, the bias-correction successfully removes mean errors at different quanta, particularly for solar radiation (Fig 3.5C) and temperature (Fig 3.5D-E), and at higher PE and rainfall values (Fig 3.5A-B). The bias-correction effectively corrects the median grid cells across much of the cumulative frequency distribution. However, the effect of the bias-correction is most apparent in cells with larger errors ([0.1, 0.9] range), shown by the much greater range of mean errors in the uncorrected simulations (the red band) compared with the bias-corrected simulations (blue band).

Performance of the multiplicative bias-correction is poorest at values at or near zero. Mean errors in PE at low values are reduced, but not removed, under cross-validation in low PE regions (e.g. western Tasmania). Here, cross-validation shows that the bias-correction is too closely fitted when PE values are near zero. We note, however, that these larger errors are at least partly explained by the proportional measure of error (%) being very sensitive for PE values very close to zero, even when the difference in values is very small.

Similarly, mean errors in rainfall for values at or near zero are improved, but not removed, by the bias-correction. The largest mean errors are in the 25th to 45th percentile range, which spans the rainfall range from no rain days to light drizzle days. Rain days are not explicitly aligned by the bias-correction, leading to instances where no-rain days are compared to days with low rain, resulting in large proportional mean errors.

The bias-correction partially corrects frequency and autocorrelation characteristics. Of the five variables, rainfall is the most difficult to correct because of its highly skewed cumulative frequency distribution, and we now focus on rainfall as the most rigorous test of the bias-correction method. The bias-corrected simulations have a tendency to slightly overstate (3-5%) the number of observed rain days (Fig 3.6A). This is a marked improvement over the uncorrected simulations in several areas, particularly over north-eastern Tasmania (Fig 3.6B), despite rain days not being explicitly corrected. The improvement in the number of rain days results from the bias-correction taking advantage of the tendency of CCAM to overstate the number of rain days (Corney et al., 2013). The number of rain days can be reduced (but not increased) by the bias-correction, resulting in better agreement with observations.

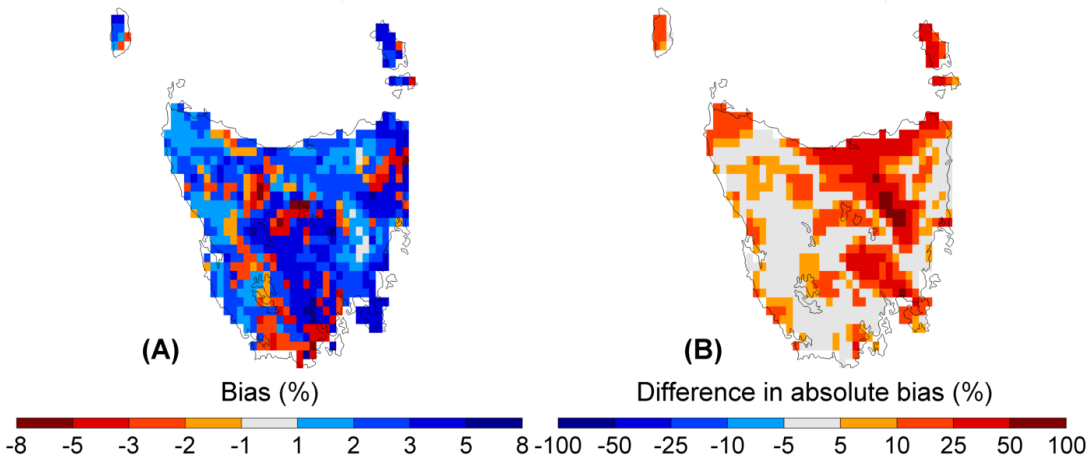

Fig 3.6 (A) Mean errors in the number of days per year where rain >1 mm. Mean errors shown are the largest errors from the six cross-validated bias-corrected CSIRO-Mk3.5 realisations at each grid cell. Where the largest absolute mean error corresponds to a negative mean error, this is plotted as a negative error. (B) Improvement of mean errors in number of days per year where rain >1 mm in the cross-validated CSIRO-Mk3.5 ensemble. Improvements are calculated by subtracting the largest absolute mean errors in the six cross-validated bias-corrected simulations from the smallest absolute mean errors in the three uncorrected CSIRO-Mk3.5 simulations. Positive values indicate improvements caused by the bias-correction; negative values show reduced performance.

However, mean errors in the duration and quanta of multi-day rain events are not improved by the bias-correction. White et al. (2013) showed that the uncorrected CCAM simulations underestimate both the number of consecutive wet days and consecutive dry days across much of Tasmania. Fig 3.7 shows the mean errors for the entire cumulative frequency distribution of rain events, where rain events are defined as consecutive rain days with rain >1 mm.d^{-1}. CCAM has a slight tendency to overestimate smaller rain events and a marked tendency to underestimate the magnitude of larger rain events (Fig 3.7A). The bias-correction improves mean errors of smaller rain events; however it somewhat exacerbates CCAM's tendency to underestimate larger rain events. The range of rain event errors between grid cells is reduced by the bias-correction by bringing all grid cell mean errors closer to the median (Fig 3.7A). The poorest performing grid cells are improved, however the median grid cells in the bias-corrected simulations tend to understate rain event magnitudes slightly more than the median grid cells in the uncorrected simulations. Similarly, the bias-correction actually increases the median error in the duration of large rainfalls (Fig 3.7B). This is because the bias-correction can only reduce the number of rain days, meaning that duration of larger rain events tends to be underestimated more in the bias-corrected simulations than in the uncorrected simulations.

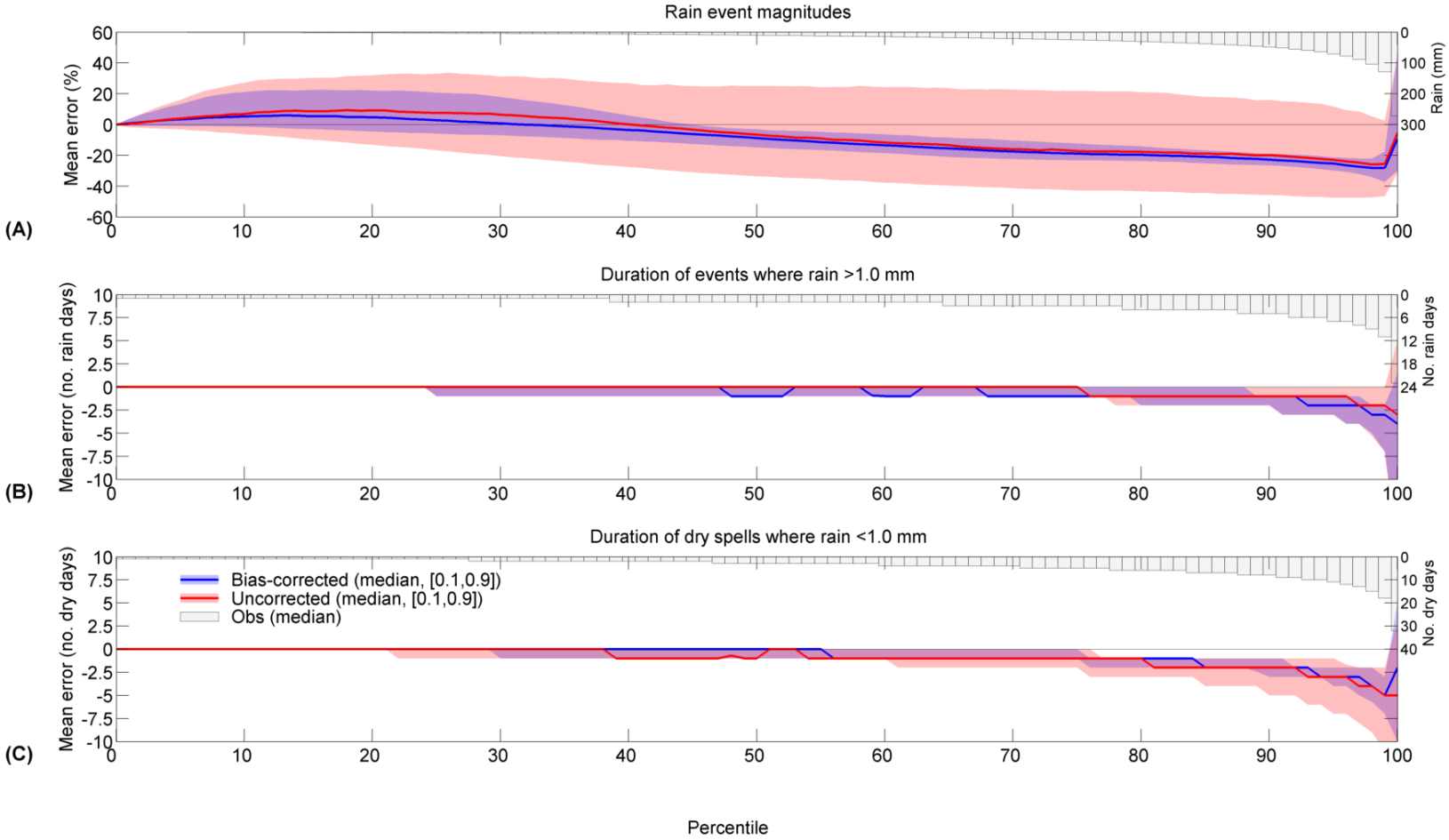

Fig 3.7 Distribution of grid-cell mean errors for the full range of values for (A) rain event magnitudes, (B) duration of rain events in the cross-validated CSIRO-Mk3.5 ensemble, and (C) duration of dry spells in the cross-validated CSIRO-Mk3.5 ensemble. Rain events are defined as consecutive rain days with rainfall >1 mm Rain event magnitudes are the accumulated rain falling in these storms. Dry spells are defined as consecutive days when rainfall <1 mm. All other elements are as described for Fig 3.5

Errors in the duration of rain events become noticeable only at very long rain events (>70th percentile – Fig 3.7B), while rainfall event magnitudes are underestimated for events greater than the median (Fig 3.7A). This indicates that CCAM's tendency to underestimate the magnitudes of multi-day rainfall events is not simply caused by underestimating the duration of these events, but also by not 'lumping' high rainfall days together sufficiently frequently. The tendency of the simulations to underestimate large rain events leads to a slight underestimation of flows by hydrological models (Bennett et al., 2012). This problem is canvassed in the discussion (Section 3.7). CCAM's tendency to underestimate long dry spells is also not changed greatly by the bias-correction (Fig 3.7C). The bias-correction slightly improves CCAM's tendency to underestimate the duration of dry spells. We note that errors in the duration of dry spells after bias-correction are reasonably small in relation to the length of dry spells – for example the median error for longer dry spells (>15 days) is around 3 days. Simulating dry spells accurately can be particularly important for accurately modelling crop yields (Ines et al., 2011). Comparisons between crop yields modelled with the bias-corrected CCAM simulations and with observed climate variables (Holz et al., 2010) demonstrated that the simulations of dry spells in the bias-corrected CCAM simulations are within the tolerance of the crop yield models.

3.6.2 Correlations between variables

A dynamical model has internal consistency and dynamical balance between variables, similar to that in observations (e.g. sunny days are usually warmer than cloudy days). Correlations between pairs of variables from CCAM run with GFDL-2.1 are shown in Fig. 9A; results are similar in all CCAM simulations (not shown). Correlations are strongly positive between solar radiation and PE, Tmax and PE and Tmax and solar radiation, and are similar to those in observations. The correlation is negative between rainfall and solar radiation, and slightly negative in some regions between rainfall and PE and rainfall and Tmax (Fig 3.8A), again similar to observations.

Bias-correcting RCM variables independently can change the dynamical relationships between variables from the RCM. This is a negative side-effect for impact modellers attempting to measure the impacts of changes to multiple variables (say, the effects of changes to temperature, rainfall and solar radiation on agricultural production). Fig 3.8B shows how temporal correlations between variables are altered by the bias-correction for a historical and future period in the GFDL-CM2.1 simulation (again, results are very similar for all simulations; not shown). In general, the bias-correction has a reasonably small effect on temporal correlations in the historical period (within ±0.1 for correlations within the range -1 to 1) (Fig 3.8B). The differences in correlations between corrected and uncorrected simulations are very similar in both the historical and future periods, showing that the effect of the bias-correction on these correlations is reasonably stable throughout the simulation.

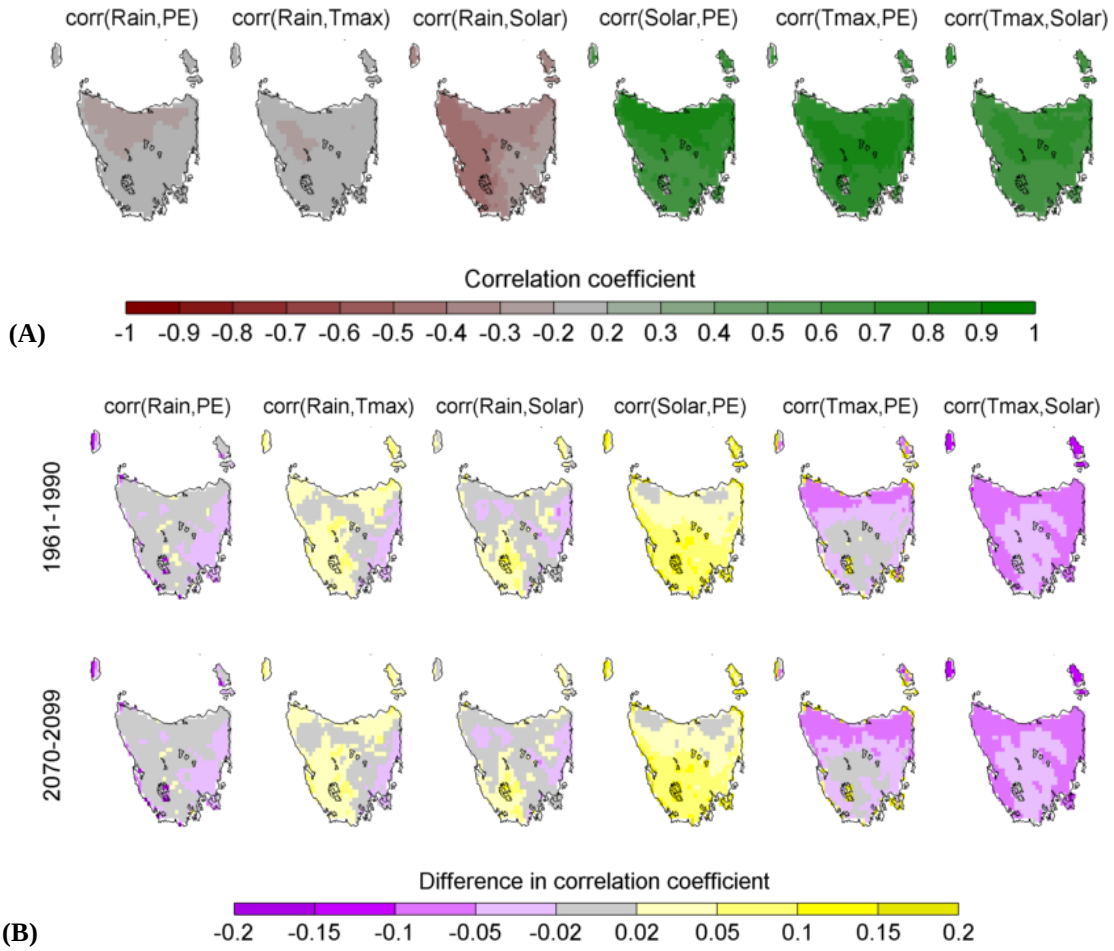

Fig 3.8 Temporal correlations between paired variables calculated for GFDL-CM2.1 (results are very similar for all simulations; not shown). (A) Correlations in raw outputs (pairs as marked), where correlation coefficients can take values from 1 (perfectly correlated) to -1 (perfectly anti-correlated), (B) difference in temporal correlation between raw and corrected outputs (pairs as marked), top row shows differences for 1961-1990; bottom row shows differences for 2070-2099.

3.6.3 Conservation of future trends

Projected changes in mean and variability are usually of most interest to impact modellers. It is therefore important that changes projected by CCAM are preserved as much as possible by the bias-correction. For a given variable simulated by CCAM, X_{RCM}, we show changes as anomalies in the mean and standard deviation (Fig 3.9, Fig 3.10).

Anomalies in mean X_{RCM} are calculated as

$$\Delta(X_{RCM,t}) = \overline{X_{RCM,t}} - \overline{X_{RCM,1961\text{-}1990}}, \quad (9)$$

where $\Delta(X_{RCM,t})$ is the anomaly in the mean at time *t* calculated with respect to 1961-1990, $\overline{X_{RCM,t}}$ is the 11-year moving average of X_{RCM} centred on *t*, and $\overline{X_{RCM,1961\text{–}1990}}$ is the average of X_{RCM} calculated for the period 1961-1990. Similarly, anomalies in standard deviations are calculated as

$$\Delta\sigma(X_{RCM,t}) = \sigma(X_{RCM,t}) - \sigma(X_{RCM,1961\text{–}1990}), \quad (10)$$

where $\Delta\sigma(X_{RCM,t})$ is the anomaly in the standard deviation of X_{RCM} at time *t* calculated with respect to 1961-1990, $\sigma(X_{RCM,t})$ is the standard deviation of X_{RCM} on the 11 years centred on *t*, and $\sigma(X_{RCM,1961\text{–}1990})$ is the standard deviation of X_{RCM} calculated for the period 1961-1990.

Examples of seasonal changes in uncorrected and bias-corrected rainfall values and variances are given at two locations in Fig 3.9. For all models and locations, the bias-corrected time series closely follow the corresponding uncorrected time series. There are slight differences in the uncorrected and bias-corrected variances (given as the standard deviation). However, the uncorrected and bias-corrected variance time series still match reasonably closely, and projected changes in the uncorrected rainfall simulations are preserved in the bias-corrected simulations. Similarly close matches are achieved for all seasons, and also for PE and solar radiation (not shown).

Changes in uncorrected and bias-corrected temperature are almost indistinguishable for all seasons and models. Fig 3.10 shows that the steady increase in Tmax for the period 2010-2100 is very well preserved in all the bias-corrected simulations, and there are negligible differences in the variances of uncorrected and bias-corrected Tmax time series.

Fig 3.9 and Fig 3.10 clearly demonstrate that the correction can be applied to long, continuous time series. Applying a consistent correction is attractive, as it allows impact models (e.g. agricultural models, hydrological models) to simulate long-term trends, rather than just time slices.

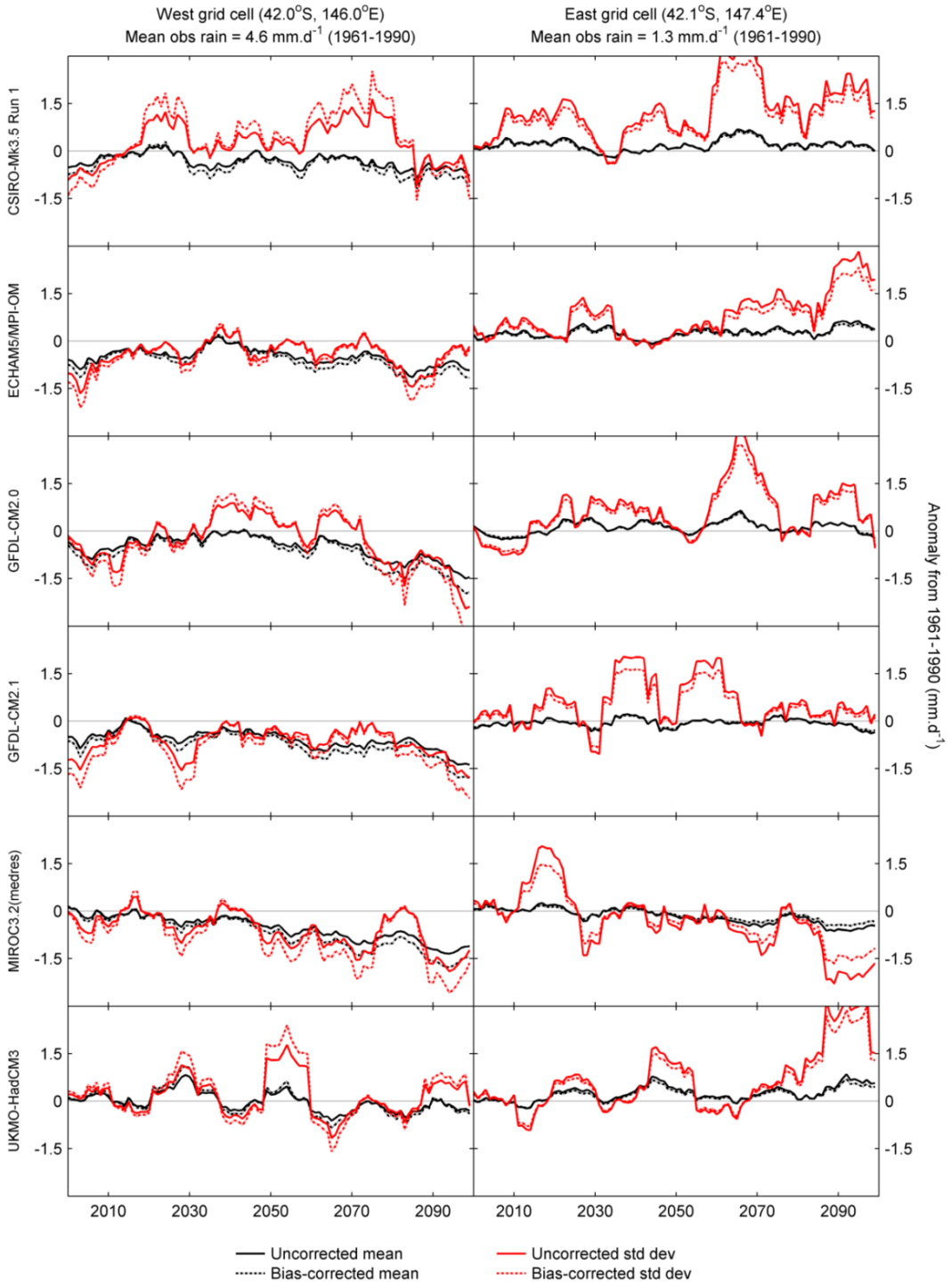

Fig 3.9 DJF anomalies of rainfall mean and standard deviation in a western and an eastern grid cell under the A2 emissions scenario. Anomalies are calculated with respect to 1961-1990, and time series are smoothed with an 11-year moving window; see text for details. Left hand panel shows changes for a grid cell in the mountainous western region of Tamania, while right hand panel gives changes for a grid cell at lower elevation in the eastern Tasmanian midlands.

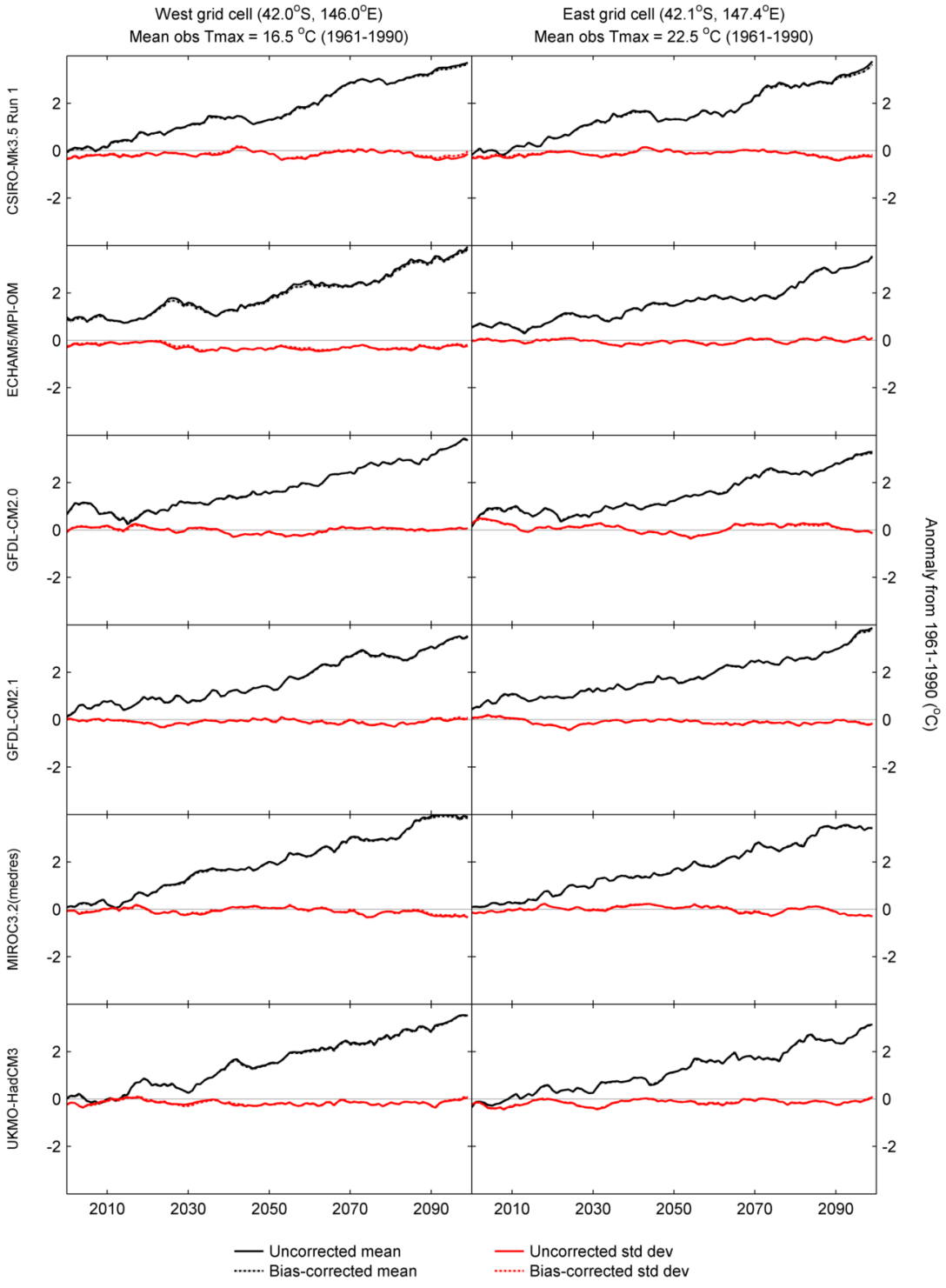

Fig 3.10 DJF anomalies of Tmax mean and standard deviation in a western and an eastern grid cell under the A2 emissions scenario. Anomalies are calculated with respect to 1961-1990, and time series are smoothed with an 11-year moving window; see text for details. Left hand panel shows changes for a grid cell in the mountainous western region of Tamania, while right hand panel gives changes for a grid cell at lower elevation in the eastern Tasmanian midlands.

3.7 Discussion

Both the multiplicative and additive quantile mapping perform well under cross-validation, even for higher quantiles. This contrasts with Lafon et al. (2013), who found that quantile mapping of empirical rainfall distributions did not perform well under cross-validation at higher quantiles. Poor performance under cross-validation may indicate poor performance outside the training period. Several elements of our method help to stabilise the bias-correction and provide confidence in the bias-corrected projections. First, because GCM biases are removed before downscaling and because CCAM is run at high horizontal resolution, the simulations require generally small corrections in many grid cells. Second, we use a long (47-year) training period for Tmax, Tmin and rainfall. We use the same period to evaluate the method under ensemble cross-validation. The large sample from the long training period used in this study produces cumulative frequency distributions that reflect natural variation in climate. In contrast, Lafon et al. (2013) used 30-year training periods and 10-year verification periods. As the long training periods contain variables that are non-stationary (in our case, Tmax and Tmin), they are detrended before bias-correction. We note that the use of a long training period is less important for PE and solar radiation as these variables tend to have lower variance than rainfall and temperature. Third, we fit bias-corrections seasonally. Most regions in Tasmania have strongly seasonal climates that are reflected in the values of all variables (a partial exception is relatively uniform monthly rainfall in some drier parts of eastern Tasmania). Applying seasonal bias-corrections groups similar values together, which tends to produce more stable cumulative frequency distributions. The seasonally distinct corrections can lead to small discontinuities in time series at seasonal boundaries, and these discontinuities may have unintended effects on impact assessments. We note, however, that these small discontinuities had no discernible effect in the outputs of several hydrological and biophysical impact models (Bennett et al., 2012; Holz et al., 2010).

Bias-correcting variables independently has been shown to disrupt the dynamical balance of climate model outputs (Piani and Haerter, 2012). Piani and Haerter (2012) advocate the use of a copula-based bias-correction to avoid this problem, as such corrections explicitly account for correlations between variables. Copula-based corrections require the use of idealised bi-variate (or multivariate) statistical distributions that need to be parameterised. We have sought to avoid using such statistical distributions, and the associated uncertainty in estimating parameters for these distributions. Despite correcting variables indepently, we have shown that inter-variable correlations are well preserved after bias-correction. This, again, can be ascribed to the relatively small corrections we apply to the RCM variables, thanks to the realistic simulation of Tasmanian climate by CCAM (Corney et al., 2013).

Multiplicative quantile mapping tends to perform less well for values at or near zero. Fortunately, these low values are unlikely to have a significant effect on the performance of most impact models, precisely because they are small. For example, hydrological models used for impact assessments often contain loss models that remove smaller quantities of rainfall before calculating runoff (e.g. Bennett et al., 2012), meaning that errors in very small rainfall quantities are unlikely to have any effect on simulated runoff.

As already noted, these corrections are not designed for assessment of extreme events, in particular for rainfall extremes. The magnitude of extreme events falling in the highest percentile bin (99-100) can vary greatly, especially for rainfall. By applying a single correction factor to all values in the top percentile bin, we generalise across events that may behave (and therefore scale) differently in a warming climate. For values in the top percentile, fitting extreme value distributions and then applying a bias-correction to these may yield more robust projections (outside the scope of this study).

The bias-correction reduces the error in the number of rain days only where the model overestimates the number, since it is a multiplicative correction. However, all climate models tend to overestimate the number of rain days, the well-documented 'drizzle problem' (e.g. Berg et al., 2013). Therefore, we see the correction as generally useful, and applicable to outputs from most RCMs.

The multiplicative bias-correction does not remove biases in the magnitude and duration of multi-day rain events. The underestimation of large, multi-day rain events inherent in the CCAM simulations can be partly attributed to the underestimation of the frequency and intensity of cutoff lows, an important driver of Tasmanian rainfall (Grose et al., 2013a), and other such synoptic systems. Despite this, Grose et al. (2013a) show that CCAM simulates the frequency and intensity of cutoff lows more realistically than a GCM. The underestimation of large rain events is an important limitation of the CFT bias-corrected simulations for impact modelling. Hydrological models run with the bias-corrected CCAM simulations tend to underestimate larger flows (Bennett et al., 2012). This can be attributed to the underestimation of large rain events reported here, as large rain events generate proportionately more runoff than smaller rain events. The underestimation of large flow events by hydrological models would be even greater if not for CCAM's tendency to overestimate large, single-day rainfalls over large areas described by Bennett et al. (2011). These rainfall biases do not seem to affect biophysical models to the same degree as hydrological models. Biophysical models forced by the bias-corrected CCAM simulations appear not to exhibit persistent biases (Holz et al., 2010).

In addition, the value of the bias-corrected outputs for use in impact models is dependent on the performance of the AWAP observations. AWAP is forced by weather station and satellite data, and weather stations are sparse in Tasmania's mountainous western areas. Hofstra et al. (2010) showed that gridded climate datasets tend to underestimate the variance of rainfall in regions with few weather stations. AWAP PE may also have systematic biases at low values. Accordingly, impact modellers using the CFT outputs should treat simulations over western Tasmania (and, indeed, the AWAP observations) with some caution.

3.8 Summary and conclusions

This study describes the method and performance of an empirical bias-correction applied to RCM simulations for Tasmania, Australia. The bias-corrected simulations are designed for use in impact models. The bias-correction is based on quantile mapping of empirical cumulative frequency distributions, which is applied to GCM model projections seasonally. Bias-correcting empirical frequency distributions avoids the need to parameterise idealised frequency distributions and the uncertainty associated with these parameters. Detrending

the variables before calculating the bias-correction ensures that projected climate change signals are conserved. The approach described here is well suited to downscaled climate model outputs in the temperate Tasmanian climate and may also be suitable for higher latitudes or in the tropics, although further testing is required in these regions.

The bias-correction performs well under cross-validation, effectively reducing biases across the range of cumulative frequency distributions, with few exceptions. The bias-correction is not as effective at correcting biases for values at or near zero (e.g. in rainfall simulations) although even here it reduces biases from the uncorrected simulations.

While cross-validating in the historical period gives some indication of how the bias-correction is likely to perform in the future, this does not conclusively demonstrate performance under future climate. Climate model biases can change over time (e.g. Boberg and Christensen, 2012; Buser et al., 2009; Christensen et al., 2008), and very large changes in the characteristics of climate model biases in future climates may undermine any bias-correction trained on historical data. While we have carefully assessed the performance of our bias-correction method in both the historical period and in future trends, we recognise that it is not certain that biases based on observations from 1961-2007 (and therefore the bias-correction) will be relevant in future.

The bias-corrected simulations inherit some of the deficiencies of the uncorrected simulations, for example the tendency to underestimate both the magnitude and duration of large, multi-day rain events. This is linked to limitations in larger scale regional climate features such as cutoff lows.

Correlations between key variables are reasonably well maintained by the bias-correction, meaning the CFT dataset is suitable for impact models that rely on input from multiple variables. Further, the key outputs of the regional climate model and the changes projected by the simulations are faithfully preserved by the bias-correction.

One of the major outcomes of this work is to generate a set of high resolution bias-corrected RCM simulations for Tasmania. The bias-corrected CFT simulations for CSIRO-Mk3.5 Run 1, ECHAM5/MPI-OM, GFDL-CM2.0, GFDL-CM2.1, MIROC3.2(medres) and UKMO-HadCM3 for the B1 and A2 emissions scenarios are available from http://www.tpac.org.au. Impact modellers who wish to use the CFT dataset are directed to Bennett et al. (2011); Bennett et al. (2012); Corney et al. (2013); Grose et al. (2013a); Grose et al. (2013b); Holz et al. (2010) and White et al. (2013) for further discussion of the performance of the CCAM simulations.

4 High-resolution projections of surface water availability for Tasmania, Australia

This is an edited version of the paper published as:

Bennett JC, Ling FLN, Post DA, Grose MR, Corney SP, Graham B, Holz GK, Katzfey JJ, Bindoff NL. 2012. High-resolution projections of surface water availability for Tasmania, Australia. *Hydrology and Earth System Sciences* **16:** 1287-1303. DOI: 10.5194/hess-16-1287-2012.

Much of the introductory material now appears in Chapter 1, while descriptions of the regional climate simulations (detailed in Chapter 2), and the bias-correction method (detailed in Chapter 3) have been abridged.

4.1 Abstract

Changes to streamflows caused by climate change may have major impacts on the management of water for hydro-electricity generation and agriculture in Tasmania, Australia. We describe changes to Tasmanian surface water availability from 1961–1990 to 2070–2099 using high-resolution simulations. Six fine-scale (10 km2) simulations of daily rainfall and potential evapotranspiration are generated with the CSIRO Conformal Cubic Atmospheric Model (CCAM), a variable-resolution regional climate model (RCM). These variables are bias-corrected with quantile mapping and used as direct inputs to the hydrological models AWBM, IHACRES, Sacramento, SIMHYD and SMAR-G to project streamflows.

The performance of the hydrological models is assessed against 86 streamflow gauges across Tasmania. The SIMHYD model is the least biased (median bias =−3%) while IHACRES has the largest bias (median bias =−22%). We find the hydrological models that best simulate observed streamflows produce similar streamflow projections.

There is much greater variation in projections between RCM simulations than between hydrological models. Marked decreases of up to 30% are projected for annual runoff in central Tasmania, while runoff is generally projected to increase in the east. Daily streamflow variability is projected to increase for most of Tasmania, consistent with increases in rainfall intensity. Inter-annual variability of streamflows is projected to increase across most of Tasmania.

This is the first major Australian study to use high resolution bias-corrected rainfall and potential evapotranspiration projections as direct inputs to hydrological models. Our study shows that these simulations are capable of producing realistic streamflows, allowing for increased confidence in assessing future changes to surface water variability.

4.2 Introduction

Human-induced climate change has been shown to contribute to changes in the spatial distribution of precipitation in the 20th century (Zhang et al., 2007). In a warmer future world, understanding the local and regional implications of changes in the hydrological cycle is critical to planning for water security (Oki and Kanae, 2006). Dynamical regional climate models (RCMs) have been used to assess climate change impacts on spatial distributions of rainfall (Kilsby, 2007), seasonal changes to rainfall (Kendon et al., 2010a), and changes to rainfall intensity (Berg et al., 2009) and frequency (Mailhot et al., 2007) at spatial scales relevant to water managers.

To assess how complex rainfall changes affect surface water availability, RCM outputs are often coupled to hydrological models. The challenge in coupling RCMs directly to hydrological models is that RCM outputs are usually too biased to allow hydrological models to produce realistic streamflows (Graham et al., 2007). Quantile mapping is a bias-correction technique shown to be highly effective at removing biases across the entire cumulative frequency distribution of a given variable (Ines and Hansen, 2006; Piani et al., 2010a). Quantile mapping has been successfully used to couple RCMs to hydrological models in several northern hemisphere studies (Akhtar et al., 2009; Boé et al., 2007; Fowler and Kilsby, 2007; Wood et al., 2004), but has not been used for major regional hydroclimatological studies in Australia, where indirect coupling methods based on pattern scaling and simple perturbation of historical observations have been more popular (Charles et al., 2010; Chiew et al., 2009; Post et al., 2012).

This paper's primary aim is to quantify seasonal and spatial changes in Tasmanian streamflows by 2100 using high-resolution RCM simulations. To better understand future changes in streamflow variability, we project streamflows using bias-corrected RCM projections as direct inputs to hydrological models. Ours is the first Australian study to use this method to produce basin-scale surface water projections, and accordingly we aim to demonstrate that our method credibly replicates historical streamflows.

Finally, this paper aims to understand whether uncertainty in the streamflow projections comes more from the RCM simulations than from the hydrological modelling. The practice of using ensembles of climate models to describe uncertainty in projections is well established. Using ensembles of hydrological models to quantify uncertainty in projections is less common, even though uncertainties in hydrological modelling may contribute significantly to uncertainties in climate change impact studies (Bastola et al., 2011). To find if the RCM simulations are a greater source of uncertainty than the hydrological models, we couple an ensemble of RCM simulations to an ensemble of hydrological models.

4.3 Data and methods

4.3.1 Regional climate modelling

We use the six RCM simulations generated with CCAM (Chapter 2, Table 2.1) run for the A2 (high) emissions scenario: CSIRO-Mk3.5 (run 1), ECHAM5/MPI-OM, GFDL-CM2.0, GFDL-CM2.1, MIROC3.2(medres) and UKMO-HadCM3.

4.3.2 Quantile mapping

Two inputs are required for the hydrological models: daily rainfall and daily APET. We use the multiplicative quantile mapping described in Chapter 3 to align daily rainfalls and APET to 10 km² gridded observations aggregated from the ~5 km² (0.05°) SILO dataset (Jeffrey et al., 2001). SILO is used here in preference to AWAP as the hydrological models were calibrated to SILO data. Rainfall is a direct output from the SILO dataset, while APET is calculated from base variables (vapour pressure, temperature and solar radiation) according to Morton's (1983) method for wet environments. Finally, bias-corrected RCM outputs are regridded from the 10 km² CCAM grid to the 5 km² grid compatible with the hydrological models.

Split-sample cross-validation of quantile mapping

When bias-corrections are applied to future projections, they are often implicitly assumed to be consistent through time (Ines and Hansen, 2006; Wood et al., 2004). However, there is some evidence that bias-corrections can vary with the choice of training period (Li et al., 2010; Piani et al., 2010b). We test this assumption using split-sample cross-validation for quantile mapping of rainfall. We carry out two sets of cross-validation:

1) We train the quantile mapping for the period 1962-1984 and validate against the period 1985-2007.
2) To minimise the effects of longer-term (decadal or greater) oscillations or trends in either the observed or simulated rainfalls, we train the quantile mapping on odd years for 1962-2007 (1963, 1965, …, 2007) and validate against even years for 1962-2007 (1962, 1964, …, 2006).

4.3.3 Hydrological modelling

We use the five hydrological models calibrated by Viney et al. (2009b): AWBM (Boughton, 2004), IHACRES (Post and Jakeman, 1999), Sacramento (Burnash et al., 1973), SIMHYD (Chiew et al., 2002) with Muskingum routing (Tan et al., 2005), and SMAR-G (Goswami et al., 2002). The hydrological models are simple conceptual models that use a variety of algorithms to partition available water into baseflows and quickflows, which are then combined to represent observed hydrographs. IHACRES is distinguished from the other models by i) employing a rainfall scaling parameter and ii) by characterising streamflow using a unit-hydrograph. Viney et al. (2009b) used a log-bias objective function (Viney et al., 2009a) to automate the calibration of the five hydrological models to 90 streamflow records for 1975-2007 for catchments around Tasmania. The stream records Viney et al. (2009b) chose were from catchments that had negligible human influence on streamflows.

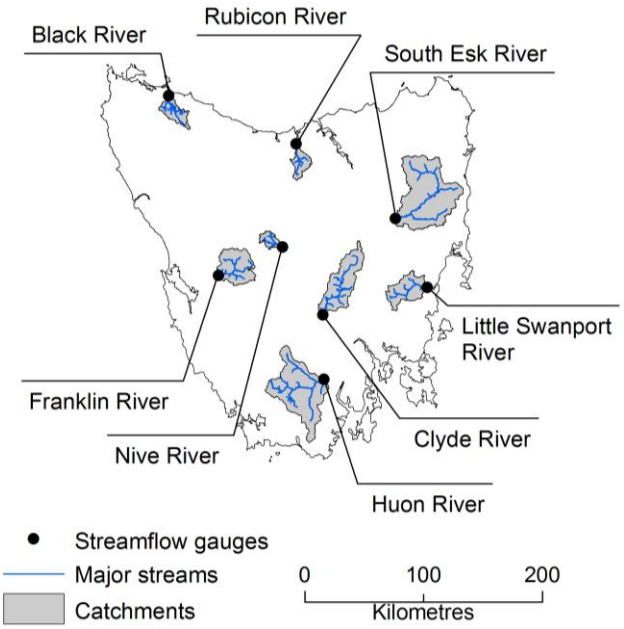

Fig 4.1 Catchments reported by this study.

For four catchments, streamflow records were augmented with estimates of irrigation extractions to simulate natural streamflows. The hydrological models produce runoff timeseries at a daily time step distributed on a ~5 km² (0.05°) grid covering all of Tasmania. To achieve Tasmania-wide coverage with the five hydrological models, Viney et al. (2009b) assigned model parameters to ungauged catchments from their nearest gauged neighbour.

We aggregate runoff to eight river catchments (Fig 4.1). Operation of storages, diversions and water extractions in these catchments are based on practices current at 31 December 2007 (Bennett et al., 2010). The eight rivers are chosen as they represent different climatic regions of Tasmania, and all have >20-year, high-quality streamflow records.

Descriptions of streamflow changes in a further 70 Tasmanian rivers, 12 large irrigation storages and the Tasmanian hydro-electric system are given by Bennett et al. (2010).

Changes are described between a baseline period, 1961-1990, and a future period, 2070-2099.

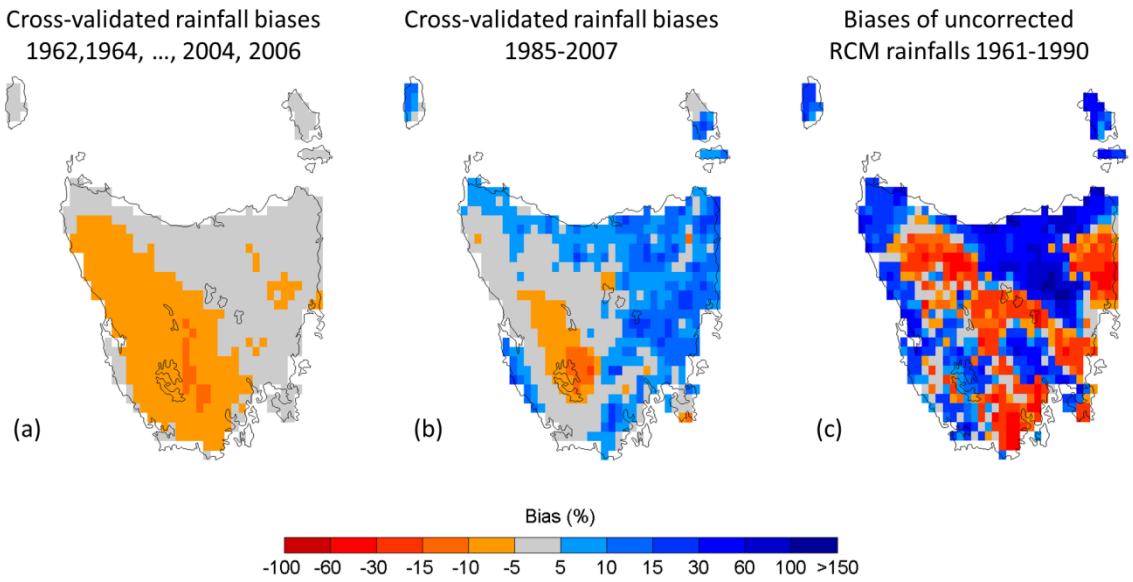

Fig 4.2 Effects of changing the training period on quantile mapping performance. Plots show biases in mean annual rainfall for the 10 km² GFDL-CM2.0 simulation. (a) Biases of bias-corrected RCM rainfall where quantile mapping is trained with the period 1962-1984; biases shown are calculated for 1985-2007. (b) Biases of bias-corrected RCM rainfall where quantile mapping is trained with odd years occurring in the period 1962-2007 (1963, 1965, …, 2007); biases shown are calculated for even years occurring during the period 1962-2007 (1962, 1964, …, 2006). (c) Biases of uncorrected RCM rainfalls for 1961-1990. Rainfall biases for the other five RCM simulations are very similar to the GFDL-CM2.0 simulation illustrated in this figure.

4.4 Results

4.4.1 Cross-validation of quantile mapping

Fig 4 shows cross-validation biases for mean annual rainfall for the GFDL-CM2.0 simulation. Rainfall biases of the GDFL-CM2.0 simulation shown in Fig 4.2 are very similar for the other RCM simulations (not shown). When the quantile mapping is trained on odd years, cross-validation biases are less than ±10% almost everywhere (Fig 4.2a). Cross-validation biases are much smaller than biases of uncorrected RCM rainfalls (Fig 4.2c). Biases of uncorrected RCM rainfalls are larger than ±30% for much of Tasmania, and exceed 150% in some cells. The relatively small cross-validation biases suggest that the quantile mapping is effective outside the training period. Accordingly, the quantile mapping is likely to be reliable for the period 2010-2100. A longer training period (e.g. 30+ years) may have produced even smaller cross-validation biases. We had 47 years of synchronous simulations and observations, which allowed 23 years to train the quantile mapping for the cross-validation tests (assuming an equally long validation period). 23 years may be an insufficiently long period to sample the natural variance in rainfall.

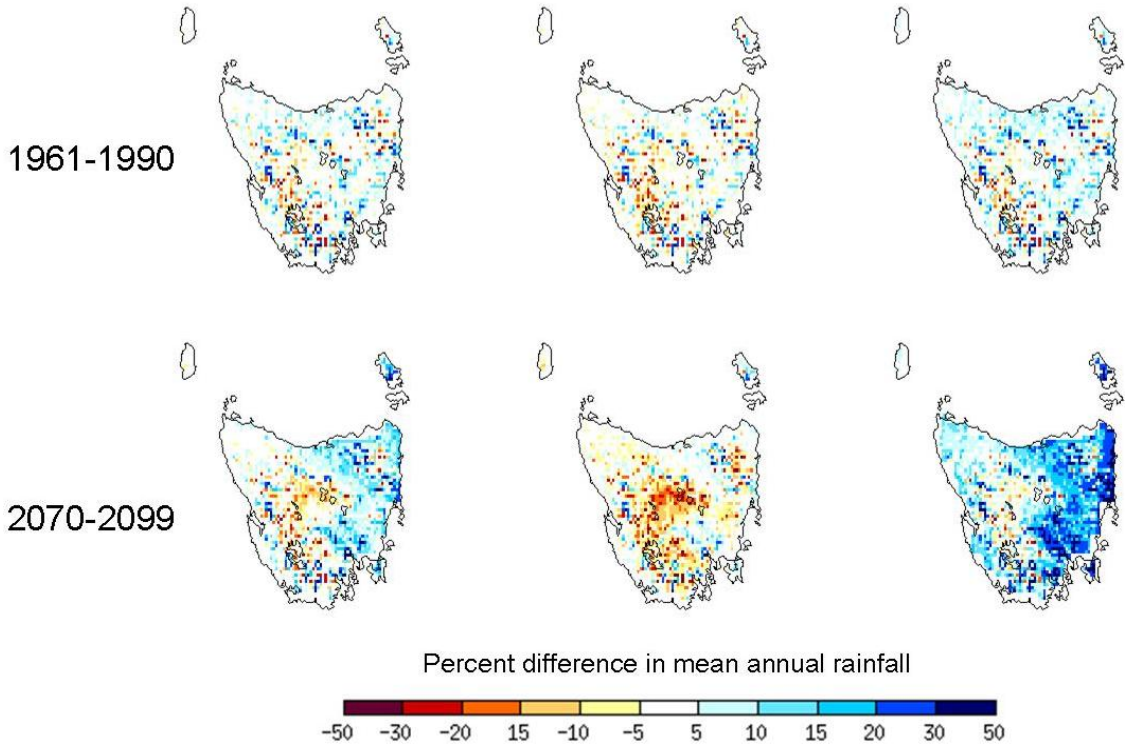

Fig 4.3 Comparison of SILO mean annual rainfall during the runoff model calibration period (1975-2007) to mean annual rainfall from RCM simulations for the reference period (top row) and end-of-century (bottom row). Left column shows percent difference of SILO (1975-2007) from mean of six RCM simulations. Middle and right columns show range of differences of SILO (1975-2007) from individual RCM simulations at each grid cell. Middle column shows lowest percent differences, right column shows highest differences**.**

When the quantile mapping is trained on 1962-1984 (Fig 4.2b), cross-validation biases are larger (±10% to ±25%), and occur over larger areas than when the quantile mapping is trained on odd years (Fig 4.2a). This discrepancy in performance is caused by changes in Tasmanian rainfall between 1962-1984 and 1985-2007. The period 1962-1984 experienced higher rainfalls over much of Tasmania than 1985-2007, particularly in eastern Tasmania. RCM simulations are not synchronised with observations, and the change in observed rainfall from 1962-1984 to 1985-2007 is not present in the RCM simulations. When the quantile mapping is trained to match the higher rainfalls of 1962-1984, it consequently overestimates rainfall during the drier period 1985-2007. (The exception to this pattern is over the south-western mountains, which experienced very wet years in 1994 and 1996; here the bias-correction underestimate rainfalls in the validation period.) These long-term changes in Tasmanian rainfall do not have the same effect on the quantile mapping when it is trained on odd years over a period that includes both wet and dry periods, resulting in lower cross-validation biases (Fig 4.2a). This illustrates the importance of sampling long periods to generate temporally stable cumulative frequency distributions for quantile mapping.

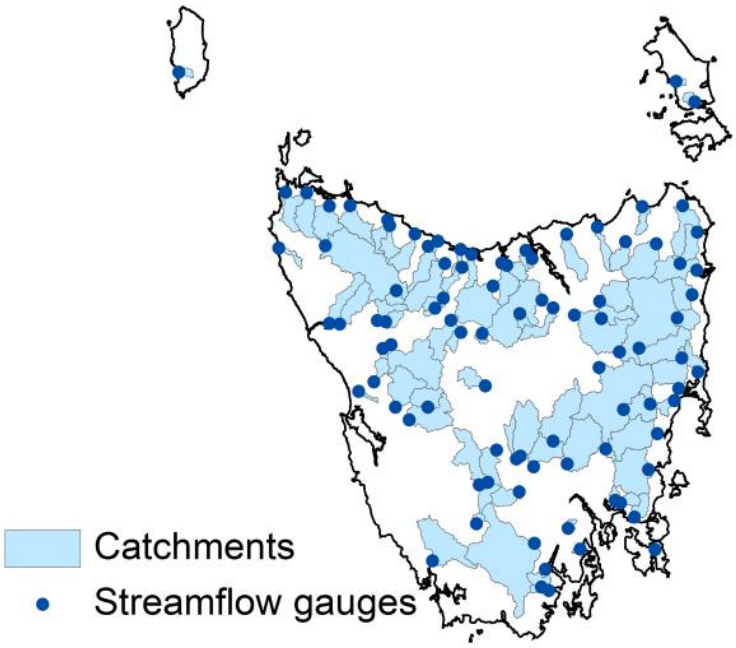

Fig 4.4 Catchments and streamflow gauges used to validate hydrological model performance.

4.4.2 Performance of hydrological modelling

Hydrological model performance under a changing climate

Performance of a hydrological model may not remain consistent under a changing climate (Merz et al., 2011). Vaze et al. (2010) found that performance of IHACRES, Sacramento, SIMHYD and SMAR-G declined sharply in periods where mean annual rainfall was more than 15% lower or more than 20% greater than mean annual rainfall in the calibration period. Differences between simulated mean annual rainfall and SILO mean annual rainfall during the calibration period (1975-2007) are between -15% and +20% for most of Tasmania for all six RCM simulations presented here (Fig 4.3), suggesting that the hydrological models should perform adequately during the baseline (1961-1990) and future (2070-2099) periods.

Comparisons of biases of hydrological models

Performance of hydrological models forced with RCM inputs (RCM-runoff) is assessed at 86 streamflow gauges for all data available for 1961-2007. The 86 catchments range in size from 8 km² to >2000 km², and give good coverage of Tasmania (Fig 4.4). Performance is assessed by calculating biases of RCM-runoff against observed streamflows. To isolate the effects of the RCM inputs on hydrological model performance, biases are also calculated for RCM- runoff against streamflows modelled with hydrological models forced by SILO (SILO-runoff).

Biases are calculated as:

$$bias = \frac{\sum_{t=1}^{T} Q_m - \sum_{t=1}^{T} Q_o}{\sum_{t=1}^{T} Q_o} \times \% \quad (4.1)$$

where Q_m is streamflow modelled with RCM-runoff and Q_o is either observed streamflow or streamflow modelled with SILO-runoff.Fig 6 shows biases of mean annual streamflows, biases of low streamflows (exceedance probability of 95%, Q_{95}) and biases of high streamflows (exceedance probability of 5%, Q_5) at 86 sites. Biases vary much more between hydrological models than between RCM simulations (Fig 4.5). Low variation between RCM simulations is caused at least in part by the bias-correction of GCM SSTs before downscaling. Low variation between RCM simulations is also consistent with the use of a single RCM for all the simulations. Because the performance of hydrological models tends not to vary greatly between RCM simulations, we focus on describing hydrological model biases for the mean of the six RCM simulations from here on.

Flows modelled with AWBM, SIMHYD and SMAR-G show similar characteristics to observed mean annual and Q_5 streamflows for 1961-2007 (Fig 4.5, Table 4.1). AWBM, SIMHYD and SMAR-G replicate observed streamflows well, with biases smaller than ±10% for more than 40% of catchments and biases smaller than ±25% for more than 85% of catchments. SIMHYD has the smallest median biases (median bias for mean annual streamflows = -3.2%) and smallest interquartile ranges of biases of any hydrological model for annual and seasonal streamflows (Table 4.1). AWBM, SIMHYD and SMAR-G show a between RCM simulations, we focus on describing hydrological model biases for the mean of the six RCM simulations from here on.

Flows modelled with AWBM, SIMHYD and SMAR-G show similar characteristics to observed mean annual and Q_5 streamflows for 1961-2007 (Fig 4.5, Table 4.1). AWBM, SIMHYD and SMAR-G replicate observed streamflows well, with biases smaller than ±10% for more than 40% of catchments and biases smaller than ±25% for more than 85% of catchments. SIMHYD has the smallest median biases (median bias for mean annual streamflows = -3.2%) and smallest interquartile ranges of biases of any hydrological model for annual and seasonal streamflows (Table 4.1). AWBM, SIMHYD and SMAR-G show a catchments) and a stronger tendency to underpredict observed Q_5 streamflows (underpredicted in >80% of catchments).IHACRES is least like observed streamflows (median bias for mean annual streamflows = -22.3%), and Sacramento biases are second largest after IHACRES. IHACRES shows a very strong tendency to underpredict observed mean and Q_5 streamflows (Fig 6), and has the largest median biases and largest interquartile ranges of biases against observed annual and seasonal streamflows (Table 4.1).

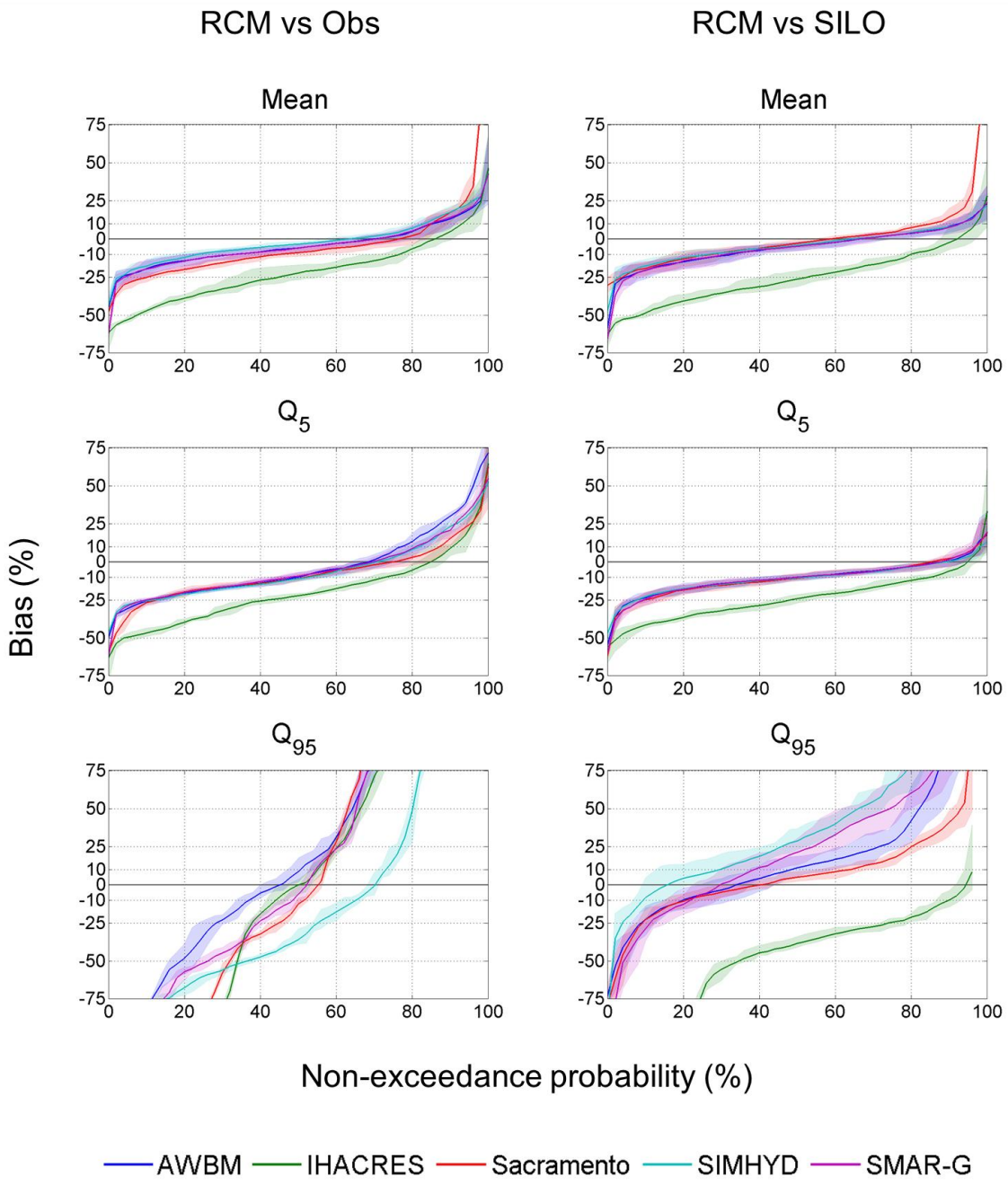

Fig 4.5 Non-exceedance probabilities of streamflow biases from the hydrological models forced with the RCM at 86 streamflow gauges for 1961-2007. Left column shows biases calculated against observed streamflows, right column shows biases calculated against streamflows simulated with the hydrological models forced by SILO variables. Biases are shown for mean streamflows (top row), high (Q_5) streamflows (middle row) and low (Q_{95}) streamflows (bottom row). Lines show mean biases from the six RCM simulations, shaded confidence intervals show the range of biases from the six simulations. For left panels positive biases mean that RCM-forced runoff overestimate observations, and for right panels positive biases mean that RCM-forced runoff overestimates SILO-forced runoff.

Table 4.1 Summary of biases of hydrological models forced by CCAM calculated at 86 streamflow gauges from the average of the six RCM simulations.

		AWBM	IHACRES	Sacramento	SIMHYD	SMAR-G
Mean annual streamflow	Median catchment bias (%)	-5.2	-22.6	-9.1	-3.2	-5.8
	Interquartile range of biases at all catchments (%)	14.9	20.5	16.1	11.6	14.1
Mean Nov-Apr streamflow	Median catchment bias (%)	-7.8	-15.6	-25.5	-6.7	-12.9
	Interquartile range of biases at all catchments (%)	22.1	25.1	35.1	25.4	23.2
Mean May-Oct streamflow	Median catchment bias (%)	-3. 9	-25.6	-3.9	-2.0	-3.8
	Interquartile range of biases at all catchments (%)	13.9	24.9	15.1	14.5	15.1
Q_{95} streamflows	Median catchment bias (%)	5.5	-1.6	-11.2	-35.3	-3.9
	Interquartile range of biases at all catchments (%)	173.3	184.9	448.8	79.7	160.9
Q_5 streamflows	Median bias (%)	-9.8	-23.4	-11.4	-11.5	-8.8
	Interquartile range of biases for all catchments (%)	26.3	26.8	17.8	20.6	23.2

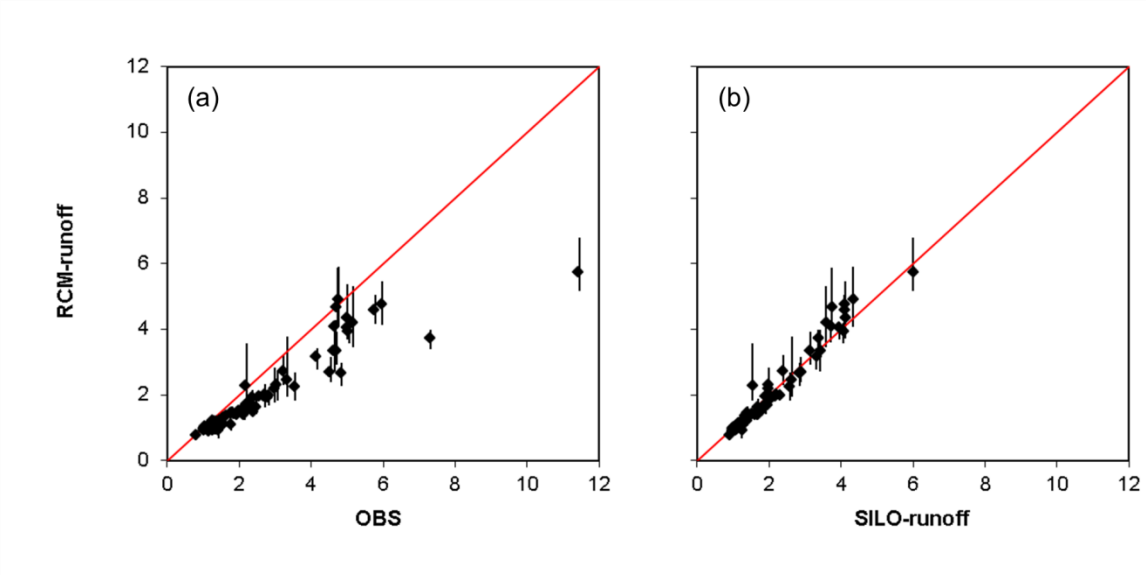

Fig 4.6 Comparison of coefficients of variation (CV) of daily streamflows generated by SIMHYD at 86 streamflow gauges for 1961-2007. (a) CV of daily streamflows generated by SIMHYD forced with the RCM (RCM-runoff) and observations (OBS). (b) CV of daily streamflows generated by RCM-runoff and SIMHYD forced with SILO (SILO-runoff). Points show the mean of the six RCM simulations, bars show the range from the six simulations.

RCM-runoff biases are generally smaller against SILO-runoff than against observations for mean streamflows and Q_5 streamflows (Fig 4.5). This is expected as biases calculated against observations add errors in the RCM inputs to errors inherent in the hydrological models, while biases calculated against SILO-runoff reflect differences only between the RCM inputs and SILO variables. In general, RCM-runoff tends to underpredict SILO-runoff. The bias-correction aligns frequency distributions of modelled and observed rainfalls, however it does not account for spatial correlations of rainstorms (how daily rainfalls in all grid cells in a catchment behave together) nor for temporal correlations of rainfall (how rainfalls behave in a multi-day rainstorm). The bias-corrected RCM rainfalls tend to overestimate large daily rainstorms over large areas (Bennett et al., 2011).Underestimation of streamflows is therefore most probably caused by inadequate replication of the temporal characteristics of rainstorms by the bias-corrected RCM inputs.

All RCM-runoff simulations tend not to replicate Q_{95} streamflows as well as higher streamflows (Table 4.1, Fig 4.5). Fig 4.5 shows that low streamflows generated from SILO-runoff do not replicate observations well. That is, many of the deficiencies in low streamflows emanate from the hydrological models as calibrated for our study, rather than from the bias-corrected RCM inputs. Nonetheless, the bias-corrected RCM inputs also contribute to poor performance of low flows. Low flow performance could have been improved by changing the tendency to underpredict observed annual streamflows (underpredicted in >60% of objective function used to calibrate the hydrological models or using different hydrological models (Staudinger et al., 2011), however, this may have reduced performance at mean and high flows.

SIMHYD model performance

SIMHYD exhibited the lowest biases of the hydrological models, and accordingly we focus on SIMHYD projections to report changes to future streamflows. We describe several additional performance tests of the SIMHYD model here.

SIMHYD RCM-runoff tends to underestimate the daily variance (measured as the coefficient of variation, CV) of observed streamflows at the 86 gauge sites (Fig 4.6a). However, when daily CV of SIMHYD RCM-runoff is compared to daily CV of SIMHYD SILO-runoff at the same sites, there is strong agreement (Fig 4.6b). This implies that the tendency of SIMHYD RCM-runoff to underestimate daily CV of observed runoff is not caused by the RCM or the bias-correction, but rather by the SILO dataset or the SIMHYD hydrological models, as calibrated for our study. The bias-corrected RCM inputs reproduce a similar level of variability to that present in SILO rainfalls for the purposes of hydrological modelling.

SIMHYD RCM-runoff matches observed seasonal streamflows reasonably well (Fig 4.7). Seasonal streamflows are particularly closely matched in northern and western catchments, illustrated by the Black River and Rubicon River. In the central, western and southern catchments (Nive, Franklin and Huon Rivers) SIMHYD RCM-runoff tends to underpredict gauged streamflows from September to December. This difference is also present in the SIMHYD SILO-runoff (black line in Fig 4.7), indicating that it is caused by hydrological model calibration or the SILO rainfalls rather than the bias-corrected RCM inputs. SIMHYD RCM-runoff varied much more between RCM simulations in the drier eastern catchments (South Esk, Little Swanport and Clyde rivers) than in the wetter western and southern catchments (Black River, Franklin River and Huon River). This is consistent with the higher variability of rainfall in eastern Tasmania. The summer (DJF) yields of the Clyde River are difficult to replicate as the upper reaches of this catchment are impounded (Lake Crescent/Sorell) and regulated for irrigation.

The effects of the bias-corrected RCM inputs on hydrological performance are more easily seen in streamflow duration curves (Fig 4.8). In general, SIMHYD RCM-runoff replicates observed streamflow durations well in larger and wetter catchments (Black River, Nive River, Franklin River, Huon River and South Esk River). As expected, SIMHYD RCM-runoff does not replicate observed streamflows as well as SIMHYD SILO-runoff. SIMHYD RCM-runoff matches or overpredicts large SIMHYD SILO-runoff daily streamflows. CCAM simulations tend to overpredict large basin-scale daily rainstorms, and this tendency is not ameliorated by the quantile mapping (Bennett et al., 2011) (Appendix A). Consequently, large daily streamflows tend to be overstated. However, overestimation of large daily streamflows is sometimes caused by the hydrological models. SIMHYD RCM-runoff strongly overpredicts large streamflows in the Clyde River and in the Little Swanport River. For both these rivers this is caused by poor replication of gauged streamflows by the SIMHYD SILO-runoff. As with low flows, alternative hydrological models or calibration methods could have improved replication of large daily streamflows in catchments where the hydrological models did not perform well.

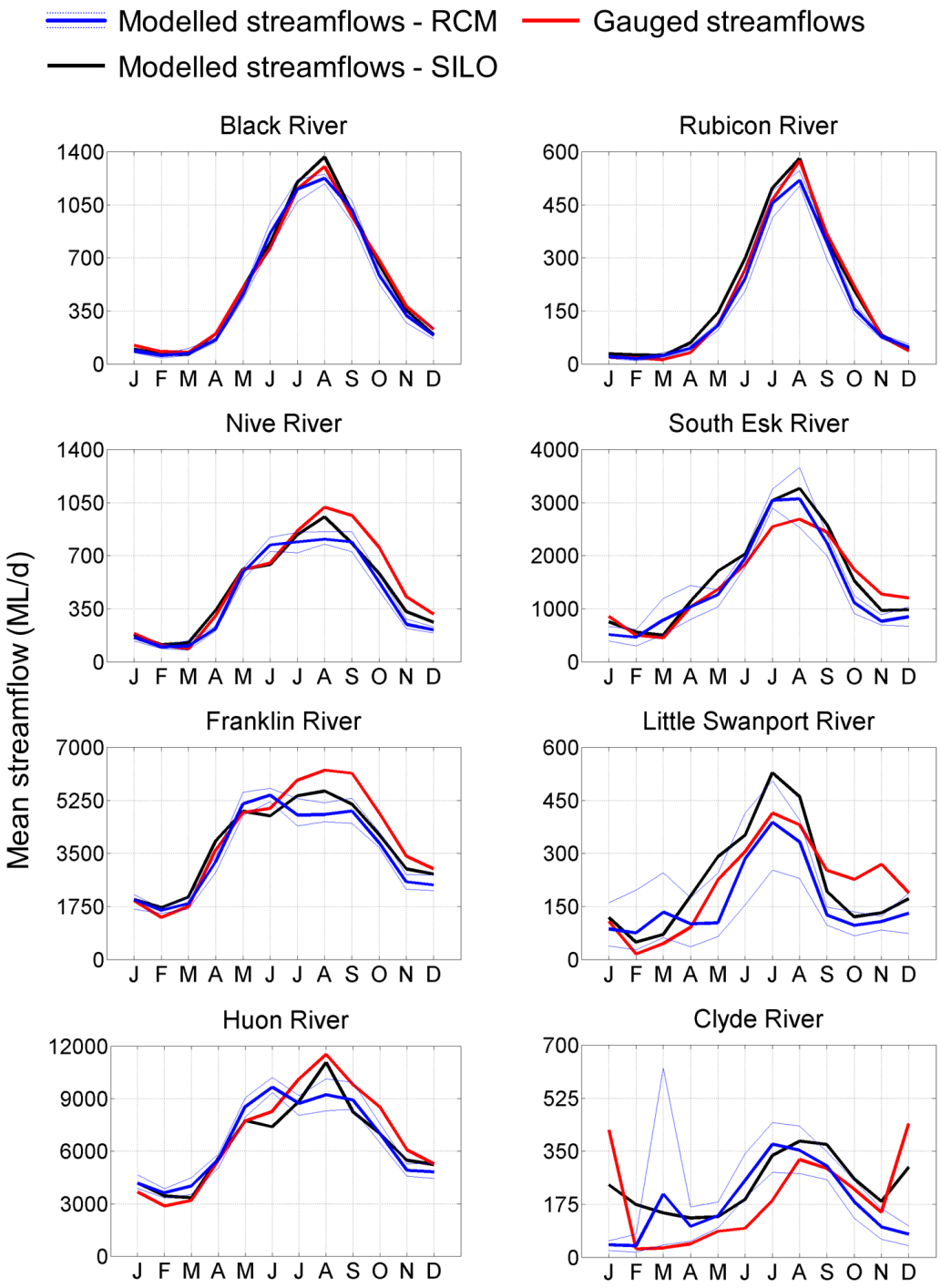

Fig 4.7 Comparison of mean monthly modelled and gauged streamflows for 1961-2007. Blue line shows streamflows modelled with SIMHYD forced by the RCM, faint blue lines give range of the six RCM simulations, black line shows SIMHYD forced by SILO and red line shows gauged streamflows.

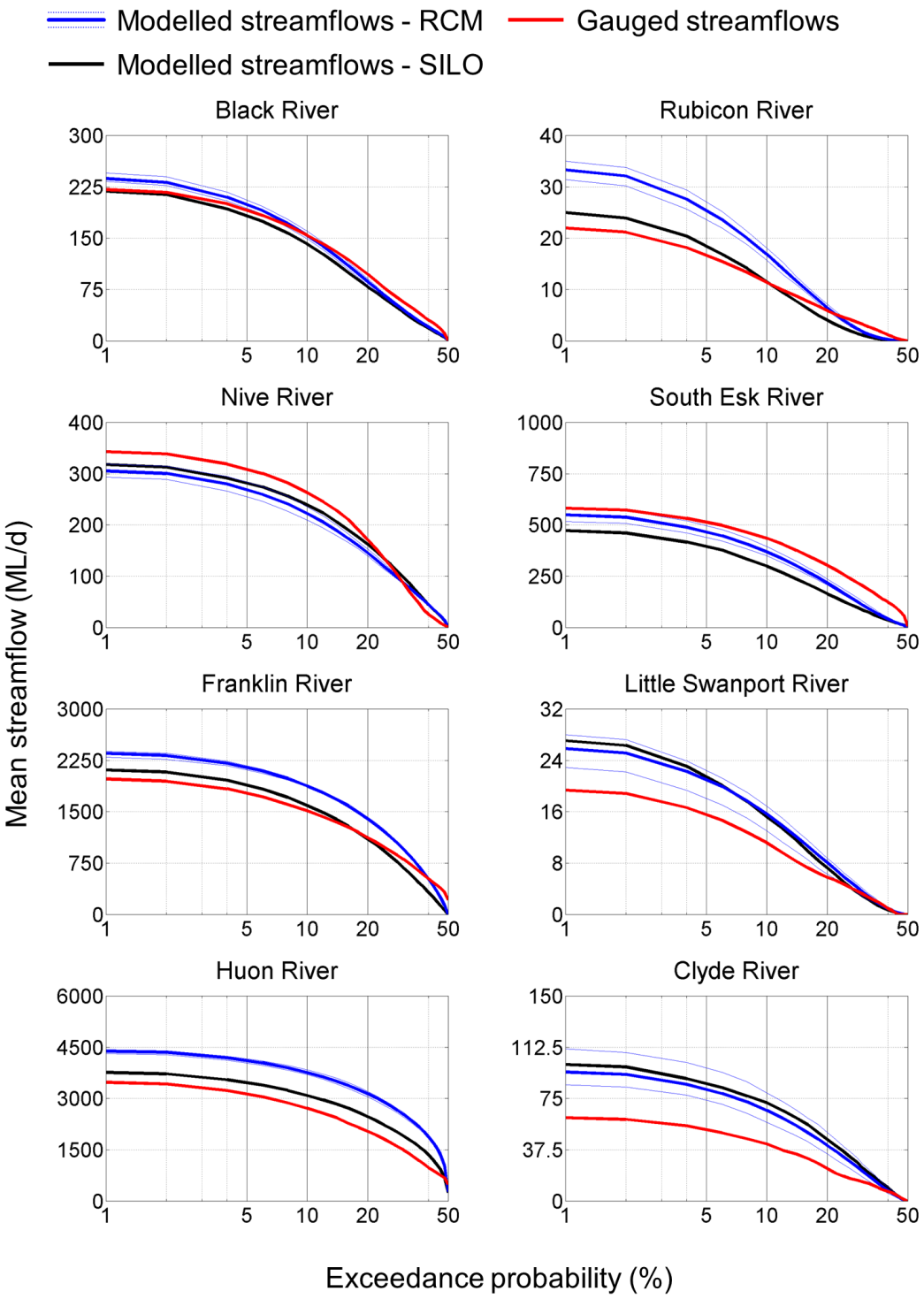

Fig 4.8 Comparison of streamflow durations for observed and modelled daily streamflows 1961-2007. Blue line shows streamflows modelled with SIMHYD forced by the RCM, faint blue lines give range of the six RCM simulations, black line shows SIMHYD forced by SILO and red line shows gauged streamflows.

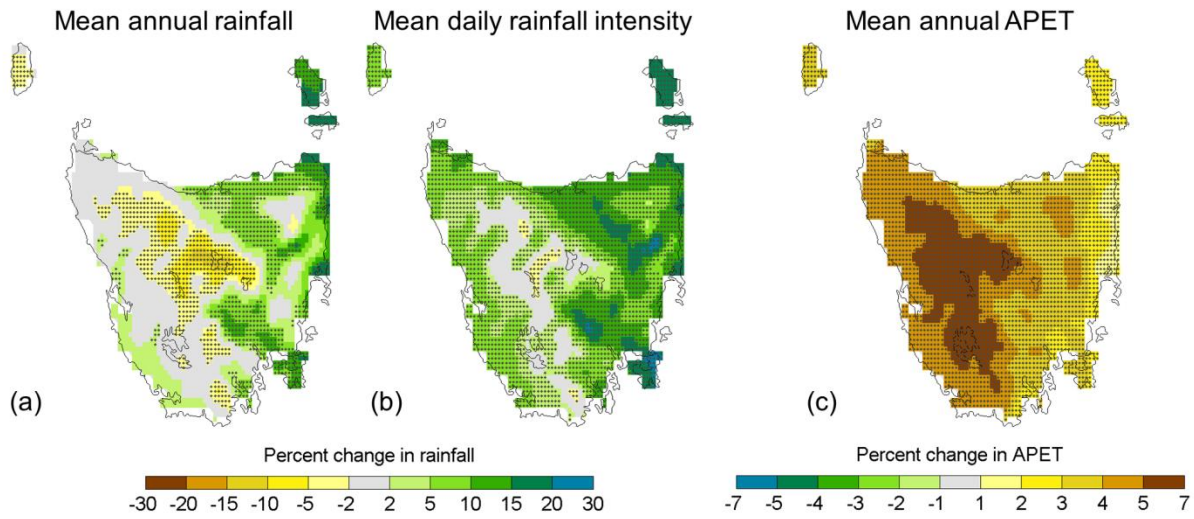

Fig 4.9 Change in rainfall and APET from 1961-1990 to 2070-2099. (a) Change in mean annual rainfall. (b) Change in mean daily rainfall intensity for rain days >1 mm. (c) Change in mean annual APET. All plots are calculated from the average of the six RCM simulations. Stippling shows regions where at least five of the six RCM simulations agree on the sign of change.

4.4.3 Projected changes in rainfall and APET

Projected changes in rainfall and APET from 1961-1990 to 2070-2099 calculated from the mean of the six RCM simulations are shown in Fig 4.9. Changes in mean annual rainfall vary spatially. Reductions in mean annual rainfall are projected for the mountainous centre (up to -15%), but marked increases (up to +30%) are projected in the east. The increases in the east tend to occur at lower elevations. An increase in mean annual rainfall is also projected along the south-west coast. The simulations agree strongly on the sign of change in the lower-lying parts of the east coast, and at high elevations in the mountainous centre (Fig 4.9a).

Mean annual APET is projected to increase across Tasmania, with the highest increases in the western mountains (Fig 4.9). Increases in APET are small compared to changes in mean annual rainfall, with mean annual APET increases always less than 7%. All RCM simulations project Tasmania-wide increases in APET by 2070-2099.

Mean daily rainfall intensity is projected to increase over most of Tasmania (Fig 4.9b). The largest proportional increases occur in the east (>15%). RCM simulations show strong agreement on the sign of change in mean daily rainfall intensity for much of Tasmania by 2070-2099 (Fig 4.9b). The general tendency of rain to fall in fewer, more intense events as the climate warms is a robust feature of theory, simulations and observations (Allan and Soden, 2008; Allen and Ingram, 2002; Min et al., 2011; Pall et al., 2007) and is at least partly consistent with an increase in atmospheric moisture (Hegerl et al., 2004; Stephens and Hu, 2010).

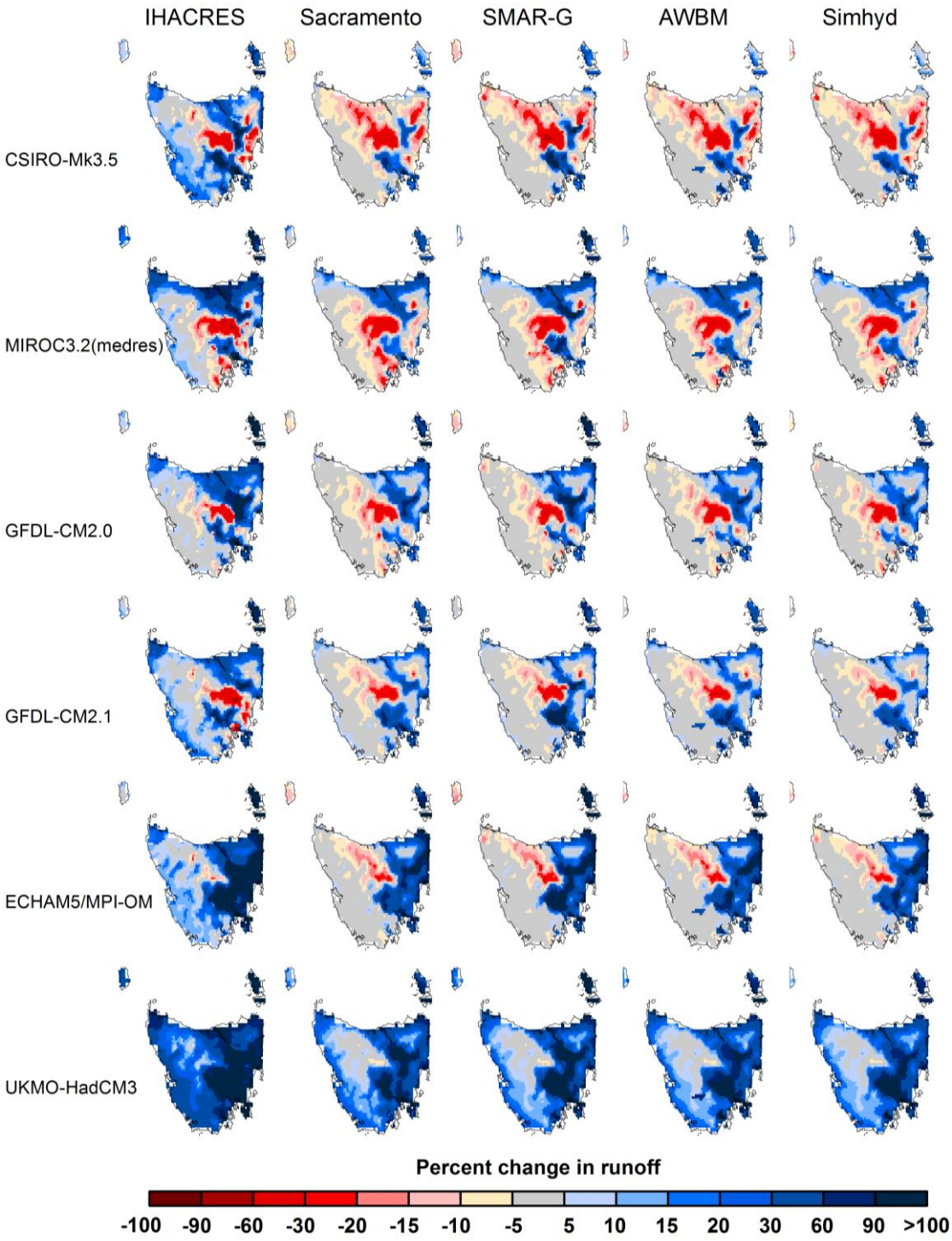

Fig 4.10 Change in mean annual runoff from 1961-1990 to 2070-2099 for all RCM simulations and hydrological models. RCM simulations are designated by the GCMs used for downscaling, and are ordered from driest projection (CSIRO-Mk3.5, top) to wettest projection (UKMO-HadCM3, bottom). Hydrological models are ordered from most biased (IHACRES, left) to least biased (SIMHYD, right).

4.4.4 Projected changes in runoff and streamflows

In describing projections we distinguish between 'runoff', defined as gridded outputs from the hydrological models, and 'streamflows', calculated by aggregating runoff to river catchments.

Variation between hydrological models and RCMs

Projected changes to future runoff vary much more between RCM simulations than between hydrological models. For a given RCM simulation, future changes to mean annual runoff projected with AWBM, Sacramento, SIMHYD and SMAR-G are very similar (Fig 4.10). Using the downscaled GFDL-CM2.1 simulation as an example, AWBM, Sacramento, SIMHYD and SMAR-G agree strongly on the spatial features of runoff change (Fig 4.10). The four hydrological models show drying in central and north-west Tasmania, little change in the south-west, and wetting in the east. AWBM, Sacramento, SIMHYD and SMAR-G are also consistent in seasonal projections and in projections of low and high streamflows (not shown). IHACRES projects more intense and more widespread wetting than other hydrological models for all RCM simulations. In the downscaled GFDL-CM2.1 example, IHACRES projects more intense wetting in the east and stronger wetting in the west and south-west than the other hydrological models. The high sensitivity of IHACRES to changes in inputs renders suspect the projections of Tasmanian runoff from IHACRES with bias-corrected RCM inputs.

Projections from the SIMHYD hydrological model

In many areas, the projected changes to rainfall are amplified in changes to runoff. Where mean annual rainfall in central Tasmania decreases by up to 15% (Fig 4.9a), runoff decreases by more than 30% (Fig 4.11a). In eastern Tasmania, rainfall increases of <20% (Fig 4.9a) are projected to increase runoff by >60% (Fig 4.11a).

Low runoff events generally decrease more than mean runoff, while high runoff events increase similarly to mean runoff. The RCM simulations agree strongly on a decrease in low runoff (represented by runoff with 75% exceedance probability, Q_{75}) over most of Tasmania (Fig 4.11d). Q_{75} runoff decreases more and over a wider area than decreases to mean runoff (Fig 4.11d). Increases in high runoff (represented by runoff with 1% exceedance probability, Q_1) are more widespread and show similar proportional increases to mean runoff (Fig 4.11e). The RCM simulations agree strongly on an increase in Q_1 runoff over the west coast, north and east. Because Q_1 runoff events are larger than mean runoff events, a proportional change in Q_1 runoff equates to a much greater increase in streamflow than the same proportional change to mean runoff.

Changes in seasonal streamflow projected with SIMHYD at the eight study catchments are shown in Fig 4.12. Projected changes to streamflows vary considerably by season. DJF runoff decreases markedly in the west (Fig 4.11b), however these seasonal decreases have little effect on annual streamflows in the Black and Franklin rivers as DJF runoff makes a small contribution to streamflow in these rivers. Similar seasonal changes are also projected in the Huon River in the south-west. The Rubicon River in the central north of Tasmania is projected to experience increases in streamflows in all seasons, particularly JJA (Fig 4.12).

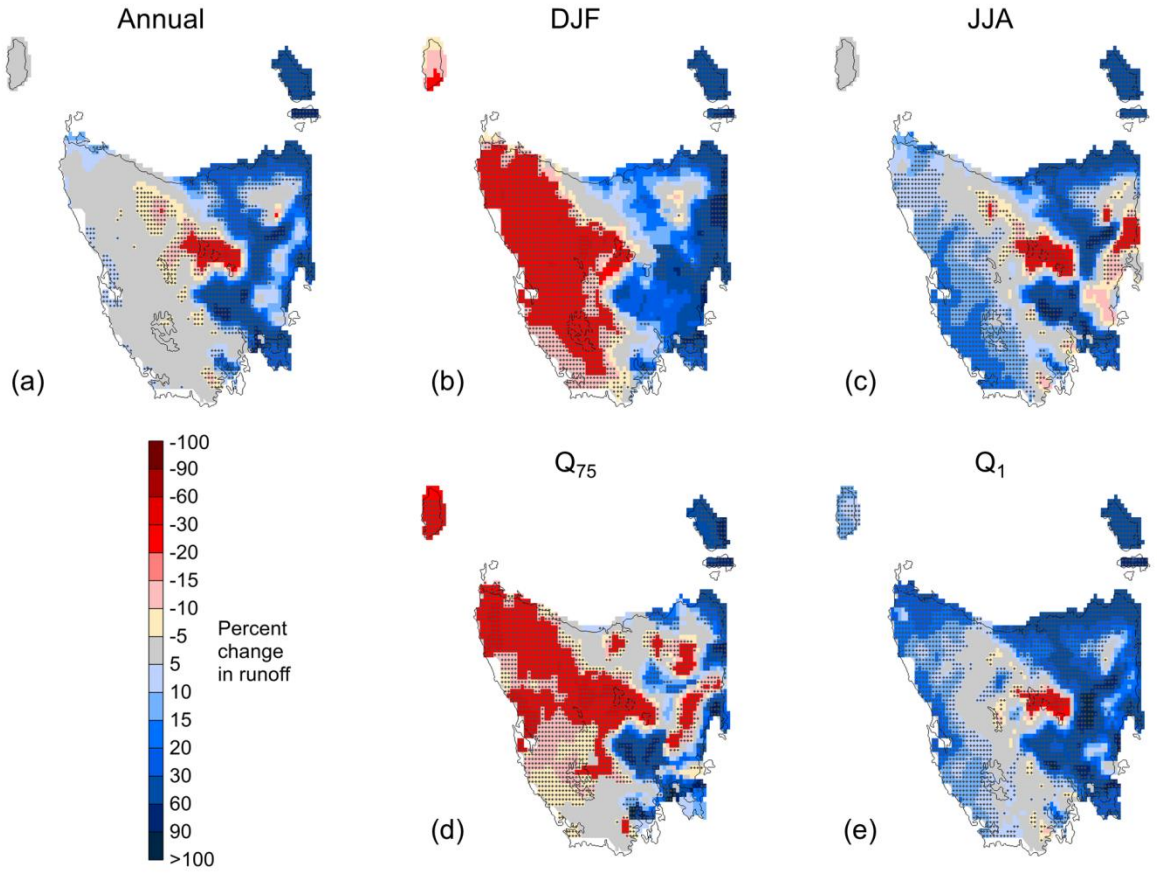

Fig 4.11 Change in runoff simulated by SIMHYD from 1961-1990 to 2070-2099. (a) Change in mean annual runoff. (b) Change in mean DJF runoff. (c) Change in mean JJA runoff. (d) Change in Q_{75} runoff. (e) Change in Q_1 runoff. Changes are calculated from the mean of the six RCM simulations. Stippling shows regions where at least five of the six RCM simulations agree on the sign of change.

Projections for rivers in the drier regions, including the north-east (South Esk River), east (Little Swanport River) and centre (Clyde River), are characterised by a high degree of variation between RCM simulations. The South Esk River and Little Swanport River are projected to experience increases in streamflow (Fig 4.12), largely during February to April.

A major feature of these projections is reduced runoff over Tasmania's central mountains in all seasons (Fig 4.11a-c). This contrasts with projected increases in mean annual runoff in many low-elevation areas in the east and in coastal areas (Fig 4.11). The high-elevation Nive River catchment is projected to experience decreases in streamflow year round, particularly in May and June (Fig 4.12). Catchments in central Tasmania that span both

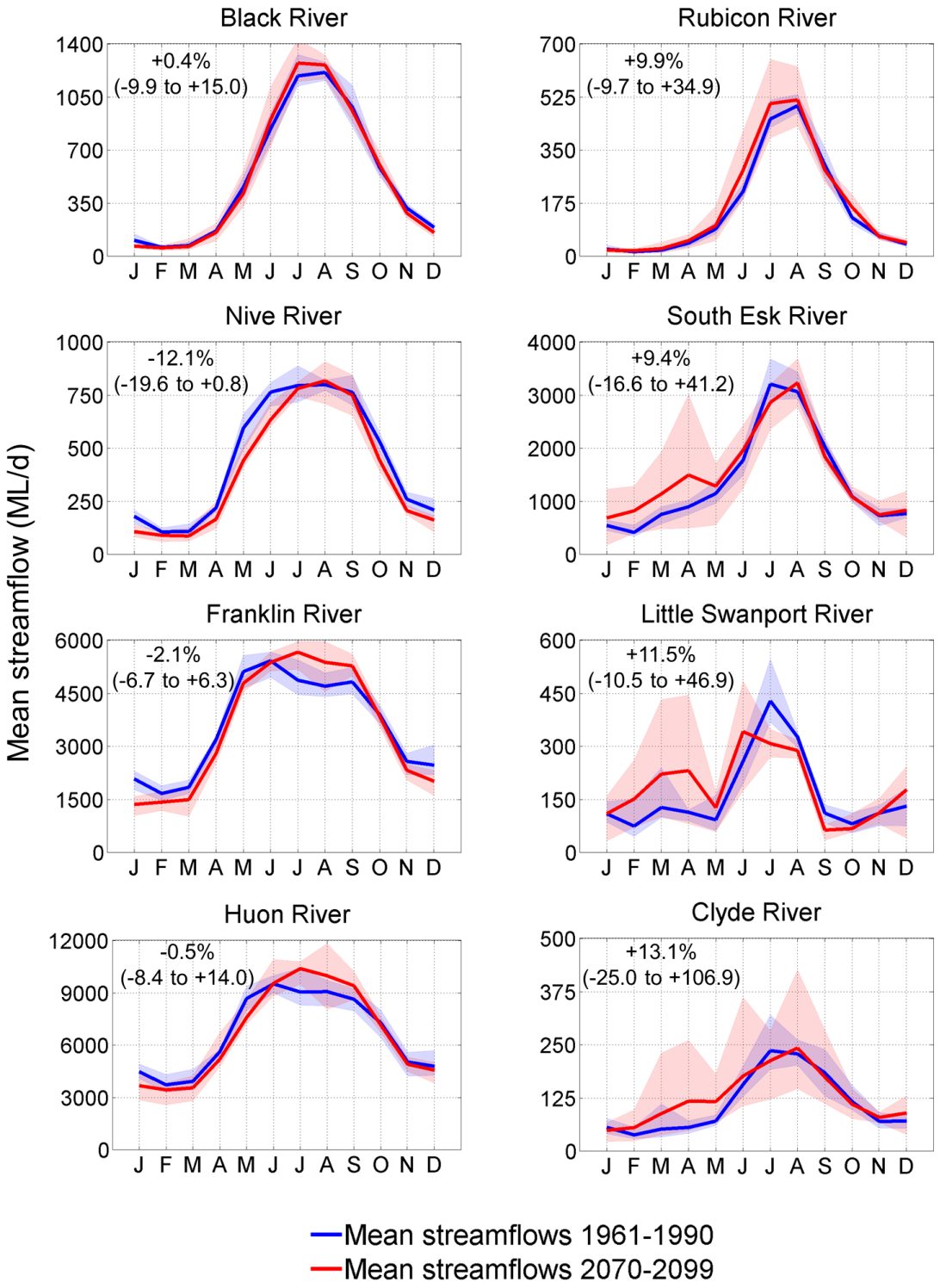

Fig 4.12 Mean monthly streamflows simulated by SIMHYD for 1961-1990 and 2070-2099. Shaded confidence intervals show range of the six RCM simulations. Numbers in plots give percent change in mean annual streamflow from the average of the six RCM simulations. Numbers in brackets give the range of percent change from the six simulations.

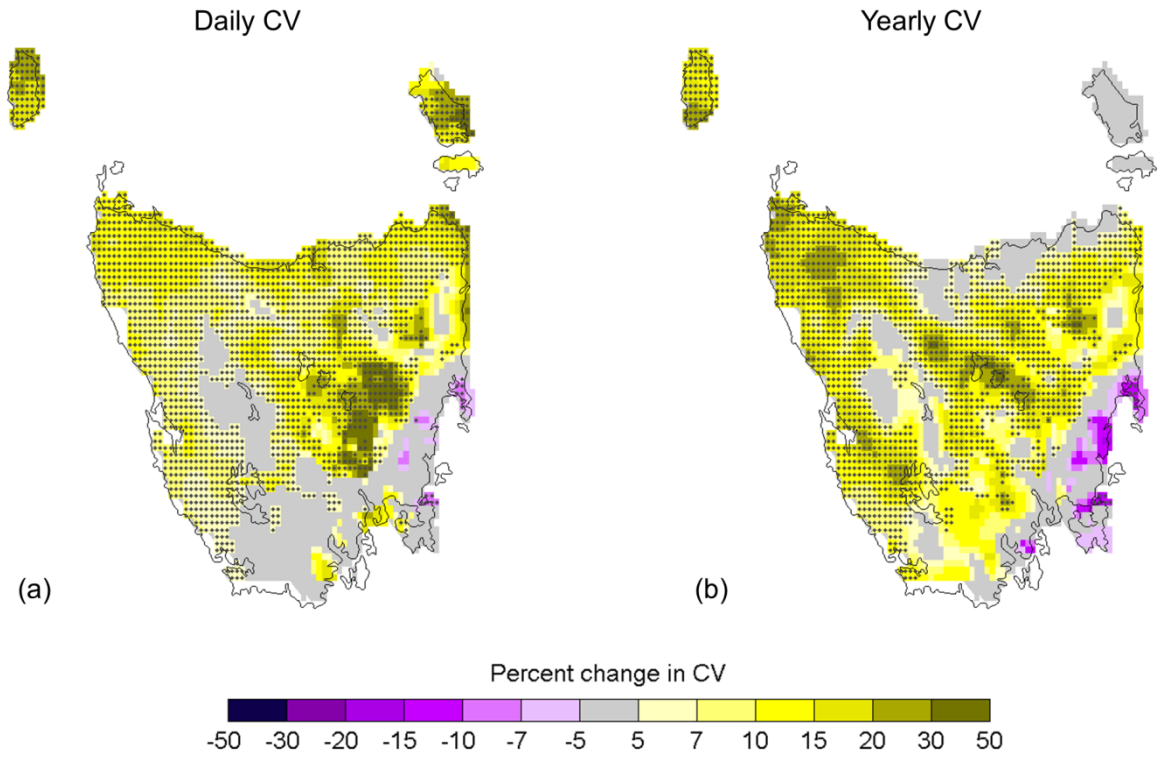

Fig 4.13 Changes to coefficient of variation (CV) of runoff simulated by SIMHYD from 1961-1990 to 2070-2099. (a) Changes to CV of daily runoff. (b) Changes to CV of annual runoff. Changes are calculated from the average of the six RCM simulations. Stippling shows regions where at least five of the six RCM simulations agree on the sign of change.

high and low elevations (e.g. Clyde River) show complex responses. The Clyde River is projected to experience year-round streamflow decreases in high elevation areas (not shown), but these decreases are offset by projected increases at lower elevations, particularly during MAM, resulting in increased mean annual streamflow at the catchment outlet. A similar elevation-sensitive streamflow response is observed for the South Esk River in the north-east.

Variance in daily and annual runoff is projected to increase in many areas of Tasmania. Increases in the variance of daily runoff occur in the northern two-thirds of Tasmania (Fig 4.13), and the RCM simulations agree strongly on projected increases in CV of daily runoff over much of Tasmania. The most marked increases in daily variance occur in the lowlands of the central east, which is consistent with an increase in mean daily rainfall intensity (Fig 4.9). Variance in annual runoff increases over most areas, with the most notable increases projected for the north-west and central highlands (4.13).

Overall, the projections suggest that there will be a greater variability of streamflows, with rivers rising to higher peaks and experiencing longer periods of low streamflow.

4.5 Discussion and conclusions

Our study demonstrates that quantile mapping can directly couple RCM outputs to hydrological models to produce realistic streamflows in a majority of catchments. Our method did not perform as well in eastern Tasmanian catchments, which are subject to higher rainfall variability. In these catchments, the poorer performance is explained largely by the bias-corrected RCM rainfalls not being sufficiently similar to observations.

We note that our method of quantile mapping may be more sensitive to changes in training period than comparable methods that fit probability distributions to observations and models before quantile mapping (e.g. Li et al., 2010). Fitting probability distributions has the advantage of smoothing frequency distributions, which may reduce variation in quantile mapping factors with changes in training period. However, Li et al. (2010) found quantile mapping varied noticeably with changes in training period, despite having fitted probability distributions before calculating their bias-corrections. Further, fitting probability distributions adds parameter uncertainties, and using empirical cumulative frequency distributions has the virtue of simplicity. Nonetheless, we reiterate that long training periods are required to generate temporally stable cumulative frequency distributions. We recommend the use of cross-validation testing as a routine measure to demonstrate the stability of quantile mapping.

The IHACRES hydrological model does not replicate observed runoff as realistically as the other hydrological models with bias-corrected RCM inputs. Further, IHACRES gives different projections of change. Viney et al. (2009a) found that IHACRES was the best performing model when calibrated, but performed worst under spatial cross-validation tests. They attributed this drop in performance to the IHACRES parameter that scales rainfall. In contrast, Vaze et al. (2010) found that IHACRES was not particularly sensitive to changes in inputs when calibrated to a range of wet and dry conditions for catchments on continental Australia. We conclude that for studies using bias-corrected RCM variables as direct inputs to hydrological models for impact studies, it is important to test a hydrological model for sensitivity to changes in inputs as a precursor to generating stable, plausible runoff projections, even if the model has been shown to be effective for climate studies elsewhere.

Projected changes in Tasmanian runoff vary far more between RCM simulations than between hydrological models. This finding is accentuated if we exclude the poorly performing IHACRES model from the projections. For our study, therefore, it is more important to consider the range of RCM simulations than the range of hydrological models to adequately describe uncertainty in projections of surface water availability. This finding supports several other studies that have shown climate models to be a more significant source of uncertainty than hydrological models for surface water projections (Prudhomme and Davies, 2009; Teng et al., 2012; Wilby and Harris, 2006).

Our fine-scale simulations project changes to Tasmanian runoff by 2100 to vary considerably by region, in contrast to near-uniform spatial changes projected by GCMs (Christensen et al., 2007). Of note are the year-round decreases in runoff projected for the central mountains, as Tasmania relies on streamflows from this

region to generate hydro-electric power and to supply irrigators. The projected decrease in runoff over the central mountains of Tasmania reported here has seasonal dependence. For winter in the future, the air is warmer and moister as it approaches the west coast of Tasmania. This causes an increase in rainfall along the west coast, which leads to increased upward motion along the western slopes of the mountains. After reaching the highest elevations, the air descends, and at a greater rate in the future as a response to the increased upward motion further west. This tendency for subsidence causes a slight decrease in rainfall in the central plateau region. In the other seasons, the decreased westerly airflow projected in the future results in weaker upward motion, and rainfall, along the western slopes. This decrease in rainfall extends to the central mountains. In addition, with decreased clouds and warmer temperatures, the surface dries out relative to the current climate (see APET changes). As a result, less moisture is available locally for evaporation. Thus for all seasons, runoff is projected to decrease in the central mountains relative to the lower-lying areas. Reduced streamflows from Tasmania's central mountains will reduce Tasmania's hydro-electric power generation capacity (Bennett et al., 2010).

The projected increases in runoff in eastern Tasmania reported here contrast with Post et al. (2012), whose median future scenario showed either no change or decreases in runoff in eastern Tasmania by 2030. This difference in sign may be attributed to the increased resolution of land-ocean boundaries in CCAM in comparison to the GCM projections used by Post et al. (2012). The increases in eastern rainfall projected by CCAM result from a tendency for increased atmospheric blocking, southward extension of the East Australian Current, and the formation of a small but significant mean sea level pressure anomaly in the Tasman Sea that enhances the onshore winds in this region (Grose et al., 2010). The pattern in the GCMs is similar but displaced further offshore to the south and east due to the coarser grid size of GCMs (Grose et al., 2011). Notwithstanding increased variability of streamflows (discussed below), increased surface water availability in Tasmania's east may present opportunities for future agricultural production.

Changes in seasonal runoff are an important feature of these projections. The projected decreases in DJF runoff over western Tasmania are caused by a reduction in the mean westerly circulation (Grose et al., 2010), associated with an expansion of the Hadley cell and a poleward movement of the mid-latitude storm tracks (Yin, 2005), including a poleward movement and strengthening of the subtropical ridge of high pressure and an increase in the high phase of the southern annular mode (Kushner et al., 2001). Even though reduced DJF streamflows in the west have little impact on annual streamflow volumes, these changes are likely to have deleterious effects on endemic freshwater fish (Morrongiello et al., 2011).

Increased runoff variability could have as great an impact on Tasmanian water management practices as changes to seasonal runoff. Projected increases to inter-annual variability in streams fed by the central highlands and western mountains could mean that the large hydropower and irrigation storages situated in these areas may not be able to buffer periods of low inflows as effectively in future as they have in the past. Projected increases in runoff occur largely in the east in lowland areas, where water is presently stored mostly in small farm dams. Small dams may be less able to buffer the projected increases in annual variability, even if there is more water

available on average. In short, the projected increases in runoff may not easily be captured by current infrastructure.

The implications for Tasmanian surface water availability and storage illustrate the virtue of using an ensemble of high-resolution RCM projections as direct inputs to hydrological models to understand the nature of future surface water changes in a warmer world. These implications cannot easily be addressed through the more common approach of perturbing historical climate data that assumes that rainfall variability is unchanged in the future. A large amount of effort has been expended in Australia in recent years building complex series of hydrological models to assess climate change impacts from pattern scaling of GCMs (Charles et al., 2010; Chiew et al., 2009; Petheram et al., 2009). Our study has shown that there is the potential to update these studies using high-resolution RCM simulations when these become available for other regions of Australia.

5 Impacts on Tasmanian hydro-power operation, irrigation storages and water allocations under future climate

This chapter describes some of the impacts that the projected changes in runoff have on the availability of water for irrigation and hydropower generation. Modelling of the hydro-electric system was carried out by Hydro Tasmania, with inputs prepared by the primary author of this thesis. In addition, Hydro Tasmania produced and supplied Fig 5.4. All other modelling and analyses presented in this chapter were carried out by the primary author of this thesis.

River models used in this chapter were originally developed for the Tasmania Sustainable Yields (TasSY) project. The primary author of this thesis contributed substantially to the development of the TasSY river models, by collecting data, developing algorithms and writing computer code.

Edited portions of this chapter have appeared in:

Bennett JC, Ling FLN, Graham B, Corney SP, Holz GK, Grose MR, White CJ, Post DA, Gaynor SM, Bindoff NL. 2010. Climate Futures for Tasmania: water and catchments. Antarctic Climate and Ecosystems Cooperative Research Centre: Hobart. Available online at http://www.climatechange.tas.gov.au/government_action/climate_futures/.

Changes in inflows to selected irrigation and hydropower storages have been published in:

Morrongiello JR, Beatty SJ, Bennett JC, Crook DA, Ikedife DNEN, Kennard MJ, Kerezsy A, Lintermans M, McNeil DG, Pusey BJ, Rayner T. 2011. Climate change and its implications for Australia's freshwater fish. *Marine and Freshwater Research* **62:** 1082-1098. DOI: 10.1071/MF10308.

5.1 Introduction

In this chapter we explore the implications of future changes in runoff for two economically important water uses in Tasmania: hydro-electric power generation and irrigation for agriculture. Tasmanian irrigated agricultural production generated more than $AUD 600 million in 2010-2011, which was more than half the value of all agricultural production in Tasmania for that year (Australian Bureau of Statistics, 2012). On average, water resources in Tasmania are not heavily utilised for irrigation. Irrigation consumes less than 10% of water by volume in 57 of the 62 agricultural catchments, and irrigation uses less than 20% of streamflow in every Tasmanian catchment (Ling et al., 2009a, 2009b, 2009c, 2009d, 2009e). We note, however, that in some

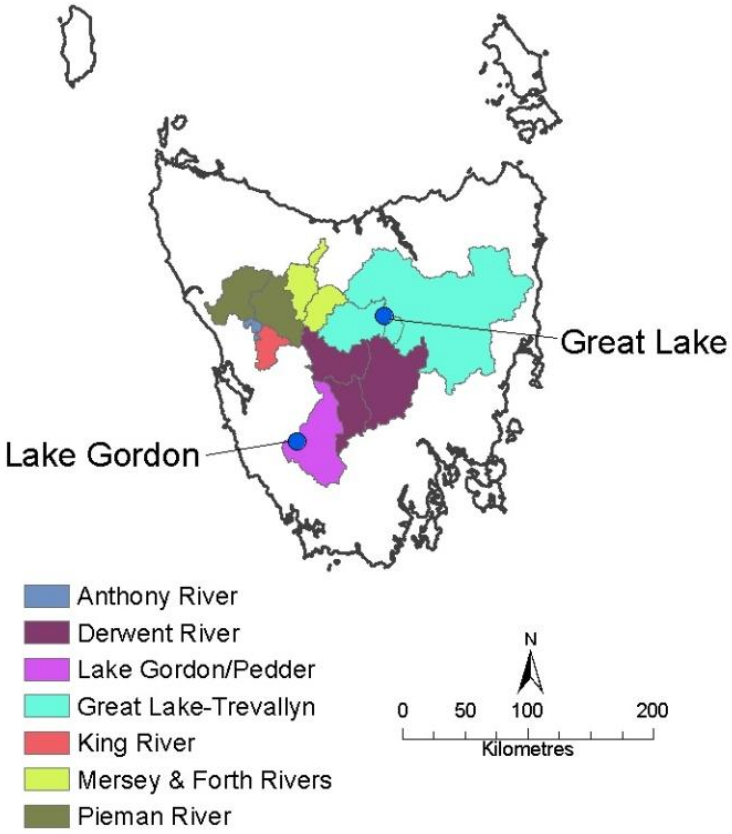

Fig 5.1 Hydro-electric power generation schemes in Tasmania.

Tasmanian catchments higher proportions of streamflow may be exploited during periods of prolonged drought. The Tasmanian government plans to substantially increase the economic value of Tasmanian irrigated agriculture through development of new irrigation infrastructure, including large irrigation storages and water distribution networks (see http://www.tasmanianirrigation.com.au/ for details).

Tasmania's hydro-electric system covers a large proportion of the western and central areas of Tasmania (Fig 5.1). It supplies more than 60% of Tasmania's electricity, and exports hydro-electricity to continental Australia by the undersea Basslink cable. The system stores significant quantities of water in reservoirs and diverts the courses of several rivers, including transferring water between catchments. The system includes Australia's largest and sixth largest lakes: Lake Gordon/Pedder (11,000 GL) and Great Lake (3,060 GL). River flows downstream of power stations can be radically altered from their natural state, particularly in systems that feature interbasin water transfers or have large storages. Diversions are frequently important to downstream water users: for example, the significant proportion of the Derwent River catchment that supplies Great Lake is now diverted north into the South Esk River basin, where irrigators have come to rely on the regular supply of diverted water.

Hydro-power and irrigation infrastructure is costly to build, and this cost is typically recouped over several decades. This makes the economic viability of this infrastructure particularly vulnerable to long-term changes in inflows. Modelling such systems under future climate can be difficult, as simulating the operation of these systems requires that 1) the systems are operated according to a predictable set of rules, and 2) that these operating rules are distilled into algorithms. Fortunately, Tasmania has existing, sophisticated models that describe the operation of both the hydro-power system and irrigated agriculture, developed by Hydro Tasmania (http://www.hydro.com.au/) and the Tasmania Sustainable Yields Project (TasSY - http://www.csiro.au/partnerships/TasSY), respectively. These models are described in detail below.

We show in Chapter 4 that the Simhyd rainfall-runoff model forced with CCAM produces realistic streamflows in Tasmania, including realistic seasonal variation in streamflows. This allows us to use projected streamflows as direct inputs to hydro-electric and water accounting models to give detailed assessments of the impacts of climate change on hydro-electric power generation and irrigation.

5.2 Simulating Tasmania's hydro-electric system

Tasmanian hydro-electric power stations are operated according to inflows to the system, to electricity demand, to market drivers, to National Electricity Market (NEM) requirements, to maintenance schedules and to operational and environmental constraints. These complex elements are all accounted for by Hydro Tasmania's Tasmanian electricity market simulation model, Temsim. Temsim is a proprietary model owned and operated by Hydro Tasmania and full operating rules are not able to be published for commercial reasons. In summary, Temsim optimises system operation to meet demand for electricity and to maximise financial return by trading in the NEM. Temsim includes environmental and other operating constraints. The catchments and storages that are used for Tasmanian hydro-electricity generation are operated as a total system rather than as individual catchments.

In its standard configuration, Temsim uses historical inflows and models the Hydro Tasmania system 20 years into the future. The historical inflows are calculated from power station outflows, storage levels and extrapolations from streamflow gauges. As these inflow time series require direct measurement of lake levels and power station outflows, they cannot be estimated for future climates. We generate inflows time series for Temsim solely from the Simhyd rainfall-runoff model. The use of inflows generated from Simhyd (rather than from historical records) produced realistic system inflows (Appendix B).

In addition, Hydro Tasmania adapted Temsim to be run for 140 years (1961-2100). Simulating the operation of the hydro-electric system for 140 years implies the ability to project electricity prices and demand for the coming 90 years. Hydro Tasmania applied the electricity demand and prices used for Temsim's standard 20-year configuration to the whole 140-year projection. This may underestimate future demand for electricity: Tasmania's population and standards of living may continue to rise, with concomitant increases in demand for electricity. Conversely, changes in consumer demand (e.g., driven by the carbon tax implemented in Australia)

Table 5.1 Large hydropower water storages described in this study

Storage Name	Capacity (GL)	Power generation scheme
Lake Gordon/Pedder	11,000	Lake Gordon/Pedder
Great Lake	3,000	Great Lake-Trevallyn
Lake Burbury	1,000	King River
Lake King William	500	Derwent River

or improvements in energy efficiency may reduce future electricity demand, even as the population continues to grow. In the absence of better information, the assumption of 'business-as-usual' electricity demand serves to illustrate the impacts of changes to inflows on the hydro-electric system as it is currently operated. We note that inflows are the dominant driver of hydropower operation, as these tend to show greater year-to-year and seasonal variance than electricity demand.

Within the larger hydro-electric system we describe changes to two types of hydro-electric scheme: large storage schemes and run-of-river schemes. Large storage schemes have very large storages in relation to their inflows, meaning they are able to buffer seasonal and annual variability in inflows. The amount and timing of power generated from these schemes are functions of long-term (e.g. 10-year) inflows, demand for power and system requirements (such as regulating lake levels). We describe impacts on the large storages listed in Table 5.1. Run-of-river schemes have small storage capacity in relation to inflows. Accordingly, run-of-river schemes are operated largely according to seasonal variation in inflows in order to maximize power generation. If run-of-river power stations are not operated during periods of inflow, valuable power-generating potential is lost as water flows over dam walls (or, more precisely, spillways), known as 'spill'. If run-of-river power stations are operating at their full capacity and inflows nonetheless exceed the water storage capacity, spill is unavoidable. Run-of-river systems are operated to minimise spill. We describe changes to run-of-river power stations in the Pieman, Mersey-Forth, Great-Lake-Trevallyn and lower Derwent schemes (Table 5.2).

5.3 Simulating river flows and water allocations

We use water accounting models to simulate flows in 78 Tasmanian rivers, covering the majority of Tasmania's land surface (Fig 5.2). While we describe overall changes to the 78 rivers, we focus on describing impacts on water allocations for the Rubicon, South Esk, and Little Swanport Rivers (Table 5.3). These rivers are important agricultural catchments in Tasmania, span a range of hydrological and climatological conditions, and have already been introduced in Chapter 4. Further description of the remaining 74 catchments is given by Bennett et al. (2010).

Table 5.2 Run-of-river power stations described in this study

Storage Name	Capacity (GL)	Power generation scheme
Lake Cethana	50	Mersey & Forth Rivers
Lake Pieman	300	Pieman River
Lake Trevallyn	12	Great Lake-Trevallyn
Meadowbank Lank	60	Derwent River

Sixty-two of the 78 river models (tan colour in Fig 5.2) were developed for the CSIRO Tasmania Sustainable Yields (TasSY) study. An additional sixteen catchments were added for this study (green coloured catchments in Fig 5.2). These 16 catchments are free-flowing rivers in remote areas that have negligible water extractions for human use and thus do not require complex water accounting rules. Accordingly, for these catchments river flow is equal to the aggregated runoff within the catchment area. The 62 TasSY river models were created byLing et al. (2009a, 2009b, 2009c, 2009d, 2009e). The river models aggregate runoff from the Simhyd runoff simulations (Chapter 4) to subareas and account for infrastructure (diversions and dams), water demands and water management rules current at 31 December 2007. Subareas vary in size, but are usually in the range of 25-50 km^2. Subareas are delineated according to points of interest to DPIPWE water managers. Each subarea is a calculation point, accounting for subarea runoff, any inflow from upstream, and any extractions, diversions and storages. The resulting outflow from a subarea is passed to downstream subareas along drainage lines.

Water extractions for agriculture and other uses are not consistently monitored in Tasmania. Water use in the TasSY models was estimated from DPIPWE water licensing information held on its Water Information Management System (WIMS) database. When water is allocated in Tasmania, both the volume of the allocation and the months during which this water may be extracted are specified. The actual rates of extractions vary, and are not monitored. The TasSY models assume that water allocation holders attempt to extract water at a single, average rate over those months when they are entitled to extract their allocation. This may be a crude simplification of how these systems are operated. Farm dams smaller than 1 ML do not need to be licensed in Tasmania. Estimates of the number of unlicensed small farm dams were made for the TasSY models using aerial photographs and Google Earth images. For calculation purposes, all unlicenced extractions are summed for each subarea, and the river models treat them as a single extraction from each subarea. Unlicensed water extractions are included in water extraction estimates for each sub-area, as described by Ling et al. (2009a, 2009b, 2009c, 2009d, 2009e). Infrastructure, water demands and water management rules vary from catchment to catchment. Details of each of the 62 TasSY river models are given by Ling et al. (2009a, 2009b, 2009c, 2009d, 2009e).

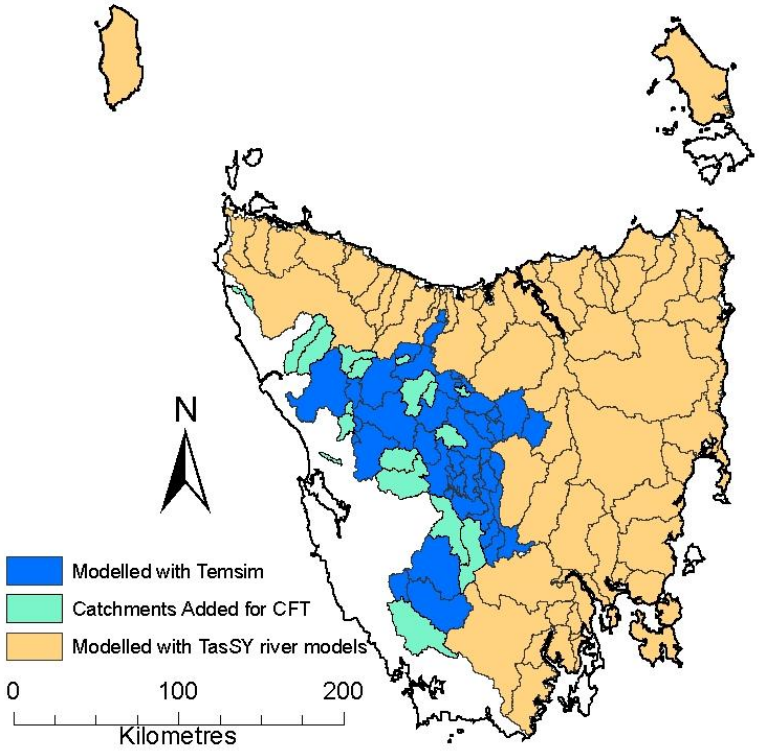

Fig 5.2 Catchments modelled for this study. Tan colour shows regions modelled with Tasmania Sustainable Yields (TasSY) river models. Regions modelled with Temsim are shown in blue. Green-coloured catchments are river models developed for this study. White areas are not covered by the river models.

Tasmanian water allocations are assigned a 'surety', which corresponds to the priority each allocation is accorded when demand for water is greater than supply. The TasSY models account for all water allocations and the priority they are accorded. To assess impacts on irrigators, we describe impacts on 'Surety 5' water allocations. Surety 5 is ascribed to water allocations for irrigation. It is accorded a lower priority than water allocated for domestic consumption. Surety 5 water is expected to be available at about 80 percent reliability. We describe changes in water allocations by calculating reliability of supply, as follows:

$$Reliability = (1 - \frac{Q_{Allocated} - Q_{Supplied}}{Q_{Allocated}}) \times 100\% \quad (5.1)$$

where $Q_{Allocated}$ is the total volume of water allocated for a given period, and $Q_{Supplied}$ is the total volume of water supplied over the same period. The TasSY models are configured so $Q_{Supplied}$ can never exceed $Q_{Allocated}$. This measure of reliability may be occasionally misleading, as a single dry year can dramatically decrease reliability,

Table 5.3 River summary characteristics (after Ling et al., 2009a, 2009b; Ling et al., 2009d)

River	Catchment area (km^2)	Rainfall (mm/yr)	Streamflow (GL/yr)	Extractions (GL/yr)
Little Swanport	875	640	127	3.1
Rubicon River	641	932	167	11.4
South Esk	3351	805	842	37.9

even if allocations are supplied in all other years. However, we calculate reliability over 30-year periods, reducing the impact of a single dry year on results. Further, acute droughts can have severe impacts on irrigators, particularly in regions where supply is generally reliable, and our calculation of reliability reflects these impacts.

5.3.1 Major irrigation storages

We describe changes to four major irrigation and water supply storages (Table 5.4). Changes to a further 10 storages are described by Bennett et al. (2010). Storages are modelled according to operating rules current at 31 December 2007. To be able to compare historical to future river flows, these operating rules were applied for the entire 140-year simulation (1961-2100). For example, construction of the Meander Dam was completed only in 2007, but the river models assume it has been in place since 1961. We calculate reliability of supply from these storages for water allocations of all sureties, following equation 5.1.

5.4 Impacts of changes to future runoff on the hydro-electric system

Historical and future inflows to Tasmania's hydro-electric system are shown in Fig 5.3. There has been an ongoing decline in observed inflows through the 20th century. Historical inflows are extrapolated from rainfall, streamflow and storage level observations. The observation network from which historical inflows is derived is not static (when more observations are available, they are used). Observations are particularly few before the 1950s (particularly in western Tasmania), and this introduces large uncertainties to the historical inflows for this period. Nonetheless, the clear decline in inflows from the 1960s can be considered a robust trend. Projections indicate that inflows will continue to decline through the 21st century, from ~47 GL/d (1961-1990) to ~43.3 GL/d (2070-2099), a decline of ~8%. Much of this decline occurs in the central highlands. The result is a decline in power generating capacity from an average of 9415 GWh/yr for 1961-1990 to 8857 GWh/yr for 2070-2099 (averaged across RCM simulations), a decline of ~6% (Fig 5.4). We note that the simulation that shows the driest future for much of the 21st century – MIROC3.2(medres) – is least adept of the six GCMs at simulating

Table 5.4 Irrigation storages described in this study

Storage Name	Capacity (GL)	Catchment	Operation described by
Lake Crescent/Sorell	80	Clyde	Ling et al (2009e)
Lake Leake	19	Macquarie	Ling et al (2009d)
Meander Dam	40	Meander	Ling et al (2009d)
Tooms Lake	21	Macquarie	Ling et al (2009d)

persistence characteristics in SSTs (Johnson et al., 2011), as we note in Chapter 2 (though we also note that this GCM simulates ENSO reasonably well as shown by van Oldenborgh et al., 2005). SST persistence characteristics may be important drivers of extended series of dry or wet years, and MIROC3.2(medres) may be the least reliable simulation of these characteristics.

Reduced inflows result in progressive declines in mean lake levels for large lakes in the hydro-electric system, including the two largest lakes, Lake Gordon and Great Lake (Fig 5.5). Inflows to Lake Gordon are not projected to change greatly, however the level in Lake Gordon declines as more water is used from this lake to compensate for reduced inflow to Great Lake and other power schemes. Lake Burbury, the third largest lake in the system, is fed by runoff from the King River on the western edge of the mountains. Rainfall in this already wet region is projected to increase through increased rainfall efficiency at lower altitudes in winter (discussed in Section 4.5), resulting in increases in mean lake levels by2100. Temsim keeps Lake Burbury at high levels to increase power generating efficiency through higher hydrostatic head, as this power station is more efficient when operated in this way. The efficiency of the Lake Gordon power station is less influenced by changes in hydrostatic head.

We note that the elevations that may be subject to increases in rainfall efficiency are somewhat uncertain, particularly in a region of steep topographic variation. A small change in the elevation experiencing increases in rainfall efficiency could have large implications for the hydro-electric system: if rainfall increases are limited to the coastal lowlands, then inflows to Lake Burbury could decrease; conversely, if rainfall increases extend further inland (and up slope), inflows to Lake Gordon may increase. We discuss assessment of uncertainties further in Chapter 6

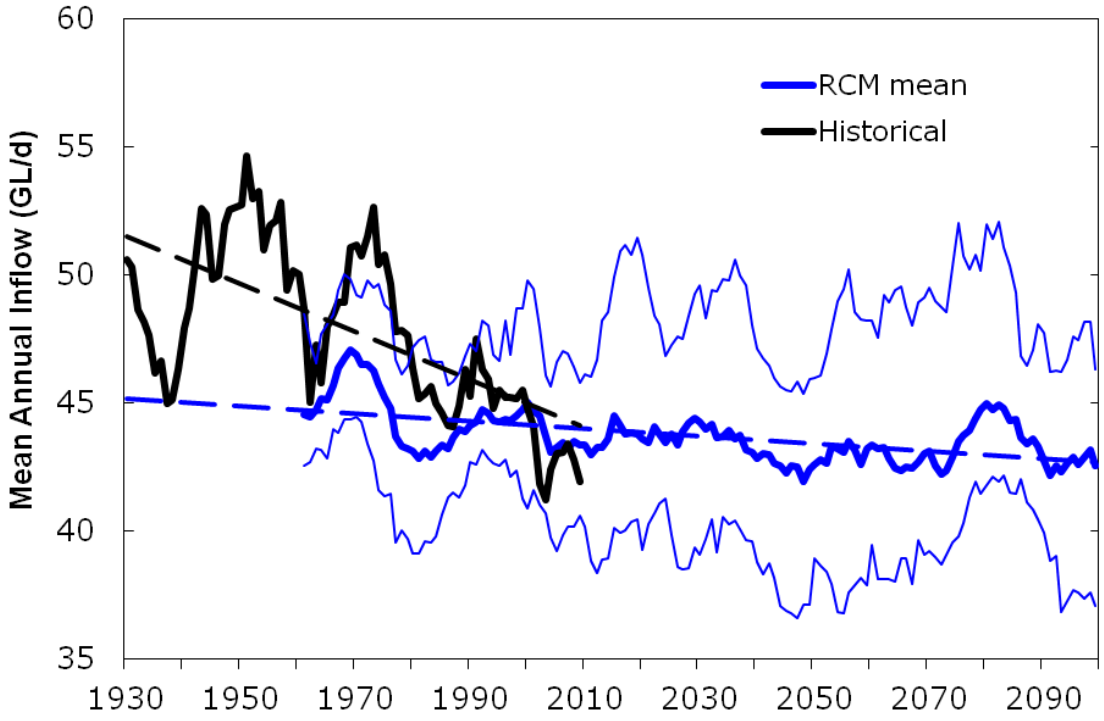

Fig 5.3 Observed and projected inflows to Hydro Tasmania catchments from 1930-2100. Curves are smoothed with an 11-year moving average. Black line shows synthesised inflow record provided by Hydro Tasmania, calculated from lake levels, power stations outflows and from regression relationships with streamflow and rainfall records. Lighter blue lines show range of RCM projections, dark blue line shows RCM mean. Dashed lines show linear trends of observed and simulated inflows.

Run-of-river power stations are affected by changes to variability of inflows as well as the quantity of inflows. Effects on run-of-river power stations are summarised in Fig 5.6 by the ratio of spill (water flowing over the dam wall) to power station discharge (water used for power generation). Fig 5.6 shows that spill:discharge ratios remain similar or increase by

2100. This is notable, as all the run-of-river storages shown are projected to experience decreased inflows. If there are no changes in inflow variability, we expect decreases in inflows either to have no effect on or to decrease spill:discharge ratios. This is because the ability for small storages to buffer variability in inflows improves as the ratio of storage capacity to inflows increases. What we see, however, is that the increases in high runoff events and interannual variability reported in Chapter 4 result in more spill being generated relative to power station discharge, even as inflows decrease. This is caused by the increases in runoff intensity in future climates reported in Chapter 4.

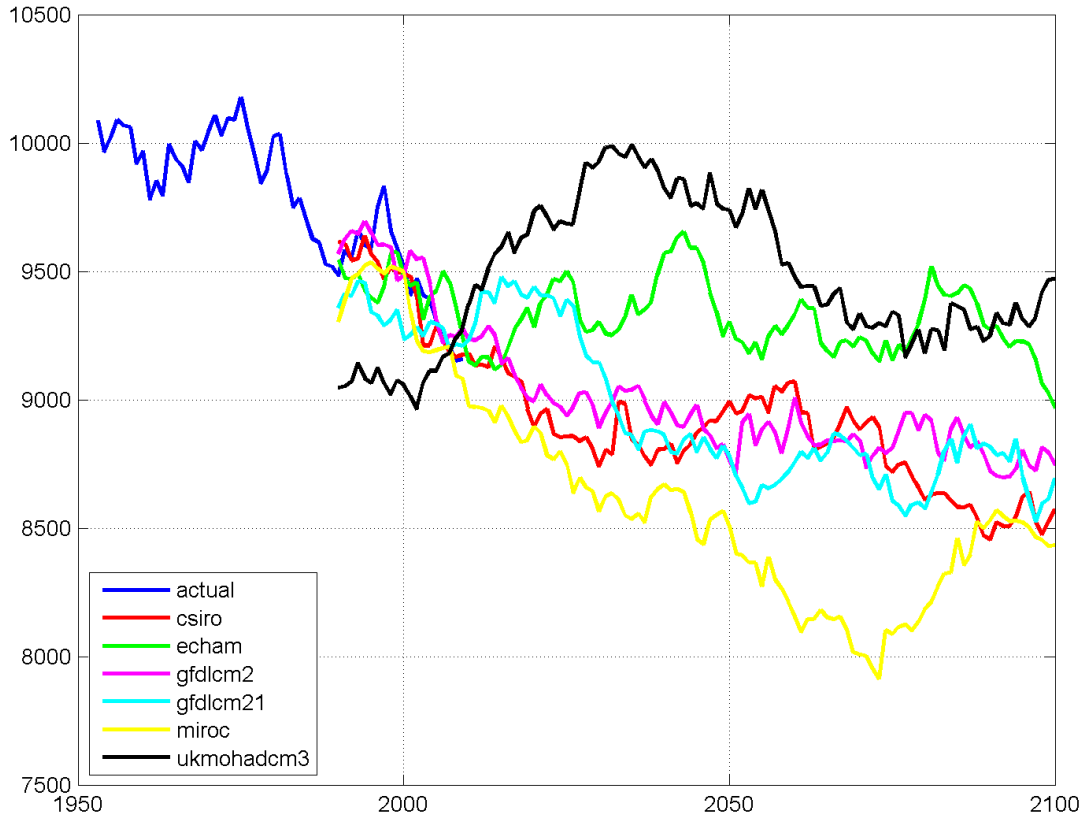

Fig 5.4 Average annual hydro-electric power generated by the Hydro Tasmania system (GWh/yr). Blue line shows historical power generating capacity synthesized from an historical inflows series generated by Hydro Tasmania. Other colours show power generation projected by individual RCM simulations. This figure was supplied by Hydro Tasmania, and is reproduced with permission.

5.5 Changes to flows in all river models

During the 21st century, there is a progressive rise in the number of rivers showing increased flows. This is largely an artifact of the large proportion of rivers modelled that are situated in eastern Tasmania. For the average of the RCM simulations, 64% of the 78 modelled catchments show a clear increase in streamflows by 2070-2099 (Fig 5.7a). These closely follow changes to runoff described in Chapter 4, as water extractions are typically small in relation to river flows in Tasmania. There are marked changes projected in annual flows for a number of rivers by 2070-2099. For the average of the RCM simulations, absolute changes to annual flows of more than 10% are projected for 32 of 78 catchments (40% of catchments) (Fig 5.7b). The changes from all RCM simulations range from 59 rivers changing by more than ±10% to 24 rivers change by more than ±10% (Fig 5.7b). Changes to flows for each catchment are given by Bennett et al. (2010).

.

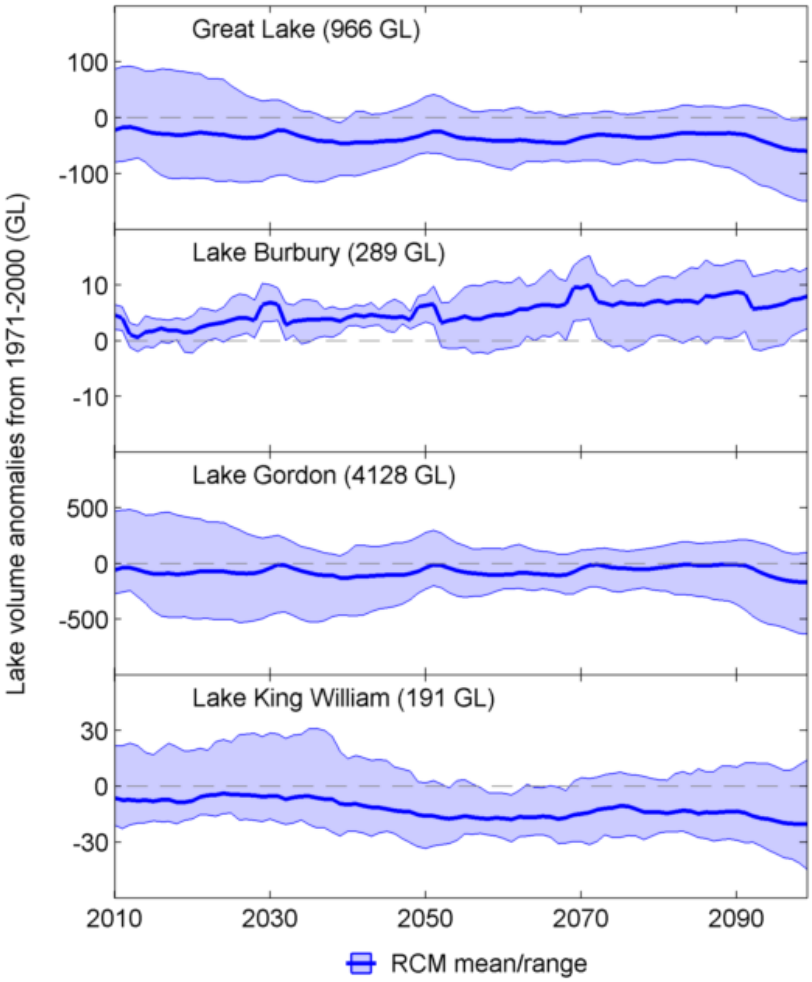

Fig 5.5 Projected lake level volumes anomalies for four large hydropower storages. Anomalies are calculated by 30-year average lake volumes less mean lake volume for 1970-2000. Dark blue line shows central estimate (mean) of six RCM simulations; confidence bands show range of RCMs. Numbers in brackets are mean effective volumes for 1970-2000 (where effective volume is water available for power generation, rather than total lake capacity).

5.6 Changes to the reliability of catchment water allocations

The mean reliability of surety 5 water allocations is projected to change little over the 21st century for the three catchments shown in Fig 5.9. Flows in the South Esk River are projected Little Swanport Rivers are projected to increase on average, and for these catchments interannual and daily variability of flows either does not change or decreases. Accordingly we expect reliability of water allocations to increase in these catchments. Fig 5.9 shows that there are essentially no changes in the reliability of Surety 5 allocations in either the Rubicon or Little Swanport catchments. This occurs because increases in streamflows are projected for months that have little impact on Surety 5 allocations in each catchment (not shown): in the Little Swanport catchment, no Surety 5

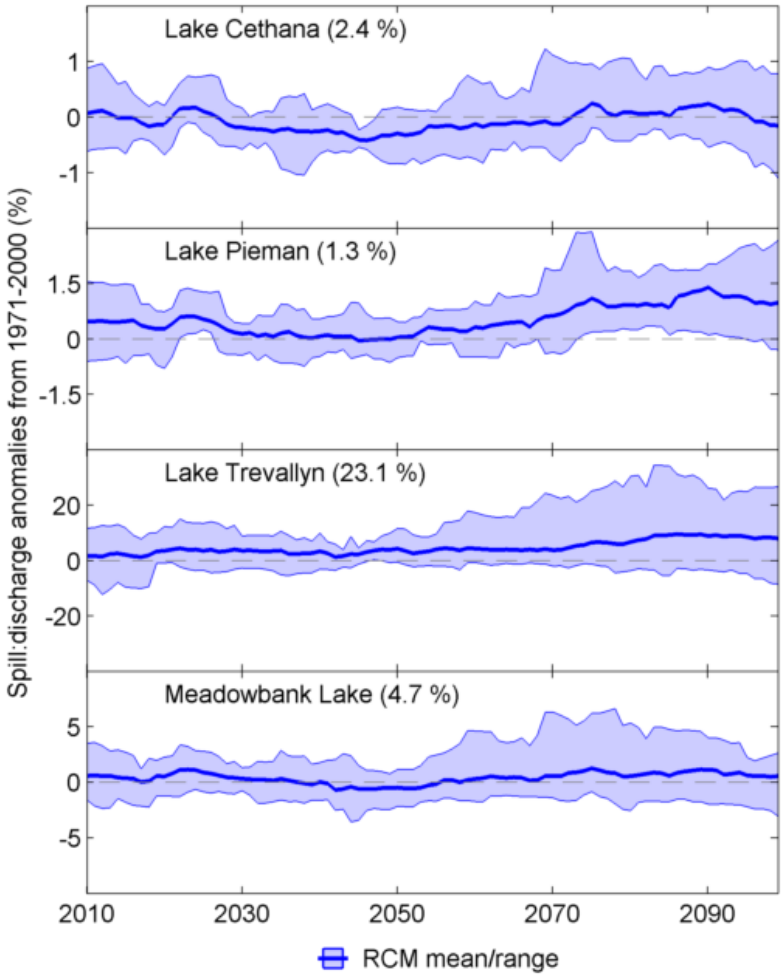

Fig 5.6 Changes in the ratio of spill to power station discharge for four run-of-river hydropower storages. Spill to discharge ratios are calculated by $Ratio = \frac{\sum Spill}{\sum Discharge}$ for 30-year periods, and anomalies are calculated by subtracting spill:discharge ratio for 1970-2000. Dark blue line shows the mean of the six RCM simulations; confidence bands show range of RCMs. Numbers in brackets are spill:discharge ratios for 1970-2000.

allocations exist for Jan-Mar, the period when flows are projected to increase most; projected flow increases in the Rubicon occur largely during the Austral winter of June-August, a period when existing Surety 5 allocations are already more than 90% reliable, leaving little scope to improve reliability in these months, and therefore overall reliability. The small changes to water allocation reliabilities serve to underscore the importance of prudent water management in Tasmanian catchments. Water management decisions such as when to grant water allocations are likely to have a far greater impact on flows than streamflow changes caused by climate change.

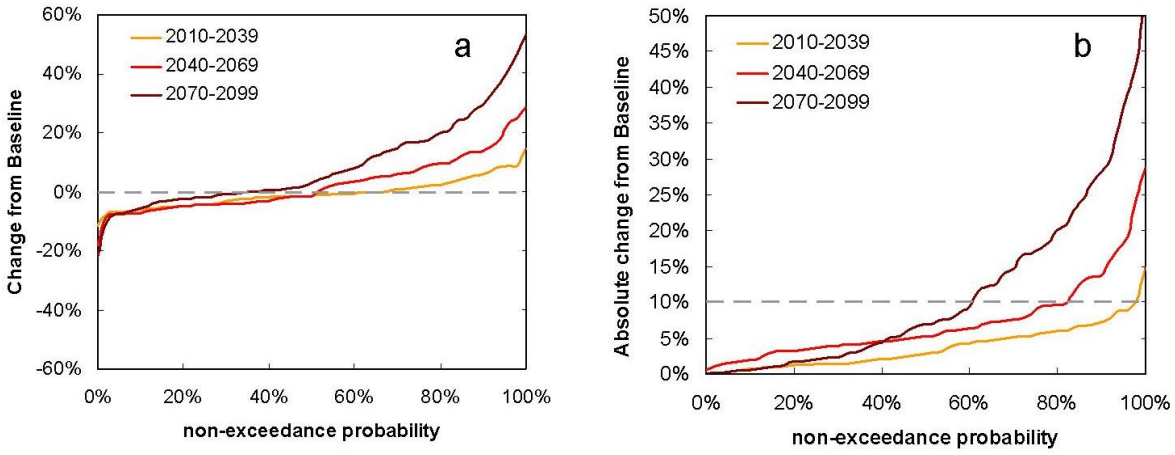

Fig 5.7 Non-exceedance probabilities of (a) percent change in river flow and (b) absolute percent change in river flow for 78 river catchments (mean of RCM simulations). Grey dashed lines show (a) no change and (b) 10% change.

5.7 Changes to inflows and reliabilities of large irrigation storages

Many catchments show changes at the subcatchment level in a future climate. These changes of river flow can affect water storage within a catchment depending on where subcatchment runoff changes occur. For example, the mean change in flow at the Clyde River catchment outlet is a projected increase of 13% by 2070-2099 (Fig 4.12). However, these increases are driven by increased runoff in the lower part of the catchment while annual inflows to Lake Crescent/Sorell at the head of the Clyde catchment – fed by runoff from the central highlands – decrease by 20% by 2070-2099 (Fig 5.11).

Four RCM simulations show that Lake Crescent/Sorell will be able to meet water demand less regularly, with the extreme case (MIROC3.2(medres)) showing a reduction in reliability of more than 60%. However, there is a wide range in the projections of reliability, with two RCM simulations showing little or no change. As we noted for the hydropower simulations, MIROC3.2(medres) may not simulate SST persistence in future as reliability as the other RCMs, and so should be treated with caution. Lake Crescent/Sorell (the two lakes form one water body) is operated as the major irrigation storage for the Clyde River, and offers an important buffer for farmers during drier years. Our projections suggest that it is likely to be less capable of fulfilling this function as reliably into the future.

Like the Clyde catchment, flows at the outlet of the Meander River decrease only slightly (-1.8% by 2070-2099), but inflows to Meander Dam (located at the head of the catchment) decrease by 12.6% (Fig 5.11a). The decrease in Meander Dam inflows has little effect on the reliability of supply, as demand from the Meander Dam is

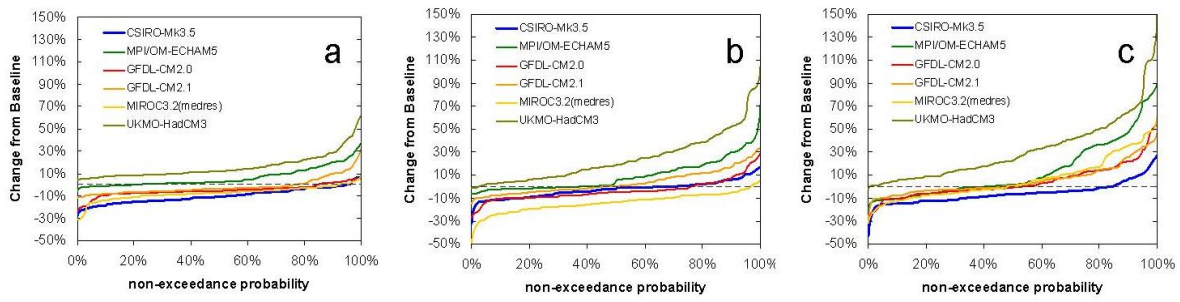

Fig 5.8 Number of catchments showing a given percent change in flows (expressed as non-exceedance probabilities) for all RCM simulations for (a) the near future (2010-2039), (b) the medium-term future (2040-2069) and (c) end-of-century (2070-2099). Grey dashed lines show no change.

substantially less than what is usually available, and this is also true in future despite decreased inflows. We note, however, that demand on Meander Dam has increased since this modelling was completed, and may increase more in future, leading to reduced reliability of supply.

Inflows to irrigation storages further to the east generally increase. Lake Leake and Tooms Lake show marked increases in inflows (Fig 5.10b,d), and this is true of other storages in the eastern catchments (Bennett et al., 2010). This improves the reliability of supply of the eastern storages, despite projected increases in the variance of interannual runoff in the east (Fig 4.13): Tooms Lake shows a slight increase in mean reliability by 2100, while Lake Leake maintains near 100% reliability for most projections. The small impact of increases in runoff variability on Tooms Lake and Lake Leake can be partly explained by the historical variability of runoff in the east of Tasmania, which has meant that these major storages have been sized to buffer this historical variability.

5.8 Discussion and conclusions

We have explored the impacts of climate change on the operation of Tasmania's hydro-electric system and irrigation storages and water allocations. Because the runoff simulations produced in this project realistically simulate the characteristics of historical runoff, we are able to use these outputs directly in hydro-electric system models and irrigation system models. This allows us to directly assess the impacts of projected spatial and seasonal changes in runoff, as well as changes in runoff intensity and variability.

Major irrigation storages fed by runoff from the central highlands are projected to experience decreases in runoff. The impacts this decline in runoff has on storages are conditioned by how the storages are managed. Lake Crescent/Sorell has a large demand on its water reserves relative to inflows. The ability of water reserves in

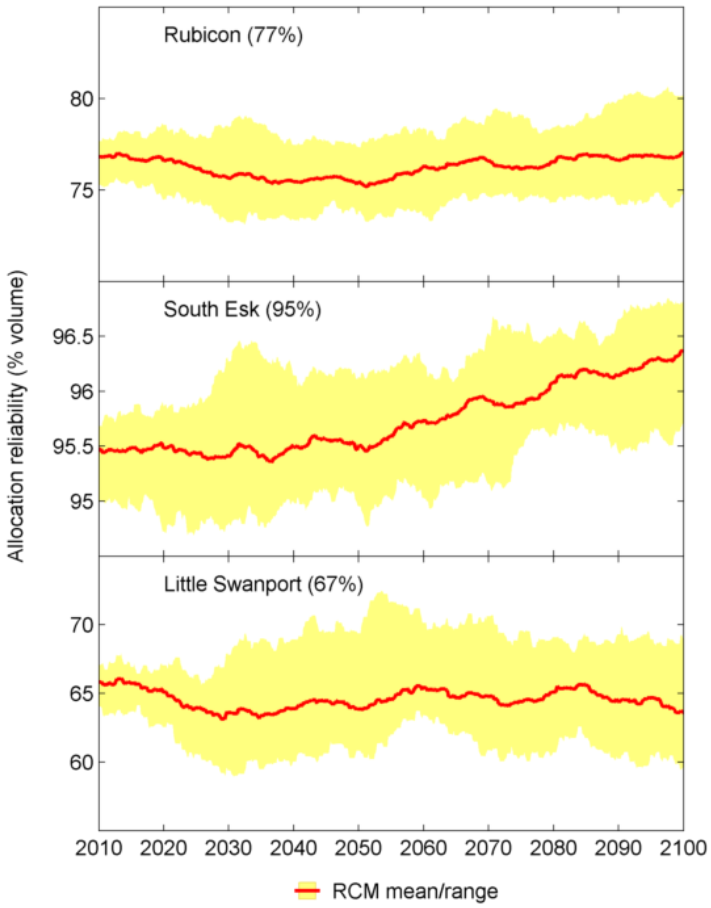

Fig 5.9 Reliabilities of surety 5 water allocations for three catchments. Reliability is defined as ratio of water supplied to water demand for a moving 30-year period. Red line shows the mean of six RCM simulations; confidence bands show range of RCMs. Numbers in brackets are mean Surety 5 water allocation reliabilities for 1961-1990.

Lake Crescent/Sorell to meet historical demand declines markedly under dry future climate scenarios. Conversely, Meander Dam is able to supply demand even under dry future climate scenarios, as historical demand on this storage is low compared to inflows. Water management also conditions the impacts of projected increases in streamflows on the reliability of water allocations in irrigation catchments. Increased streamflows do not necessarily improve the reliability of irrigation water allocations under current allocation rules, as seen in the Little Swanport and Rubicon catchments and Tooms Lake.

Actual reliabilities of Surety 5 water allocations may be greater than described in this study, because the TasSY models assume that water allocations are extracted at a constant daily rate. When streamflows fall below certain thresholds (defined differently for each catchment), water allocations cannot be extracted. Water allocation holders may, in reality, extract large quantities of water at times of high streamflow and store this water for use during times of lower streamflow when cease-to-take restrictions apply. Developing more sophisticated demand

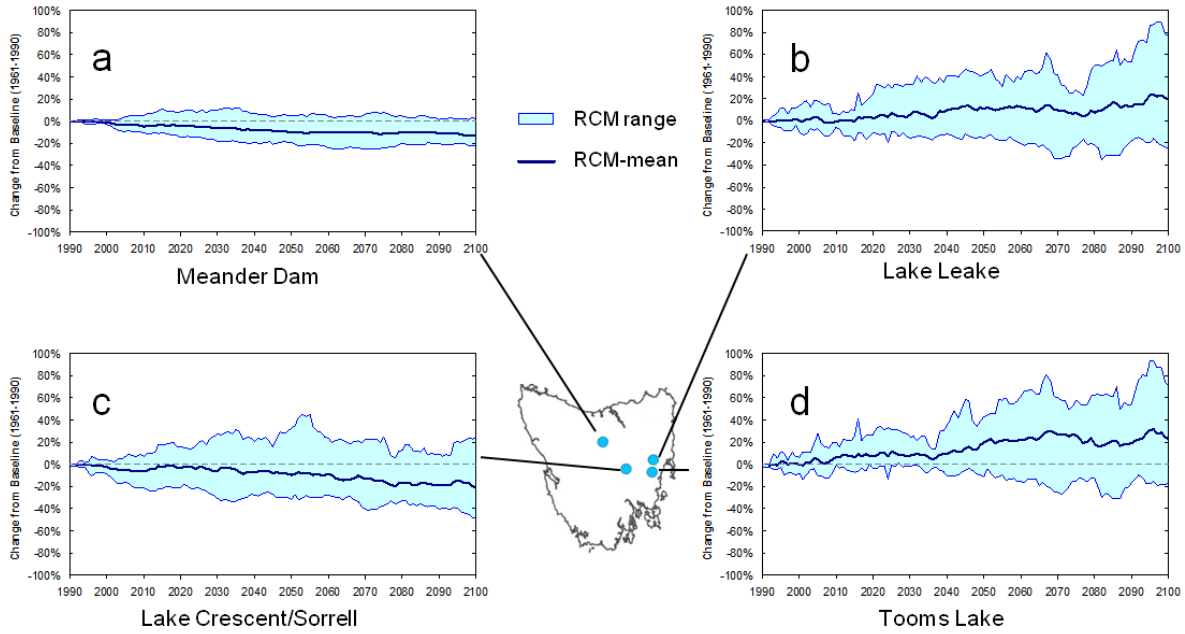

Fig 5.10 (a)-(d) Change in inflows to four large irrigation storages. Changes plotted are anomaly (%) of 30-year moving average inflows from average inflow during 1961-1990.

modelling (e.g. based on soil moisture accounting or on-farm water storage size) was outside the scope of this thesis. We have assumed that because operating rules are applied consistently in historical and future periods, the TasSY models will give a consistent account of climate change impacts on irrigation reliabilities. If more data on current rates of extraction of water allocations becomes available, future extractions may be modelled more accurately.

Impacts on the Tasmanian hydro-electric system are less equivocal, and indicate that generating capacity will decline. This is largely from declines in inflows, particularly over the central highlands, but also from increases in runoff variability, which results in more spill in relation to inflows in run-of-river hydropower schemes. This results in lower water volumes in large hydropower storages, on average. Several of these storages are important habitats for native fauna, particularly endemic fish, and minimising any deleterious impact on endemic species may require additional management (see review by Morrongiello et al., 2011).

Declines in generating capacity are not simply because of the overall reduction in inflows, but also because of the spatial distribution of changes to inflows and increased variability in inflows. Declines to inflows to Great Lake have a serious impact on power generation, because these catchments feed Poatina power station - a high-capacity (300 MW), large hydrostatic-head (900 m) power station. Because of the large hydrostatic head, this

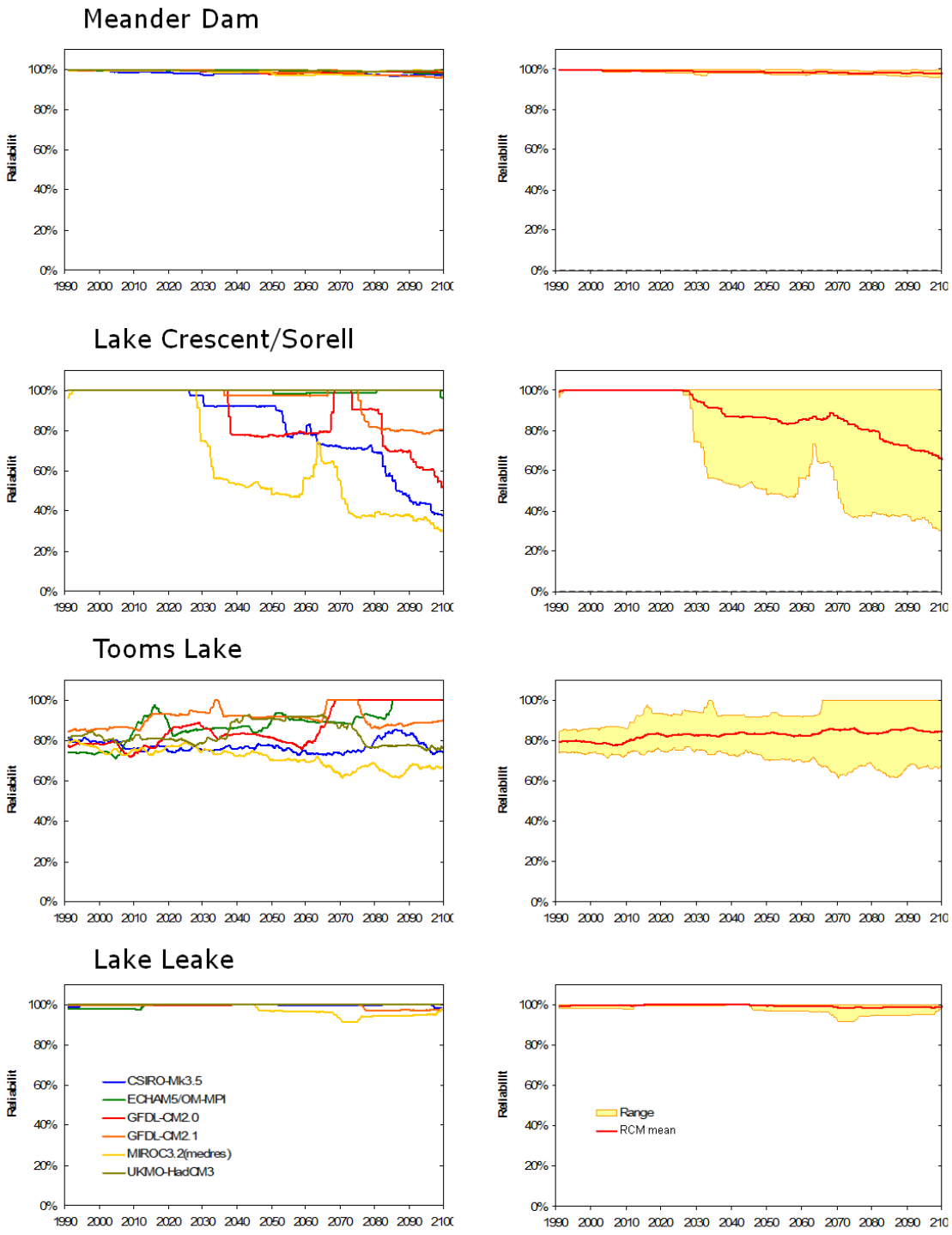

Fig 5.11 Reliabilities of supply for four example large-irrigation storages. Reliability is defined as ratio of water supplied to water demanded for a moving 30-year period. Plots on left give change for each RCM simulation, plots on right show changes to RCM mean and range.

power station produces a very large amount of power per unit volume of water, meaning that small declines in water volumes lead to large declines in power generation. This reduction affects the remainder of the Hydro Tasmania system, for example by reducing storage levels in Lake Gordon, which is used to compensate for the reduced Great Lake generation, even though there are only small reductions in annual inflows to Lake Gordon.

The decreases in power generating capacity (~6%) are slightly less than decreases in inflows (~8%) where we would expect the reverse, given the importance of hydropower storages that suffer decreases in inflow. This indicates that the hydro-power system is able to offset losses in power stations fed by the central highlands.

We have not examined the effect of long-term persistence characteristics of precipitation – for example the tendency of dry years to occur simultaneously – and any influence this has on hydropower storages. Such long dry or wet spells can have a strong influence on hydrological changes (Johnson and Sharma, 2011), and could dramatically affect the ability large storages to buffer inflows: for example, the long dry period extending from 1996-2008 resulted in record low lake levels in the Great Lake and Tasmania became a net importer of electricity for the latter part of this period. We selected our GCMs partly on their strong ability to simulate ENSO, and a subsequent study has found that five of the six GCMs we chose reproduced SST persistence characteristics very well in relation to other GCMs at a range of time scales (Johnson et al., 2011) (see Chapter 2). Further, there is generally a strong relationship between a GCM's ability to represent SST persistence characteristics and its ability to represent precipitation persistence (Johnson et al., 2011), but this has not been explicitly tested for CCAM. We caution that the representation of precipitation persistence characteristics is a potential weakness of our study, and our findings should be interpreted in this light.

We note that impacts on the hydro-electric system are more readily apparent than on irrigated agriculture partly because operation of the hydro-electric system is heavily optimised in order to be as profitable as possible. Irrigation storages are often operated to maintain high storage levels in order to buffer unforeseen dry periods that may occur in future: for example, water allocations from storages are often restricted in certain months. This conservative operation means irrigation storages are able to buffer future increases in variability in inflows better than hydro-electric storages. Nonetheless, the overall impact projected for Tasmanian hydro-electric power generation (a reduction of 6% in generating capacity) appears to be moderate in comparison to other regions. This is particularly true of regions where projected changes in seasonal snow-melt can have a large effect, for example a 36% decline in power generating capacity reported for Switzerland (Schaefli et al., 2007) or a >20% decline projected for the American Pacific North-West by a majority of climate models evaluated by Markoff and Cullen (2008).

We have represented uncertainty in projections of hydropower generation and irrigation reliabilities with ranges of RCM simulations. More rigorous treatment of uncertainties have been proposed that attempt to account for uncertainties in different tiers of impact and climate models (e.g. Schaefli et al., 2007). We have shown in Chapter 4 that uncertainties in the RCM simulations largely subsume uncertainties from a range of hydrological models. Further, both Temsim and the TasSY river models generate essentially linear responses to inputs; that is,

they do not respond chaotically to changes in inputs or initial conditions as climate models do, and accordingly these models are unlikely to be a significant source of uncertainty in their present configurations (Teng et al., 2012). As we have already remarked, however, the management and operation of these systems plays a crucial part in any impacts that changes in inflow may have. We have chosen to apply a fixed set of operating rules based on historical habit to these systems. This assumption is almost certain to lapse, even in the near future, and therefore our range of uncertainty is likely to underestimate – quite possibly grossly underestimate – the uncertainty in future impacts on hydropower and irrigation systems in Tasmania. A more comprehensive treatment of uncertainties – for example by including a range of possible adaptive management strategies – is outside the scope of this thesis. We offer possible strategies to improve uncertainty estimates in the final chapter of this thesis.

In this chapter we have used the CCAM-Simhyd hydroclimate projections described in Chapter 4 as direct inputs into hydropower and irrigation system models. This allows the combined effects of projected changes in the spatial distribution of runoff, in the seasonal distribution of runoff, in the variance of runoff and in the intensity of runoff to be accounted by the impact models, and as a result gives water managers the most plausible and coherent future impact scenarios possible.

6 Summary and conclusions

The main scientific outcomes of the work presented in this thesis are:

- Assessment of the value added to GCM simulations by a recent generation regional climate model for producing high-resolution projections for Tasmania (Chapter 2)
- Development and testing of a bias-correction method to enable regional climate model outputs to be used as direct inputs to conceptual rainfall-runoff models (Chapter 3 and Appendix A). We show that the bias-correction is effective in correcting the full statistical distribution of RCM rainfall outputs, while biases in spatial and temporal characteristics of rainfalls are not corrected.
- The first high-resolution (5 km) projections of runoff for Tasmania to 2100, from an ensemble of regional climate simulations and rainfall-runoff models (Chapter 4).
- Further evidence that the chaotic fluctuations of climate simulations are a far greater source of uncertainty in hydroclimate projections than differences in hydrological models.
- Assessment of changes to spatial distributions and variability of runoff over Tasmania by 2100 (Chapter 4). These changes include marked decreases (up to 30%) in runoff over the central highlands in all seasons; increases in runoff in the eastern lowlands; decreases in summer runoff and increases in winter runoff over western Tasmania; increases in runoff intensity over most of Tasmania; increases in daily and annual runoff variability over most of Tasmania.
- Assessment of impacts of future changes to runoff on hydropower generation and irrigation water allocations in Tasmania (Chapter 4 and Appendix B). We report a decrease in overall hydropower generating capacity of 6%, mainly caused by declines in inflows to hydropower storages fed by the central highlands.

The work presented in this thesis forms the core of two scientific papers: one published in the international journal Hydrology and Earth System Sciences (Bennett et al., 2012) and the other published in the International Journal of Climatology (Bennett et al., 2013). In addition, this work contributes to three other scientific papers published in international scientific journals (Corney et al., 2013; Grose et al., 2013b; Morrongiello et al., 2011).

This work substantially increases our understanding of the possible impacts of climate change on surface water availability in Tasmania. This work has generated the first high-resolution projections of surface water for Tasmania to 2100. The study was designed so that projections would be able to be used directly in impact models used by Tasmania's two largest water managers: the Department of Primary Industry, Parks, Water and Environment and Hydro Tasmania.

Chapter 2 describes the high-resolution projections that are the foundation of this work. The use of the global, stretched grid model, CCAM, to downscale GCM projections allows the bias-correction of GCM SSTs before

downscaling. This substantially improves the simulation of precipitable water and rainfall. The high horizontal resolution of CCAM over Tasmania significantly improves the representation of Tasmanian topography, resulting in much more realistic representation of rainfall distribution over Tasmanian catchments. Chapter 2 shows that the spatial representation of rainfall over Tasmania by CCAM is better than the spatial representation of rainfall over Australia by the host GCMs.

Chapter 3 describes the quantile mapping bias-correction applied to the RCM simulations. The bias-correction aligns modelled and observed frequency distributions of daily data. It is distinguished from similar methods by using empirical frequency distributions, by being trained independently for each season, and by being applied to de-trended simulations. The bias-correction effectively removes biases across the frequency distributions of RCM variables. However, biases in temporal characteristics of rainfall – notably the tendency of CCAM to underestimate large, multi-day rainfalls – are not corrected by the quantile mapping. The season-specific corrections and the use of empirical frequency distributions introduces the possibility that the quantile-mapping will be over fitted, and therefore not perform reliably when applied outside the training period. A new technique, ensemble cross-validation, shows that the bias-correction is not over fitted, and thus is likely to perform well outside the training period. This is further demonstrated by the strong agreement between projected trends of uncorrected and bias-corrected rainfalls. The tendency of the bias-correction to disrupt physical relationships between RCM variables is investigated for simulations of past and future climates. The bias-correction had only a minimal effect on the physical relationships between RCM variables.

Chapter 4 describes the simulations of Tasmanian runoff and river flows to 2100. Simulations are generated by forcing five different conceptual rainfall-runoff models with bias-corrected RCM rainfall and potential evaporation. This method explicitly accounts for changes in rainfall variability, rainfall intensity, seasonal rainfall distributions, and spatial distributions of rainfall, as well changes to evaporation, in simulations of runoff. Historical simulations of river flows with the AWBM and Simhyd hydrological models forced by bias-corrected CCAM outputs agreed closely with observed streamflows. Hydrological models that were more sensitive to changes in inputs, in particular the IHACRES model, produced biased streamflow simulations. A slight tendency to underestimate streamflow magnitudes was present even in the best performing hydrological models (AWBM and Simhyd), and this is explained by the tendency of CCAM to underestimate the magnitude and the frequency of multi-day rain events, described in Chapter 3. Changes to spatial and seasonal runoff distributions are described, including increases in the inter-annual variability in runoff, increases in large runoff events for most of Tasmania, and decreased summer runoff over western Tasmania. The most pronounced feature of the runoff simulations are the decline in runoff over the central highlands in all seasons by 2100. Runoff from this region is economically important for hydropower generation and irrigated agriculture. In addition, this region has high conservation values, including serving as habitat to several species of endemic freshwater fish.

Chapter 5 presents the effects of runoff changes on hydropower generation and irrigation water allocations. Impacts on hydropower are assessed with Temsim, Hydro Tasmania's system model. This chapter describes the

projected 6% decline in hydropower generating capacity in Tasmania, resulting principally from projected runoff reductions in the central highlands. Chapter 5 shows that increased variability in runoff had an effect on hydropower generation, causing increased spill from run-of-river hydropower storages in relation to power station outflow, even as total inflows decreased. The reliability of supply of water allocated for irrigation is investigated in Chapter 5 with water accounting models that apply historical demand rules under future climate scenarios. The reliability of water supplied from large irrigation storages is influenced both by demand and by changes to inflows. For example, Meander Dam and Lake Crescent/Sorell are both supplied by runoff from the central highlands. Future reliability of supply of Lake Crescent/Sorell declines. Conversely the reliability of water supplied by Meander Dam is not affected by the decline in inflows because historical demand on this storage is low compared to supply (though demand on Meander Dam is very likely to increase in future). This underscores the importance of prudent water management and planning in Tasmania, particularly in light of attempts to increase the value of irrigated agriculture and the probable increases to the interannual variability of streamflows.

6.1 Confidence and uncertainty in hydro-climate projections

Uncertainty in hydro-climate simulations emanates from many sources, including estimates of future greenhouse gas concentrations, imperfectly understood or imperfectly represented climate processes in GCMs and RCMs, as well as the bias-correction and hydrological modelling. The uncertainty of future human emissions is typically handled using a scenario approach, and this approach is taken here.

Throughout this thesis the range of climate simulations for a given emissions scenario is used as the principal estimate of uncertainty in the hydro-climate projections, following many other studies (e.g. IPCC AR4). This is partly justified if the uncertainty described by the range of climate simulations largely encapsulates other sources of uncertainty, including the hydrological modelling and the bias-correction. We have shown that uncertainties from the range of climate simulations are much larger than the uncertainties from an ensemble of conceptual rainfall runoff models, echoing findings by other studies (e.g. Prudhomme and Davies, 2009; Wilby and Harris, 2006). In addition, we have shown that trends in the bias-corrected RCM variables are very similar to trends in the uncorrected variables, showing that uncertainties introduced by the bias-correction are also small in relation to the range of the climate simulations, as found by Chen et al. (2011).

However, the range of uncertainties we describe is unlikely to reflect the true range of uncertainty in these projections for a given emissions scenario. This is in part due to limitations in horizontal and spatial resolution of even the high-resolution climate simulations presented here. This can be illustrated by considering fine-scale spatial changes in rainfall. CCAM strongly underestimates the rain shadow over the Tamar Valley in the north of Tasmania in the 10 km simulations, resulting in rainfall biases of more than 100% (Chapter 1). The projected changes in the spatial distribution of rainfall and runoff presented in this thesis are often related to elevation: all six RCM simulations project rainfall/runoff decreases in the central highlands and rainfall increases in the Tamar valley to the north-east, and the simulations generally show strong agreement on the location of the boundary

between the drying and wetting regions (Fig 4.11a). If we rely only on the range of climate simulations to describe the range of uncertainty, we would place a high confidence on the location of this wetting-drying boundary. In light of the inability of CCAM to represent the steep rainfall gradient in this region effectively, this level of confidence is likely to be too high. Other resolution-dependent changes, including land-sea boundaries, are subject to similar uncertainties.

It is worthwhile to consider as many lines of evidence as possible when assigning confidence to hydroclimate projections. For example, additional climate simulations with another RCM (not possible due to time and cost constraints) would have added another line of evidence and strengthened the conclusions of this study. An additional RCM would have offered alternative parameterisation schemes and algorithms, and possibly different horizontal and temporal resolutions. The choice of RCM has been shown to contribute significant uncertainties to hydroclimate simulations, although RCMs are generally a smaller source of uncertainty than the driving GCMs (Kendon et al., 2010b). In the absence of additional RCM simulations, the confidence in projected changes can also be fortified by comparison to theoretical dynamical and thermodynamical changes. It is also possible to assess the plausibility of local changes by gathering evidence from wider-scale changes projected by CCAM. This is unusually straightforward in a variable resolution RCM, because regional and global atmospheric changes cohere with local projections as they are simulated by the same atmospheric model. The coherence of regional changes with local changes in the CCAM simulations has been investigated by Grose et al. (2013a) and Grose et al. (2013b). Drawing various lines of evidence together allows us to qualitatively assign very high confidence to the following projected changes in Tasmanian hydrology by 2100:

- **Increases in potential evaporation for all of Tasmania**, projected by all six RCM simulations. Increases in potential evaporation are strongly tied to increases in temperature in temperate regions, and these increases are supported by recent observed trends and climate studies. Increased evaporation magnifies the effects of any reductions in rainfall on runoff. In addition, more water can be expected to be evaporated from standing water bodies such as large hydropower or irrigation storages.
- **Summer reductions in rainfall and runoff in western Tasmania**, projected by all six RCM simulations. This is associated with a southward shift in the subtropical ridge of high pressure simulated by CCAM (Grose et al., 2013b), which causes moist westerly air to be pushed further south. This southward shift is a manifestation of the poleward expansion of the Hadley cell, which has strong empirical, modelled and theoretical support as a consequence of global warming (Chapter 1). One notable consequence of the decline in western summer rainfall is that seasonal periods of low flow will experience lower flows. Much of western Tasmania is covered by a thin layer of soil, providing little subsurface water storage. This means baseflows are unlikely to buffer projected decreases in summer rainfall, resulting in lower flows during dry periods.
- **Winter increases in rainfall and runoff in western Tasmania**, projected by most CCAM simulations and also present in most GCMs. In contrast to summer, the mid-latitude westerly circulation is projected to strengthen and not move markedly pole-ward in this season (Grose et al. 12013b), leading

to a greater incidence of rain-bearing systems crossing western Tasmania. This generally leads to increases in soil moisture and runoff in this season.

- **Increases in rainfall and runoff intensity for many regions of Tasmania**, projected by all six RCM simulations. Increases in rainfall intensity in temperate climates with increased temperature have a strong basis in theory, climate model studies and recent observations (see Chapter 1). The increases in rainfall intensity drive even larger increases in runoff intensity, as proportionately more water flows into rivers under more intense rainfall.

More inclusive, formally quantified uncertainties in hydro-climate projections are also possible, if somewhat difficult. A common approach in shorter-term probabilistic hydrometeorological forecasts is to ensure the forecasts are 'well-calibrated' or statistically 'reliable' (Toth et al., 2003). A probabilistic forecast is well-calibrated if forecast probabilities align with observed frequencies of occurrence. For example, for a well-calibrated forecast, if a forecast probability of 70% is assigned to an event, this event will actually occur 70% of the time in the historical record (and *does not* occur 30% of the time). Forecasts can be calibrated after they are issued, by increasing (or reducing) the spread of uncertainty to align with historical observations (e.g. Schepen, 2012). There are many barriers to calibrating hydro-climate projections in this way, including (but not limited to): 1) effectively calibrating forecasts requires very long historical simulations and observation records; 2) calibration methods have been traditionally applied to forecasting models, which are synchronous with observations (unlike climate models); and 3) calibrations reflect historical uncertainties, not possible future uncertainties. Devising such a calibration is outside the scope of this thesis; however, the concept of a well-calibrated hydro-climate forecast is highly attractive, and deserves future attention.

6.2 Suggested further work

We suggest the following work to build on this study:

- The tendency of CCAM to underestimate the incidence and magnitude of multi-day rainfall events could be investigated and improved. Improvements in the representation of rainfalls will improve streamflow simulations.
- The ability to simulate long-term persistence characteristics in rainfall could have significant impacts on water resources assessments (Johnson and Sharma, 2011), and investigating CCAM's ability to represent rainfall persistence characteristics on a range of time scales would add insight to the investigation of future surface water availability in Tasmania presented in this thesis.
- The CCAM 10 km outputs are generated at a 6-minute time step, and CCAM rainfall outputs have been saved at 3-hour intervals. This admits the possibility of investigating the impacts of future climate change on sub-daily rainfall and runoff, and in particular on the possible impacts on flooding in Tasmanian catchments.
- Graham et al. (2009) quantified the environmental implications of changed stream flows for the TasSY project. Outputs from our modelling are directly compatible with the software Graham et al. (2009)

used to quantify environmental impacts, and this work could be extended using modelling outputs from our study.

- Additional case studies that combine the hydrological assessments presented here with other analyses carried out using CCAM outputs. For example, assessments of changes to agricultural productivity carried out by Holz et al. (2010) could be paired with more detailed analyses of water reliabilities to assess the viability of agricultural development in particular basins or regions.

References

Akhtar M, Ahmad N, Booij MJ. 2009. Use of regional climate model simulations as input for hydrological models for the Hindukush-Karakorum-Himalaya region. *Hydrology and Earth System Sciences* **13:** 1075–1089. DOI: 10.5194/hess-13-1075-2009.

Alexander LV, Zhang X, Peterson TC, Caesar J, Gleason B, Klein Tank AMG, Haylock M, Collins D, Trewin B, Rahimzadeh F, Tagipour A, Rupa Kumar K, Revadekar J, Griffiths G, Vincent L, Stephenson DB, Burn J, Aguilar E, Brunet M, Taylor M, New M, Zhai P, Rusticucci M, Vazquez-Aguirre JL. 2006. Global observed changes in daily climate extremes of temperature and precipitation. *Journal of Geophysical Research-Atmospheres* **111:** 22. DOI: 10.1029/2005JD006290.

Allan RP, Soden BJ. 2008. Atmospheric warming and the amplification of precipitation extremes. *Science* **321:** 1481-1484. DOI: 10.1126/science.1160787.

Allen MR, Ingram WJ. 2002. Constraints on future changes in climate and the hydrologic cycle. *Nature* **419:** 224-232. DOI: 10.1038/nature01092.

Allison I, Alley RB, Fricker HA, Thomas RH, Warner RC. 2009. Ice sheet mass balance and sea level. *Antarctic Science* **21:** 413-426. DOI: 10.1017/S0954102009990137.

Arrhenius S. 1896. On the influence of carbonic acid in the air upon the temperature of the ground. *The London, Edinburgh and Dublin Philosophical Magazine and Journal of Science* **5:** 237–276

Ashfaq M, Skinner CB, Diffenbaugh NS. 2010. Influence of SST biases on future climate change projections. *Climate Dynamics* **36:** 1303-1319. DOI: 10.1007/s00382-010-0875-2.

Australian Bureau of Statistics. 2012. Gross value of irrigated agricultural production, 2010-11, catalogue number 4610.0.55.008. Australian Bureau of Statistics: Canberra. Available online at http://www.abs.gov.au/. Accessed: May 2013.

Bastola S, Murphy C, Sweeney J. 2011. The role of hydrological modelling uncertainties in climate change impact assessments of Irish river catchments. *Advances in Water Resources* **34:** 562-576. DOI: 10.1016/j.advwatres.2011.01.008.

Bennett JC, Grose MR, Post DA, Ling FLN, Corney SP, Bindoff NL. 2011. Performance of quantile-quantile bias-correction for use in hydroclimatological projections. *MODSIM2011, 19th International Congress on Modelling and Simulation*. Modelling and Simulation Society of Australia and New Zealand: Perth. Available online at http://www.mssanz.org.au/modsim2011/F5/bennett.pdf. Accessed: Jan 2013.

Bennett JC, Grose MR, Corney SP, White CJ, Holz GK, Katzfey JJ, Post DA, Bindoff NL. 2013. Performance of an empirical bias-correction of a high-resolution climate dataset. *International Journal of Climatology***:** published online. DOI: 10.1002/joc.3830.

Bennett JC, Ling FLN, Post DA, Grose MR, Corney SP, Graham B, Holz GK, Katzfey JJ, Bindoff NL. 2012. High-resolution projections of surface water availability for Tasmania, Australia. *Hydrology and Earth System Sciences* **16:** 1287-1303. DOI: 10.5194/hess-16-1287-2012.

Bennett JC, Ling FLN, Graham B, Corney SP, Holz GK, Grose MR, White CJ, Post DA, Gaynor SM, Bindoff NL. 2010. Climate Futures for Tasmania: water and catchments. Antarctic Climate and Ecosystems Cooperative Research Centre: Hobart. Available online at http://www.climatechange.tas.gov.au/government_action/climate_futures/.

Berbery EH, Fox-Rabinovitz MS. 2003. Multiscale Diagnosis of the North American Monsoon System Using a Variable-Resolution GCM. *Journal of Climate* **16:** 1929-1947. DOI: 10.1175/1520-0442(2003)016<1929:MDOTNA>2.0.CO;2.

Berg P, Wagner S, Kunstmann H, Schädler G. 2013. High resolution regional climate model simulations for Germany: part I—validation. *Climate Dynamics* **40:** 401-414. DOI: 10.1007/s00382-012-1508-8.

Berg P, Haerter JO, Thejll P, Piani C, Hagemann S, Christensen JH. 2009. Seasonal characteristics of the relationship between daily precipitation intensity and surface temperature. *Geophysical Research Letters* **114:** D18102. DOI: 10.1029/2009JD012008.

Boberg F, Christensen JH. 2012. Overestimation of Mediterranean summer temperature projections due to model deficiencies. *Nature Clim. Change* **2:** 433-436. DOI: 10.1038/nclimate1454.

Boé J, Terray L. 2007. A weather-type approach to analyzing winter precipitation in France: twentieth-century trends and the role of anthropogenic forcing. *Journal of Climate* **21:** 3118-3133. DOI: 10.1175/2007JCLI1796.1.

Boé J, Terray L, Habets F, Martin E. 2007. Statistical and dynamical downscaling of the Seine basin climate for hydro-meteorological studies. *International Journal of Climatology* **27:** 1643-1655. DOI: 10.1002/joc.1602.

Boughton WC. 2004. The Australian water balance model. *Environmental Modelling & Software* **19:** 943-956. DOI: 10.1016/j.envsoft.2003.10.007.

Burnash RJC, Ferral RL, McGuire RA. 1973. A generalized streamflow simulation system-conceptual modeling for digital computers. Joint Federal and State River Forecast Center: Sacramento.

Buser CM, Künsch HR, Lüthi D, Wild M, Schär C. 2009. Bayesian multi-model projection of climate: bias assumptions and interannual variability. *Climate Dynamics* **33:** 849-868. DOI: 10.1007/s00382-009-0588-6.

Charles SP, Bari MA, Kitsios A, Bates BC. 2007. Effect of GCM bias on downscaled precipitation and runoff projections for the Serpentine catchment, Western Australia. *International Journal of Climatology* **27:** 1673-1690. DOI: 10.1002/joc.1508.

Charles SP, Silberstein R, Teng J, Fu G, Hodgson G, Gabrovsek C, Crute J, Chiew FHS, Smith IN, Kirono DGC, Bathols JM, Li LT, Yang A, Donohue RJ, Marvanek SP, McVicar TR, Van Niel TG, Cai W. 2010. Climate analyses for south-west Western Australia. A report to the Australian Government from the CSIRO South-West Western Australia Sustainable Yields Project. CSIRO: Australia. Available online at http://www.clw.csiro.au/publications/waterforahealthycountry/swsy/pdf/SWSY_Climate_TechRpt.pdf.

Chen C, Haerter JO, Hagemann S, Piani C. 2011. On the contribution of statistical bias correction to the uncertainty in the projected hydrological cycle. *Geophysical Research Letters* **38:** L20403. DOI: 10.1029/2011GL049318.

Chiew FHS, Peel MC, Western AW. 2002. Application and testing of the simple rainfall-runoff model SIMHYD. *Mathematical models of small watershed hydrology and applications*, V. P. Singh and D. K. Frevert, Eds. Water Resources Publications: Littleton, USA, 335–367.

Chiew FHS, Teng J, Vaze J, Post DA, Perraud JM, Kirono DGC, Viney NR. 2009. Estimating climate change impact on runoff across southeast Australia: Method, results and implications of the modeling method. *Water Resources Research* **45:** W10414. DOI: 10.1029/2008WR007338.

Chiew FHS, Kirono DGC, Kent DM, Frost AJ, Charles SP, Timbal B, Nguyen KC, Fub G. 2010. Comparison of runoff modelled using rainfall from different downscaling methods for historical and future climates. *Journal of Hydrology***:** 10-23. DOI: 10.1016/j.jhydrol.2010.03.025.

Chou C, Neelin JD. 2004. Mechanisms of global warming impacts on regional tropical precipitation. *Journal of Climate* **17:** 2688–2701. DOI: 10.1175/1520-0442(2004)017<2688:MOGWIO>2.0.CO;2.

Christensen JH, Boberg F, Christensen OB, Lucas-Picher P. 2008. On the need for bias correction of regional climate change projections of temperature and precipitation. *Geophysical Research Letters* **35:** L20709. DOI: 10.1029/2008GL035694.

Christensen JH, Hewitson B, Busuioc A, Chen A, Gao X, Held I, Jones R, Kolli RK, Kwon W-T, Laprise R, Magaña Rueda V, Mearns L, Menéndez CG, Räisänen J, Rinke A, Sarr A, Whetton P. 2007. Regional Climate Projections. *Climate Change 2007: The Physical Science Basis*, S. Solomon, D. Qin, M. Manning, Z. Chen, M. Marquis, K. B. Averyt, M. Tignor and H. L. Miller, Eds. Cambridge University Press: Cambridge, United Kingdom and New York, NY, USA.

Corney S, Grose M, Bennett J, White C, Katzfey J, McGregor J, Holz G, Bindoff NL. 2013. Performance of downscaled regional climate simulations using a variable-resolution regional climate model: Tasmania as a test case. *Journal of Geophysical Research: Atmospheres***:** 2013JD020087. DOI: 10.1002/2013jd020087.

Corney SP, Katzfey JJ, McGregor JL, Grose MR, White CJ, Holz GK, Bennett JC, Gaynor SM, Bindoff NL. 2010. Climate Futures for Tasmania: methods and results on climate modelling. Antarctic Climate and Ecosystems Cooperative Research Centre: Hobart. Available online at http://www.climatechange.tas.gov.au/government_action/climate_futures/. Accessed: Jan 2013.

Dai A. 2011. Drought under global warming: a review. *WIREs Climate Change* **2:** 45–65. DOI: 10.1002/wcc.81.

Dai A, Trenberth KE, Qian T. 2004. A global dataset of Palmer drought severity index for 1870–2002: relationship with soil moisture and effects of surface warming. *Journal of Hydrometeorology* **5:** 1117-1130. DOI: 10.1175/JHM-386.1.

Di Luca A, de Elía R, Laprise R. 2013. Potential for small scale added value of RCM's downscaled climate change signal. *Climate Dynamics* **40:** 601-618. DOI: 10.1007/s00382-012-1415-z.

Domingues CM, Church JA, White NJ, Gleckler PJ, Wijffels SE, Barker PM, Dunn JR. 2008. Improved estimates of upper-ocean warming and multi-decadal sea-level rise. *Nature* **453:** 1090-1093. DOI: 10.1038/nature07080.

Dosio A, Paruolo P. 2011. Bias correction of the ENSEMBLES high-resolution climate change projections for use by impact models: evaluation on the present climate. *Journal of Geophysical Research* **116:** D16106. DOI: 10.1029/2011JD015934.

Durack PJ, Wijffels SE, Matear RJ. 2012. Ocean salinities reveal strong global water cycle intensification during 1950 to 2000. *Science* **336:** 455-458. DOI: 10.1126/science.1212222.

Ehret U, Zehe E, Wulfmeyer V, Warrach-Sagi K, Liebert J. 2012. Should we apply bias correction to global and regional climate data? *Hydrology and Earth System Sciences* **16:** 3391-3404. DOI: 10.5194/hess-16-3391-2012.

Engelbrecht FA, McGregor JL, Engelbrecht CJ. 2009. Dynamics of the Conformal-Cubic Atmospheric Model projected climate-change signal over southern Africa. *International Journal of Climatology* **29:** 1013-1033. DOI: 10.1002/joc.1742.

Fawcett R, Trewin B, Barnes-Keoghan I. 2010. Network-derived inhomogeneity in monthly rainfall analyses over western Tasmania. *17th National Conference of the Australian Meteorological and Oceanographic Society*. IOP Publishing: Canberrra.

Feser F, Rockel B, von Storch H, Winterfeldt J, Zahn M. 2011. Regional climate models add value to global model data: a review and selected examples. *Bulletin of the American Meteorological Society* **92:** 1181–1192. DOI: 10.1175/2011BAMS3061.1.

Fowler HJ, Kilsby CG. 2007. Using regional climate model data to simulate historical and future river flows in northwest England. *Climatic Change* **80:** 337-367. DOI: 10.1007/s10584-006-9117-3.

Fowler HJ, Blenkinsop S, Tebaldi C. 2007. Linking climate change modelling to impacts studies: recent advances in downscaling techniques for hydrological modelling. *International Journal of Climatology* **27:** 1547-1578. DOI: 10.1002/joc.1556.

Fox-Rabinovitz M, Côté J, Dugas B, Déqué M, McGregor JL, Belochitski A. 2008. Stretched-Grid Model Inter-comparison Project: decadal regional climate simulations with enhanced variable and uniform-resolution GCMs. *Meteorology and Atmospheric Physics* **100:** 159-177. DOI: 10.1007/s00703-008-0301-z.

Giorgi F, Im E-S, Coppola E, Diffenbaugh NS, Gao XJ, Mariotti L, Shi Y. 2011. Higher Hydroclimatic Intensity with Global Warming. *Journal of Climate* **24:** 5309–5324. DOI: 10.1175/2011JCLI3979.1.

Goswami M, O'Connor KM, Shamseldin AY. 2002. Structures and performances of five rainfall-runoff models for continuous river-flow simulation. *1st Biennial Meeting of International Environmental Modeling and Software Society*: Lugano, Switzerland, 476–481.

Graham B, Hardie S, Gooderham J, Gurung S, Hardie D, Marvanek S, Bobbi C, Krasnicki T, Post DA. 2009. Ecological impacts of water availability for Tasmania. CSIRO Water for a Healthy Country Flagship: Australia. Available online at http://www.csiro.au/partnerships/TasSY.html.

Graham LP, Hagemann S, Jaun S, Beniston M. 2007. On interpreting hydrological change from regional climate models. *Climatic Change***:** 97–122. DOI: 10.1007/s10584-006-9217-0.

Grose MR, Corney SP, Katzfey JJ, Bennett JC, Bindoff NL. 2011. Improving projections of rainfall trends through regional climate modeling and wide-ranging assessment. *MODSIM2011 International Congress on Modelling and Simulation*. Modelling and Simulation Society of Australia and New Zealand: Perth. Available online at http://www.mssanz.org.au/modsim2011.

Grose MR, Pook MJ, McIntosh P, Risbey J, Bindoff NL. 2013a. The simulation of cutoff lows in a regional climate model: reliability and future trends. *Climate Dynamics* **39:** 445-459. DOI: 10.1007/s00382-012-1368-2.

Grose MR, Corney SP, Katzfey JJ, Bennett JC, Holz GK, White CJ, Bindoff NL. 2013b. A regional response in mean circulation and rainfall to projected climate warming. *Climate Dynamics* **40:** 2035-2048. DOI: 10.1007/s00382-012-1405-1.

Grose MR, Barnes-Keoghan I, Corney SP, White CJ, Holz GK, Bennett JC, Gaynor SM, Bindoff NL. 2010. Climate Futures for Tasmania: general climate. Antarctic Climate and Ecosystems Cooperative Research Centre: Hobart. Available online at http://www.climatechange.tas.gov.au/government_action/climate_futures/.

Hagemann S, Göttel H, Jacob D, Lorenz P, Roeckner E. 2009. Improved regional scale processes reflected in projected hydrological changes over large European catchments. *Climate Dynamics* **32:** 767-781. DOI: 10.1007/s00382-008-0403-9.

Hansen J, Sato M, Kharecha P, von Schuckmann K. 2011. Earth's energy imbalance and implications. *Atmospheric Chemistry and Physics* **11:** 13421-13449. DOI: 10.5194/acp-11-13421-2011.

Hansen J, Nazarenko L, Ruedy R, Sato M, Willis J, Del Genio A, Koch D, Lacis A, Lo K, Menon S, Novakov T, Perlwitz J, Russell G, Schmidt GA, Tausnev N. 2005. Earth's energy imbalance: confirmation and implications. *Science* **308:** 1431–1435. DOI: 10.1126/science.1110252.

Hegerl GC, Zwiers FW, Stott PA, Kharin VV. 2004. Detectability of anthropogenic changes in annual temperature and precipitation extremes. *Journal of Climate* **17:** 3683-3700. DOI: 10.1175/1520-0442(2004)017<3683:DOACIA>2.0.CO;2.

Held IM, Soden BJ. 2006. Robust responses of the hydrological cycle to global warming. *Journal of Climate* **19:** 5686-5699. DOI: 10.1175/JCLI3990.1.

Hock R, de Woul M, Radić V, Dyurgerov M. 2009. Mountain glaciers and ice caps around Antarctica make a large sealevel rise contribution. *Geophysical Research Letters* **36:** L07051. DOI: 10.1029/2008GL037020.

Hofstra N, New M, McSweeney C. 2010. The influence of interpolation and station network density on the distributions and trends of climate variables in gridded daily data. *Climate Dynamics* **35:** 841–858. DOI: 10.1007/s00382-009-0698-1.

Holz GK, Grose MR, Corney SP, White CJ, Bennett JC, Gaynor SM, Bindoff NL. 2010. Climate Futures for Tasmania: agricultural impacts. Antarctic Climate and Ecosystems Cooperative Research Centre: Hobart. Available online at http://www.climatechange.tas.gov.au/government_action/climate_futures/. Accessed: Jan 2013.

Ines AVM, Hansen JW. 2006. Bias correction of daily GCM rainfall for crop simulation studies. *Agricultural and Forest Meteorology* **138:** 44-53. DOI: 10.1016/j.agrformet.2006.03.009.

Ines AVM, Hansen JW, Robertson AW. 2011. Enhancing the utility of daily GCM rainfall for crop yield prediction. *International Journal of Climatology* **31:** 2168-2182. DOI: 10.1002/joc.2223.

IPCC. 2007. Climate change 2007: The Physical Science Basis. Contribution of Working Group I to the Fourth Assessment Report of the Intergovernmental Panel on Climate Change. Cambridge University Press: Cambridge, United Kingdom and New York, NY, USA.

Jeffrey SJ, Carter JO, Moodie KM, Beswick AR. 2001. Using spatial interpolation to construct a comprehensive archive of Australian climate data. *Environmental Modelling & Software* **16:** 309-330. DOI: 10.1016/S1364-8152(01)00008-1.

Johnson F, Sharma A. 2011. Accounting for interannual variability: A comparison of options for water resources climate change impact assessments. *Water Resources Research* **47:** W04508. DOI: 10.1029/2010wr009272.

Johnson F, Westra S, Sharma A, Pitman AJ. 2011. An Assessment of GCM Skill in Simulating Persistence across Multiple Time Scales. *Journal of Climate* **24:** 3609-3623. DOI: 10.1175/2011jcli3732.1.

Jones DA, Wang W, Fawcett R. 2009. High-quality spatial climate data-sets for Australia. *Australian Meteorological and Oceanographic Journal* **58:** 233-248

Katzfey JJ, McGregor J, Nguyen KC, Thatcher M. 2009. Dynamical downscaling techniques: impacts on regional climate change signals. *18th World IMACS Congress and MODSIM09 International Congress on Modelling and Simulation*, R. S. Anderssen, R. D. Braddock and L. T. H. Newham, Eds. Modelling and Simulation Society of Australia and New Zealand and International Association for Mathematics and Computers in Simulation: Cairns, 3942-3947. Available online at http://www.mssanz.org.au/modsim09.

Kendon EJ, Rowell DP, Jones RG. 2010a. Mechanisms and reliability of future projected changes in daily precipitation. *Climate Dynamics* **35:** 489-509. DOI: 10.1007/s00382-009-0639-z.

Kendon EJ, Jones RG, Kjellström E, Murphy JM. 2010b. Using and designing GCM–RCM ensemble regional climate projections. *Journal of Climate* **23:** 6485–6503. DOI: 10.1175/2010JCLI3502.1.

Kerr RA. 2011. Vital details of global warming are eluding forecasters. *Science* **334:** 173-174. DOI: 10.1126/science.334.6053.173.

Kilsby CG. 2007. Context and aims. *Hydrology and Earth System Sciences* **11:** 1065-1068. DOI: www.hydrol-earth-syst-sci.net/11/1065/2007.

Kilsby CG, Tellier SS, Fowler HJ, Howles TR. 2007. Hydrological impacts of climate change on the Tejo and Guadiana rivers. *Hydrology and Earth System Sciences* **11:** 1175-1189. DOI: 10.5194/hess-11-1175-2007.

Kushner PJ, Held IM, Delworth TL. 2001. Southern hemisphere atmospheric circulation response to global warming. *Journal of Climate* **14:** 2238-2249. DOI: 10.1175/1520-0442(2001)014<0001:SHACRT>2.0.CO;2.

Lafon T, Dadson S, Buysa G, Prudhomme C. 2013. Bias correction of daily precipitation simulated by a regional climate model: a comparison of methods. *International Journal of Climatology* **33:** 1367-1381. DOI: 10.1002/joc.3518.

Lal M, McGregor JL, Nguyen KC. 2008. Very high-resolution climate simulation over Fiji using a global variable-resolution model. *Climate Dynamics* **30:** 293-305. DOI: 10.1007/s00382-007-0287-0.

Lavery B, Joung G, Nicholls N. 1997. An extended high-quality historical rainfall dataset for Australia. *Australian Meteorological Magazine* **46:** 27-38

Li H, Sheffield J, Wood EF. 2010. Bias correction of monthly precipitation and temperature fields from Intergovernmental Panel on Climate Change AR4 models using equidistant quantile matching. *Journal of Geophysical Research* **115:** D10101. DOI: doi:10.1029/2009JD012882.

Ling FLN, Gupta V, Willis M, Bennett JC, Robinson KA, Paudel K, Post DA, Marvanek S. 2009a. River modelling for Tasmania. Volume 5: the Derwent-South East region. CSIRO Water for a Healthy Country Flagship: Australia. Available online at http://www.csiro.au/partnerships/TasSY.html.

——. 2009b. River modelling for Tasmania. Volume 4: the South Esk region. CSIRO Water for a Healthy Country Flagship: Australia. Available online at http://www.csiro.au/partnerships/TasSY.html.

——. 2009c. River modelling for Tasmania. Volume 3: the Pipers-Ringarooma region. CSIRO Water for a Healthy Country Flagship: Australia. Available online at http://www.csiro.au/partnerships/TasSY.html.

——. 2009d. River modelling for Tasmania. Volume 2: the Mersey-Forth region. CSIRO Water for a Healthy Country Flagship: Australia. Available online at http://www.csiro.au/partnerships/TasSY.html.

——. 2009e. River modelling for Tasmania. Volume 1: the Arthur-Inglis-Cam region. CSIRO Water for a Healthy Coun try Flagship: Australia. Available online at http://www.csiro.au/partnerships/TasSY.html.

Lucas C, Nguyen H, Timbal B. 2012. An observational analysis of Southern Hemisphere tropical expansion. *Journal of Geophysical Research* **117:** D17112. DOI: 10.1029/2011JD017033.

Lüthi D, Le Floch M, Bereiter B, Blunier T, Barnola J-M, Siegenthaler U, Raynaud D, Jouzel J, Fischer H, Kawamura K, Stocker TF. 2008. High-resolution carbon dioxide concentration record 650,000–800,000 years before present. *Nature* **453:** 379-382. DOI: 10.1038/nature06949.

Mailhot A, Duchesne S, Caya D, Talbot G. 2007. Assessment of future change in intensity–duration–frequency (IDF) curves for Southern Quebec using the Canadian Regional Climate Model (CRCM). *Journal of Hydrology* **347:** 197-210. DOI: 10.1016/j.jhydrol.2007.09.019.

Mann ME, Zhang Z, Hughes MK, Bradley RS, Miller SK, Rutherford S, Ni F. 2008. Proxy-based reconstructions of hemispheric and global surface temperature variations over the past two millennia. *Proceedings of the National Academy of Sciences* **105:** 13252–13257. DOI: 10.1073/pnas.0805721105.

Maraun D. 2012. Nonstationarities of regional climate model biases in European seasonal mean temperature and precipitation sums. *Geophysical Research Letters* **39:** L06706. DOI: 10.1029/2012GL051210.

Maraun D, Wetterhall F, Ireson A, Chandler R, Kendon E, Widmann M, Brienne S, Rust H, Sauter T, Themeßl M, Venema V, Chun K, Goodess C, Jones R, Onof C, Vrac M, Theile-Eich I. 2010. Precipitation downscaling under climate change: recent developments to bridge the gap between dynamical models and the end user. *Reviews of Geophysics* **48:** RG3003. DOI: 10.1029/2009RG000314.

Markoff MS, Cullen AC. 2008. Impact of climate change on Pacific Northwest hydropower. *Climatic Change* **87:** 451-469. DOI: 10.1007/s10584-007-9306-8.

McGregor JL, Dix MR. 2008. An updated description of the Conformal-Cubic Atmospheric Model. *High resolution numerical modelling of the atmosphere and ocean*, K. Hamilton and W. Ohfuchi, Eds. Springer New York51-75.

Meehl G, Covey A, C., Delworth T, Latif M, McAvaney B, Mitchell JFB, Stouffer RJ, Taylor KE. 2007. The WCRP CMIP3 multi-model dataset: A new era in climate change research. *Bulletin of the American Meteorological Society* **88:** 1383-1394. DOI: 10.1175/BAMS-88-9-1383.

Merz R, Parajka J, Blöschl G. 2011. Time stability of catchment model parameters: implications for climate impact analyses. *Water Resources Research* **47:** W02531. DOI: 10.1029/2010WR009505.

Milly PCD, Dunne KA. 2011. On the hydrologic adjustment of climate-model projections: the potential pitfall of potential evapotranspiration. *Earth Interactions* **15:** 1–14. DOI: 10.1175/2010EI363.1.

Min S-K, Zhang X, Zwiers FW, Hegerl GC. 2011. Human contribution to more-intense precipitation extremes. *Nature* **470:** 378-381. DOI: 10.1038/nature09763.

Mitchell T. 2003. Pattern scaling. *Climatic Change* **60:** 217-242. DOI: 10.1023/A:1026035305597.

Morrongiello JR, Beatty SJ, Bennett JC, Crook DA, Ikedife DNEN, Kennard MJ, Kerezsy A, Lintermans M, McNeil DG, Pusey BJ, Rayner T. 2011. Climate change and its implications for Australia's freshwater fish. *Marine and Freshwater Research* **62:** 1082-1098. DOI: 10.1071/MF10308.

Morton FI. 1983. Operational estimates of areal evapotranspiration and their significance to the science and practice of hydrology. *Journal of Hydrology* **66:** 1–76. DOI: 10.1016/0022-1694(83)90177-4.

Nakićenović N, Swart R. 2000. Special Report on Emissions Scenarios. A Special Report of Working Group III of the Intergovernmental Panel on Climate Change: Cambridge, United Kingdom.

Nguyen H, Evans A, Lucas C, Smith I, Timbal B. 2013. The Hadley circulation in reanalyses: climatology, variability, and change. *Journal of Climate* **26:** 3357–3376. DOI: 10.1175/JCLI-D-12-00224.1.

Nguyen KC, Katzfey JJ, McGregor JL. 2011. Global 60 km simulations with CCAM: evaluation over the tropics. *Climate Dynamics* **39:** 637-654. DOI: 10.1007/s00382-011-1197-8.

Oki T, Kanae S. 2006. Global hydrological cycles and world water resources. *Science* **313:** 1068-1072. DOI: 10.1126/science.1128845.

Pall P, Allen MR, Stone DA. 2007. Testing the Clausius-Clapeyron constraint on changes in extreme precipitation under CO2 warming. *Climate Dynamics* **28:** 351-363. DOI: 10.1007/s00382-006-0180-2.

Pall P, Aina T, Stone DA, Stott PA, Nozawa T, Hilberts AGJ, Lohmann D, Allen MR. 2011. Anthropogenic greenhouse gas contribution to flood risk in England and Wales in autumn 2000. *Nature* **470:** 382-385. DOI: 10.1038/nature09762.

Petheram C, Hughes D, Rustomji P, Smith K, Van Neil T, Yang A. 2009. River modelling for Northern Australia. A report to the Australian Government from the CSIRO Northern Australia Sustainable Yields Project. Australia.

Piani C, Haerter JO. 2012. Two dimensional bias correction of temperature and precipitation copulas in climate models. *Geophysical Research Letters* **39:** L20401. DOI: 10.1029/2012GL053839.

Piani C, Haerter J, Coppola E. 2010a. Statistical bias correction for daily precipitation in regional climate models over Europe. *Theoretical and Applied Climatology* **99:** 187-192. DOI: 10.1007/s00704-009-0134-9.

Piani C, Weedon GP, Best M, Gomes SM, Viterbo P, Hagemann S, Haerter JO. 2010b. Statistical bias correction of global simulated daily precipitation and temperature for the application of hydrological models. *Journal of Hydrology* **395:** 199-215. DOI: 10.1016/j.jhydrol.2010.10.024.

Pielke RA, Wilby RL. 2012. Regional climate downscaling: What's the point? *Eos, Transactions American Geophysical Union* **93:** 52-53. DOI: 10.1029/2012EO050008.

Post DA, Jakeman AJ. 1999. Predicting the daily streamflow of ungauged catchments in SE Australia by regionalising the parameters of a lumped conceptual rainfall–runoff model. *Ecological Modeling* **123:** 91–104. DOI: 10.1016/S0304-3800(99)00125-8.

Post DA, Chiew FHS, Teng J, Viney NR, Ling FLN, Harrington G, Crosbie RS, Graham B, Marvanek S, McLoughlin R. 2012. A robust methodology for conducting large-scale assessments of current and future water availability and use: a case study in Tasmania, Australia. *Journal of Hydrology* **412-413:** 233-245. DOI: 10.1016/j.jhydrol.2011.02.011.

Prudhomme C, Davies H. 2009. Assessing uncertainties in climate change impact analyses on the river flow regimes in the UK. Part 1: baseline climate. *Climatic Change* **93:** 177–195. DOI: 10.1007/s10584-008-9464-3.

Rahmstorf S, Cazenave A, Church JA, Hansen JE, Keeling RF, Parker DE, Somerville RCJ. 2007. Recent climate observations compared to projections. *Science* **316:** 709. DOI: 10.1126/science.1136843.

Randall DA, Wood RA, Bony S, Colman R, Fichefet T, Fyfe J, Kattsov V, Shukla APJ, Srinivasan J, Stouffer RJ, Sumi A, Taylor KE. 2007. Climate models and their evaluation. *Climate Change 2007: The Physical Science Basis. Contribution of Working Group I to the Fourth Assessment Report of the Intergovernmental Panel on Climate Change*, S. Solomon, D. Qin, M. Manning, Z. Chen, M. Marquis, K. B. Averyt, M.Tignor and H. L. Miller, Eds. Cambridge University Press: Cambridge, United Kingdom, New York, NY, USA.

Reynolds RW. 1988. A real-time global sea surface temperature analysis. *Journal of Climate* **1:** 75-86. DOI: 10.1175/1520-0442(1988)001<0075:ARTGSS>2.0.CO;2.

Schaefli B, Hingray B, Musy A. 2007. Climate change and hydropower production in the Swiss Alps: quantification of potential impacts and related modelling uncertainties. *Hydrology and Earth System Sciences* **11:** 1191-1205. DOI: 10.5194/hess-11-1191-2007.

Schepen A, Q. J. Wang, and D. E. Robertson. 2012. Combining the strengths of statistical and dynamical modeling approaches for forecasting Australian seasonal rainfall. *Journal of Geophysical Research* **117:** D20107. DOI: 10.1029/2012JD018011.

Sherwood SC. 2010. Direct versus indirect effects of tropospheric humidity changes on the hydrologic cycle. *Environmental Research Letters* **5:** 025206. DOI: 10.1088/1748-9326/5/2/025206.

Sherwood SC, Roca R, Weckwerth TM, Andronova NG. 2010a. Tropospheric water vapor, convection, and climate. *Reviews of Geophysics* **48:** RG2001. DOI: 10.1029/2009RG000301.

Sherwood SC, Ingram W, Tsushima Y, Satoh M, Roberts M, Vidale PL, O'Gorman PA. 2010b. Relative humidity changes in a warmer climate. *Journal of Geophysical Research* **115:** D09104. DOI: 10.1029/2009JD012585.

Smith I, Chandler E. 2010. Refining rainfall projections for the Murray Darling Basin of south-east Australia-the effect of sampling model results based on performance. *Climatic Change* **102:** 377-393. DOI: 10.1007/s10584-009-9757-1.

Staudinger M, Stahl K, Seibert J, Clark MP, Tallaksen LM. 2011. Comparison of hydrological model structures based on recession and low flow simulations. *Hydrology and Earth System Sciences* **15:** 3447–3459. DOI: 10.5194/hess-15-3447-2011.

Stephens GL, Hu Y. 2010. Are climate-related changes to the character of global-mean precipitation predictable? *Environmental Research Letters* **5:** 025209. DOI: 10.1088/1748-9326/5/2/025209.

Tan KS, Chiew FHS, Grayson, R.B., Scanlon PJ, Siriwardena L. 2005. Calibration of a daily rainfall-runoff model to estimate high daily flows. *MODSIM 2005 International Congress on Modelling and Simulation*, A. Zerger and R. M. Argent, Eds. Modelling and Simulation Society of Australia and New Zealand: Melbourne, 2960-2966. Available online at http://www.mssanz.org.au/modsim05/index.htm.

Taylor KE. 2001. Summarizing multiple aspects of model performance in a single diagram. *Journal of Geophysical Research* **106:** 7183-7192. DOI: 10.1029/2000JD900719.

Teng J, Vaze J, Chiew FHS, Wang B, Perraud J-M. 2012. Estimating the relative uncertainties sourced from GCMs and hydrological models in modelling climate change impact on runoff. *Journal of Hydrometeorology* **13:** 122-139. DOI: 10.1175/JHM-D-11-058.1.

Teutschbein C, Seibert J. 2012. Is bias correction of Regional Climate Model (RCM) simulations possible for non-stationary conditions? *Hydrology and Earth System Sciences Discussions* **9:** 12765-12795. DOI: 10.5194/hessd-9-12765-2012.

Thatcher M, McGregor JL. 2009. Using a scale-selective filter for dynamical downscaling with the Conformal Cubic Atmospheric Model. *Monthly Weather Review* **137:** 1742-1752. DOI: 10.1175/2008MWR2599.1.

Thatcher M, McGregor JL. 2011. A technique for dynamically downscaling daily-averaged GCM datasets using the Conformal Cubic Atmospheric Model. *Monthly Weather Review* **139:** 79-95. DOI: 10.1175/2010MWR3351.1.

Thompson DWJ, Kennedy JJ, Wallace JM, Jones PD. 2008. A large discontinuity in the mid-twentieth century in observed global-mean surface temperature. *Nature* **453:** 646-649. DOI: 10.1038/nature06982.

Timbal B, Drosdowsky W. 2013. The relationship between the decline of Southeastern Australian rainfall and the strengthening of the subtropical ridge. *International Journal of Climatology* **33:** 1021–1034. DOI: 10.1002/joc.3492.

Toth Z, Talgrand O, Candille G, Zhu Y. 2003. Probability and ensemble forecasts. *Forecast verification: a practitioner's guide in atmospheric science*, I. T. Jolliffe and D. B. Stephenson, Eds. John Wiley & Sons Ltd: Chichester, West Sussex, England, 137-164.

Trenberth KE. 2011. Changes in precipitation with climate change. *Climate Research* **47:** 123-138. DOI: 10.3354/cr00953.

Trenberth KE, Jones PD, Ambenje P, Bojariu R, Easterling D, Tank AK, Parker D, Rahimzadeh F, Renwick JA, Rusticucci M, Soden B, Zhai P. 2007. Observations: Surface and Atmospheric Climate Change. *Climate Change 2007: The physical science basis. Contribution of Working Group I to the Fourth Assessment Report of the Intergovernmental Panel on Climate Change*, S. Solomon, D. Qin, M. Manning, Z. Chen, M. Marquis, K. B. Averyt, M. Tignor and H. L. Miller, Eds. Cambridge University Press: Cambridge, United Kingdom and New York, NY, USA.

van den Hurk B, Hirschi M, Schär C, Lenderink G, van Meijgaard E, van Ulden A, Rockel B, Hagemann S, Graham P, Kjellström E, Jones R. 2005. Soil control on runoff response to climate change in regional climate model simulations. *Journal of Climate* **18:** 3536–3551. DOI: 10.1175/JCLI3471.1.

van Dijk AIJM, Beck HE, Crosbie RS, de Jeu RAM, Liu YY, Podger GM, Timbal B, Viney NR. 2013. The Millennium Drought in southeast Australia (2001–2009): Natural and human causes and implications for water resources, ecosystems, economy, and society. *Water Resources Research* **49:** 1-18. DOI: 10.1002/wrcr.20123.

van Oldenborgh GJ, Philip YS, Collins M. 2005. El-Nino in a changing climate: a multi-model study. *Ocean Science* **1:** 81-95. DOI: 10.5194/os-1-81-2005.

Vaze J, Post DA, Chiew FHS, Perraud J-M, Viney N, Teng J. 2010. Climate nonstationarity – Validity of calibrated rainfall-runoff models for use in climate change studies. *Journal of Hydrology* **394:** 447-457. DOI: 10.1016/j.jhydrol.2010.09.018.

Viney NR, Perraud J, Vaze J, Chiew FHS, Post DA, Yang A. 2009a. The usefulness of bias constraints in model calibration for regionalisation to ungauged catchments. *18th World IMACS Congress and MODSIM09 International Congress on Modelling and Simulation*, R. S. Anderssen, R. D. Braddock and L. T. H. Newham, Eds. Modelling and Simulation Society of Australia and New Zealand and International Association for Mathematics and Computers in Simulation: Cairns, 3421-3427. Available online at http://mssanz.org.au/modsim09.

Viney NR, Post DA, Yang A, Willis M, Robinson KA, Bennett JC, Ling FLN, Marvanek S. 2009b. Rainfall-runoff modelling for Tasmania. CSIRO Water for a Healthy Country Flagship: Australia. Available online at http://www.csiro.au/science/TASSY.html.

Wentz FJ, Ricciardulli L, Hilburn K, Mears C. 2007. How much more rain will global warming bring? *Science* **317:** 233-235. DOI: 10.1126/science.1140746.

White CJ, McInnes KL, Cechet RP, Corney SP, Grose MR, Holz GK, Katzfey JJ, Bindoff NL. 2013. On regional dynamical downscaling for the assessment and projection of future temperature and precipitation extremes across Tasmania, Australia. *Climate Dynamics***:** Published Online. DOI: 10.1007/s00382-013-1718-8.

Wilby RL, Harris I. 2006. A framework for assessing uncertainties in climate change impacts: Low-flow scenarios for the River Thames, UK. *Water Resources Research* **42:** W02419. DOI: 10.1029/2005WR004065.

Willett KM, Gillett NP, Jones PD, Thorne PW. 2007. Attribution of observed surface humidity changes to human influence. *Nature* **449:** 710–712. DOI: 10.1038/nature06207.

Willett KM, Jones PD, Gillett NP, Thorne PW. 2008. Recent Changes in Surface Humidity: Development of the HadCRUH Dataset. *Journal of Climate* **21:** 5364–5383. DOI: 10.1175/2008JCLI2274.1.

Wood A, Leung LR, Sridhar V, Lettenmaier DP. 2004. Hydrologic implications of dynamical and statistical approaches to downscaling climate outputs. *Climatic Change* **62:** 189-216. DOI: 10.1023/B:CLIM.0000013685.99609.9e.

Yin JH. 2005. A consistent poleward shift of the storm tracks in simulations of 21st century climate. *Geophysical Research Letters* **32:** L18701. DOI: 10.1029/2005GL023684.

Zhang X, Zwiers FW, Hegerl GC, Lambert FH, Gillett NP, Solomon S, Stott PA, Nozawa T. 2007. Detection of human influence on twentieth-century precipitation trends. *Nature* **448:** 461-465. DOI: 10.1038/nature06025.

Zou L, Zhou T, Li L, Zhang J. 2010. East China summer rainfall variability of 1958–2000: dynamical downscaling with a variable-resolution AGCM. *Journal of Climate* **23:** 6394-6408. DOI: 10.1175/2010JCLI3689.1.

This chapter has been removed for copyright or proprietary reasons.

Appendix A

Performance of quantile-quantile bias-correction for use in hydroclimatological projections

Published in:

This paper has been published in the proceedings of the MODSIM2011 19th International Congress on Modelling and Simulation as:

Bennett JC, Grose MR, Post DA, Ling FLN, Corney SP, Bindoff NL. 2011. Performance of quantile-quantile bias-correction for use in hydroclimatological projections. MODSIM2011, 19th International Congress on Modelling and Simulation. Modelling and Simulation Society of Australia and New Zealand: Perth.
Available online at:
http://www.mssanz.org.au/modsim2011/F5/bennett.pdf

Appendix B Adapting Temsim to operate with inflows from rainfall-runoff simulations

Temsim was designed to apply assumptions of future electricity prices and demand to historical inflows in order to predict system operation, storage levels and power yield for 20 years. Historical inflows used in Temsim are calculated retrospectively with a series of models that employ a variety of methods, depending on available data. These methods include regression analyses with available data and water balances based on measured storage volumes and known outflows – for convenience we will collectively term these the 'volume balance method'. The input data and models are reviewed annually, but the models have remained reasonably consistent since a major revision in 1992.

The volume balance method assumes that historical inflows will reflect future inflows. We sought to assess the impacts of changes to future inflows, so it was not enough to rely on historical inflows to the hydropower system. To calculate future inflows to the hydro-electric system we digitally delineated 47 catchments in the system, accounting for all diversions and other hydropower infrastructure. Projected runoff (Chapter 4) was then aggregated to generate inflows to each of these catchments – we will term this the 'runoff aggregation method'.

The runoff aggregation method differs from the volume balance method in two important ways:

1) The two methods rely on different and independent sets of input data.

2) The volume balance method uses measured changes in storage volumes, meaning evaporation from storages is calculated implicitly. This can result in negative inflows during the summer months at certain sites. The runoff models used in the runoff aggregation method account for evaporation from a catchment, but not the elevated rates of evaporation that can be expected from a large water body. Inflows aggregated from runoff can never be negative.

Despite these differences, the two methods yield acceptably similar inflows. Daily inflows to the 47 catchments were generated for the period 1992-2008 with the runoff aggregation method using SILO interpolated observations as inputs to the Simhyd runoff models. These inflows were then compared to those calculated with the volume balance method. Annual volumes at each of the 47 sites agree reasonably well (Fig B.1a). The runoff aggregation method tends to slightly overpredict annual total system inflows (bias = +4%) and replicates seasonal patterns reasonably well (Fig B.1b), though there is considerable variation in seasonal matches from site to site (not shown). The runoff aggregation method tends to overpredict summer flows, indicating that evaporation from large water bodies is underestimated. Nonetheless, the runoff aggregation method is reasonably efficient at replicating inflows calculated with the volume balance method, with about half the catchments giving daily Nash-Sutcliffe efficiencies (Nash & Sutcliffe 1970) of 0.6 or more (Fig B.1c). The runoff aggregation method also gives realistic power station ouflows and power yield (not shown) when processed through Temsim.

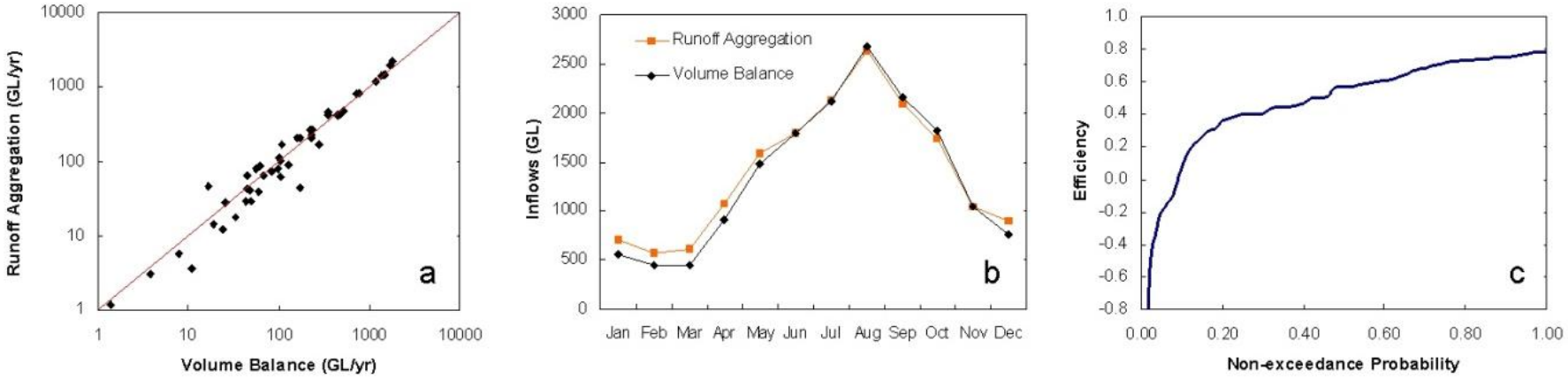

Fig B.1 Comparison of inflows to the hydro-electric system 1992-2008 generated using the volume balance and runoff aggregation methods (see text for details): (a) annual inflows at 47 sites (b) monthly system inflows (c) efficiency of runoff aggregation method measured against volume balance method for 47 sites.